CN9800580

CNIC-01230
CNDC-0021
INDC(CPR)-043-L

中国核科技报告

CHINA NUCLEAR SCIENCE AND TECHNOLOGY REPORT

COMMUNICATION OF NUCLEAR DATA PROGRESS

No. 18 (1997)

China Nuclear Data Center

中国核情报中心
原子能出版社

China Nuclear Information Centre
Atomic Energy Press

CNIC-01230
CNDC-0021
INDC(CPR)-043 / L

COMMUNICATION OF NUCLEAR DATA PROGRESS

No.18 (1997)

China Nuclear Data Center

China Nuclear Information Centre

Atomic Energy Press

Beijing, December, 1997

EDITORIAL NOTE

This is the 18th issue of *Communication of Nuclear Data Progress* (CNDP), in which the achievements of nuclear data field for the last year in P. R. China are carried. It includes the measurements of angular distributions and energy spectra for ^{58}Ni(n,p)^{58}Co reaction at 4.1 MeV, and activation cross sections for ^{159}Tb(n,γ) ^{160}Tb and ^{169}Tb(n,γ) ^{170}Tb reactions at 0.4~4.0 MeV and 0.16~3.0 MeV, respectively; n+^{239}Pu coupled channel optical model and DWBA calculations, analysis of d+^{16}O and p+^{18}F reactions, calculations of (n,p) reaction cross sections for Zinc isotopes and n+^{176}Hf; evaluations of n+^{235}U fission product data and study of the dependence of fission yield data on neutron energy, decay data evaluation for radionuclide ^{7}Be, evaluations of ^{55}Mn, ^{54}Fe, ^{59}Co, ^{62}Ni, and ^{63}Cu(n,α) reaction cross sections, evaluations and calculations of ^{158,159}Tb(n,2n), (n,3n), (n,γ) and (n,x) reaction cross sections below 20 MeV; the systematics research on (p,n) and (p,2n) reaction excitation functions; and the sub-library of atomic masses and characteristic constants of nuclear ground states (CENPL-MCC 2).

The editors hope that our readers and colleagues will not spare their comments, in order to improve this publication.

Please write to Drs. Liu Tingjin and Zhuang Youxiang

Mailing Address: China Nuclear Data Center
China Institute of Atomic Energy
P.O.Box 275 (41), Beijing 102413
People's Republic of China

Telephone: 86-10-69357729 or 69357830

Telex: 222373 IAE CN

Facsimile: 86-10-6935 7008

E-mail: cndc @ mipsa.ciae.ac.cn

EDITORIAL BOARD

Editor-in-Chief

Liu Tingjin Zhuang Youxiang

Members

Cai Chonghai Li Manli Li Qiankun Liu Jianfeng
Liu Tingjin Liu Tong Ma Gonggui Shen Qingbiao
Song Qinglin Tang Guoyou Tang Hongqing Wang Yansen
Wang Yaoqing Zhang Jingshang Zhuang Youxiang

Editorial Department

Li Qiankun Xu Ling Li Shuzhen

CONTENTS

CN9800581

I EXPERIMENTAL MEASUREMENT

Tests of the GIC and Measurements of Angular Distributions and Energy Spectra for $^{58}Ni(n,p)^{58}Co$ Reaction at 4.1 MeV

Tang Guoyou Zhang Guohui Chen Jinxiang Shi Zhaomin
(Institute of Heavy Ion Physics, Peking University, Beijing 100871, China)

Yu. M. Gledenov M. Sedysheva G. Khuukhenkhuu
(Joint Institute for Nuclear Research, Dubna 141980, Russia)

Chen Zemin Liang Wei Zhang Xuemei
(Department of Physics, Tsinghua University, Beijing 100084, China)

Abstract

On the basis of measurements of double differential cross sections for (n,α) reactions in 5−7 MeV neutron energy region using gridded ionization chamber (GIC)[1-3], we constructed a new GIC which, compared with the old ones[4], can bear higher pressure and makes it possible to measure (n,p) reactions up to 6 MeV and (n,xα) reactions up to 20 MeV.

To test the new chamber, the saturation property for argon and krypton mixed with a few percent CO_2 was studied using ^{241}Am and compound Pu α source and tritium from $^{6}Li(n_{th},t)^{4}He$, and the two dimensional spectra for ^{241}Am and Pu α source, $^{6}Li(n_{th},t)^{4}He$ and H(n,p) reactions were measured. The measured energy spectra and angular distributions for α and tritium are reasonable, and the derived $\overline{X}$ data for α, proton and tritium in argon and krypton from the measured spectra data were compared with the calculated ones. They are in good agreement.

The angular distributions and energy spectra for $^{58}Ni(n,p)^{58}Co$ reaction at 4.1 MeV neutron energy were measured using the new chamber. The results were compared with other data.

Introduction

Neutron induced charged particle emission reaction data are of great interest since they not only can provide important information for the theoretical study of reaction mechanism, but also are very important in reactor technology, particularly in the estimation of nuclear heating, radiation damage and induced activity in structural materials.

The gridded ionization chamber (GIC) has many advantages in charged particle measurements, such as the high geometrical efficiency, the capability of energy-angle determination and particle selection. In our previous GIC works, we have measured ^{40}Ca, ^{58}Ni, ^{64}Zn, ^{54}Fe(n,α) reactions in 5−7 MeV neutron region[1−3].

In order to measure (n,p) reactions and higher energy region (n,xα) reactions, we constructed a new twin GIC. It was made at the Frank Laboratory of Neutron Physics, JINR, Dubna, Russia. Compared to the old ones[4], the new chamber can bear higher gas pressure, so it is suitable for (n,p) and (n,xα) reaction measurements. In addition, the volume of the new GIC is much smaller than the old ones and, with a sample changer, five samples can be placed in it, thus saved a lot of counting gas. As a result, it is affordable for us to use krypton instead of argon as working gas to reduce the background.

1 Tests of the New Chamber

1.1 Working State Determination

(1) Saturation Property and Electrodes Voltage Determination

By measuring the anode pulse-height of α-particles from ^{241}Am and Pu α source (compound α source, including ^{238}Pu, ^{239}Pu, ^{234}U and ^{244}Cm), and tritium from ^{6}Li(n$_{th}$,t)^{4}He as a function of the reduced field strength between the cathode and the grid at different pressures, we derived the saturation curves.

Fig.1 shows the saturation curves for ^{241}Am α particles in argon with CO_2(3.78%). The saturation curves for tritium are similar to that for α particles. It can be seen from the curves that the saturation of charge collection was reached after the reduced field strength E_{cg}/p higher than 200−250 V·cm^{-1}·atm^{-1}*. For krypton +CO_2(2.73%) the required reduced field strength is just a little higher (250−300 V·cm^{-1}·atm^{-1}). The voltage difference between cathode and grid can be decided from this value.

---

* 1atm=0.101MPa

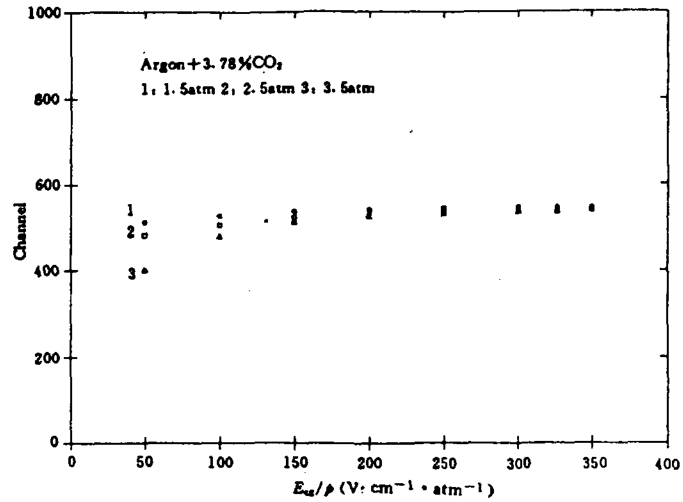

Fig.1 Saturation curves for Ar+3.78%CO_2

To decide the needed voltage difference between anode and grid, we measured the anode pulse-heights from Pu α source at different ratios of field strength between anode and grid to that between cathode and grid (E_{ag}/E_{cg}). From the curve showed in Fig.2, for our GIC, the value of E_{ag}/E_{cg} should be greater than 1.4 to avoid electron capture by the grid. According to the structure of the grid (parallel wires 2 mm in distance, 0.1 mm in diameter), this value is 1.372 in theory. We normally set this value 1.6—2.0 during measurements.

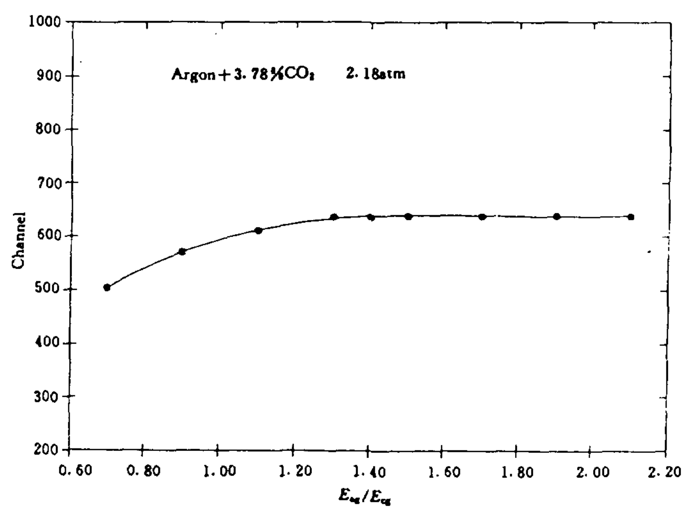

Fig.2 The relations between the channel of alpha peak and E_{ag}/E_{cg}

With our high voltage equipment (±5000 V), using krypton as working gas, we can measure protons up to 6 MeV, and α-particles up to 20 MeV.

(2) Cathode-grid and Anode-grid Distances and Gas Pressure

To ensure the uniformity of the field, the distance from cathode to grid is set 4.35 cm, much shorter than the length of one side of the square electrodes 18.5 cm. The distance between anode and grid is 1.75 cm. In this arrangement, the grid inefficiency is about 0.011.

The gas pressure was determined by the range of the measured particles in the working gas and the distance from cathode to grid. The pressure should be high enough to ensure the particles to be stopped before reaching the grid. On the other hand, the pressure shouldn't be too high. As the pressure increases, the angular resolution becomes worse, as well as wasting more gas.

1.2 Measurements of ^{241}Am and Pu α Source, ^{6}Li(n_{th},t)^{4}He and H(n,p)n Reactions

Two dimensional spectra of ^{241}Am, Pu α source and ^{6}Li(n_{th},t)^{4}He, H(n,p)n reactions were measured. Fig.3 is the typical anode spectrum of Pu α source. The energy resolution is better than 2%. Fig.4 is the results of angular distributions of the compound Pu α source. The results are reasonable.

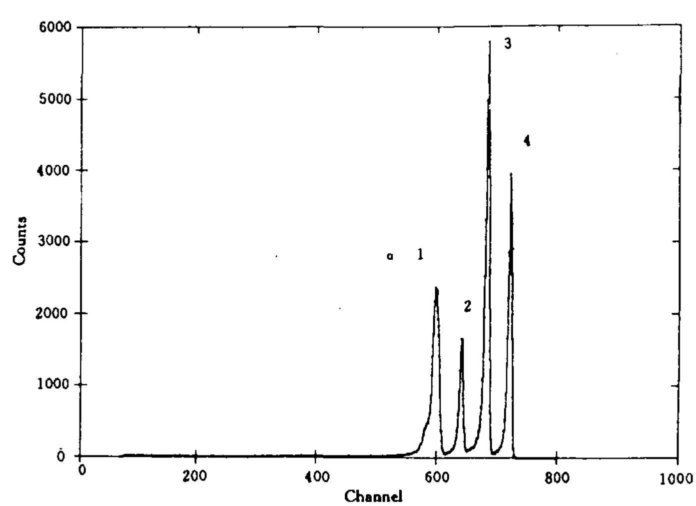

Fig.3 Typical anode spectrum for the compound alpha source

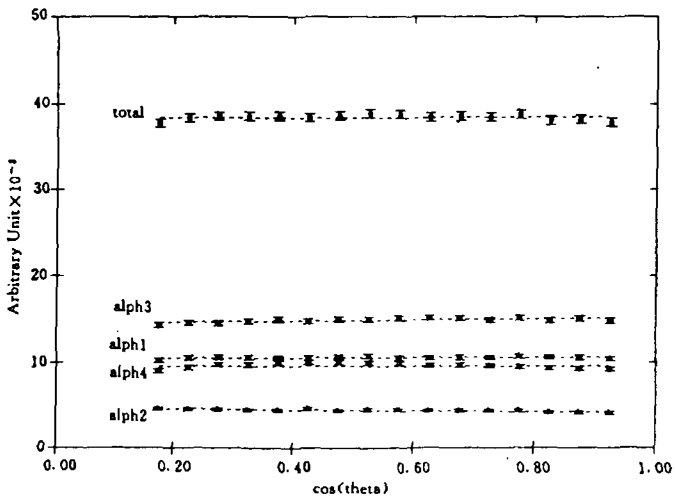

Fig.4 Alpha angular distributions

1.3 Measurement and Calculation of $\overline{x}$ Data for α, Proton and Tritium in Argon and Krypton

$\overline{x}$ is the average distance from the centre of gravity of the electron-ion pair track to the origin of the trace. In general it is a function of particle energy, mass and charge. $\overline{x}$ data are needed in the work of GIC measurement[5]. As far as we know, there are no such data published, so it is important to study $\overline{x}$ data experimentally and theoretically.

According to reference[5], $\overline{x}$ data for α-particle from α source or for tritium from $^6Li(n_{th},t)^4He$ can be measured from the upper and lower edges of the cathode spectrum of α or tritium, whose energy is known. As for protons, since it is difficult to get mono-energy proton source, we used recoil protons from n-p reaction on a polyethylene film.

We measured the $\overline{x}$ data for α, proton, and tritium in argon and krypton. Then, using the stopping power data calculated from program TRIM, we calculated the range data and $\overline{x}$ data for these particles in argon and krypton. The experiments and the calculations are in good agreement. Fig.5 shows the result of proton in krypton.

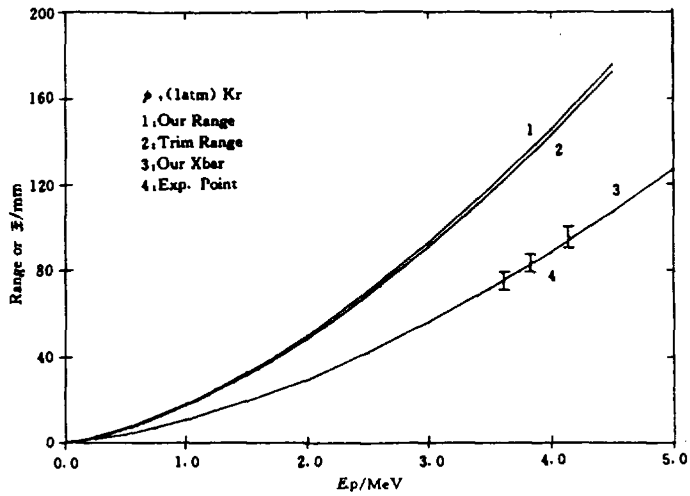

Fig.5 The measurement and calculation of $\overline{X}$ data for proton in Kr

2 Measurement of ^{58}Ni(n,p) Reaction at 4.1 MeV

2.1 Experiment

The experiment was performed at the Institute of Heavy Ion Physics, Peking University. The neutron was produced through D(d,n)^{3}He reaction on the 4.5 MV Van de Graaff accelerator. The neutron flux was monitored by a fission chamber with enriched ^{238}U sample (99.997%), and a BF_3 long counter.

The counting gas was krypton with CO_2(2.73%), and the pressure was 4.0 atm. The nickel sample was 3.57 cm in diameter, 1.04 mg/cm^2 in thickness. The distance from the neutron source to the nickel sample was 37.5 cm. We used a collimator made from copper and iron with a thickness of 15.3 cm to reduce the background.

First, the forward events plus background and backward background were measured at the same time, and then we turned the GIC 180° to measure the backward events plus background and forward background. The measuring time for each side was about 10 hours.

2.2 Results and Discussion

Figs.6 and 7 show the proton energy spectra in the forward and backward directions. From the spectra we know that the emitted protons can be divided into two groups, the lower energy group and the higher energy group. In Fig.8 is shown the angular distribution of the total protons in the center of mass system, as well as those of the two groups. The angular distribution for the lower energy group is a little steeper than that of the higher energy group. The angular distribution for the total protons and for the lower energy group is 90° symmetric, not isotropic, as given in ENDF/B-VI library.

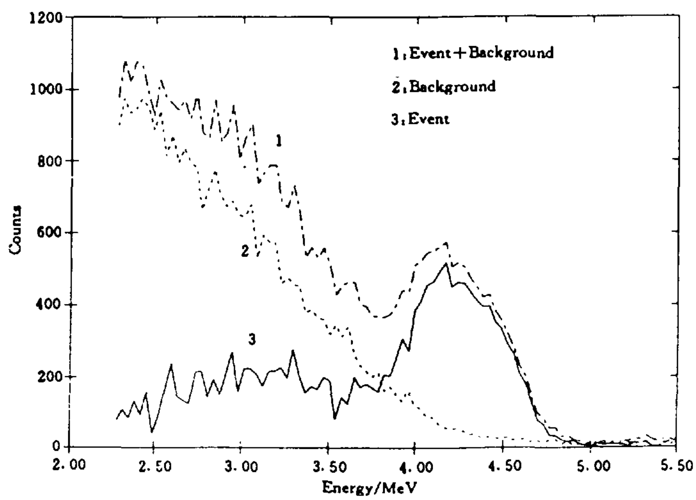

Fig.6 The energy spectrum for proton from ^{58}Ni(n,p) in the forward direction (E_n=4.1 MeV)

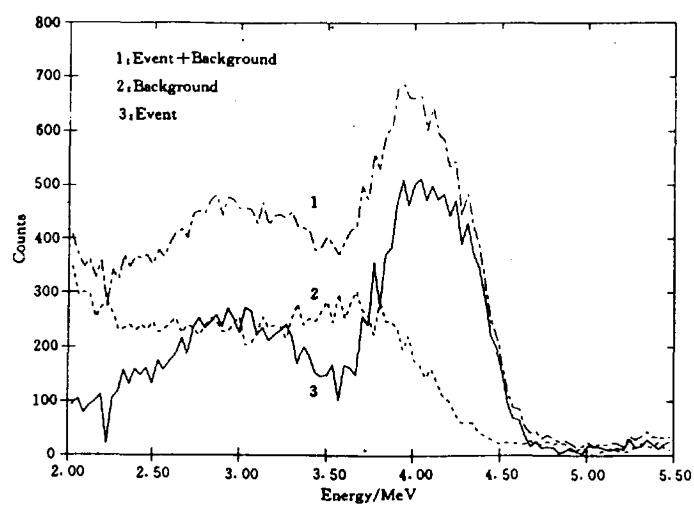

Fig.7 The energy spectrum for proton from ^{58}Ni(n,p) in the backward direction (E_n=4.1MeV)

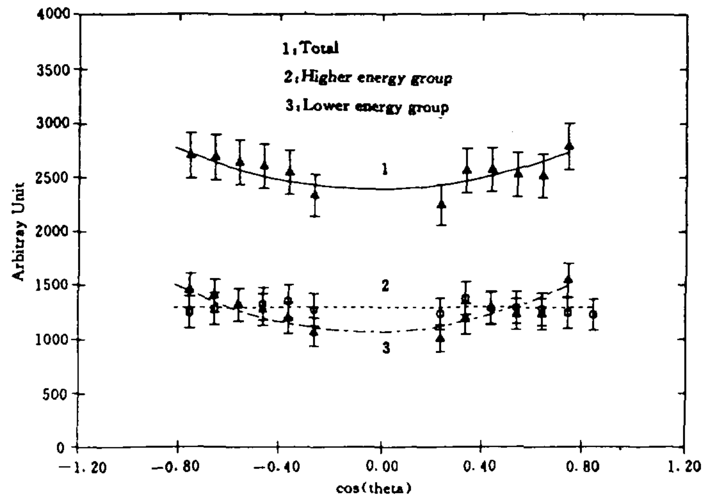

Fig.8 The angular distribution in the center of mass system

Since the statistics are not good enough, the error bars are large. Further experiments are needed. In the process of experiment, we found that in the forward two dimensional spectra, there were recoil protons. To reduce this interference, only 35°−90° proton spectra were selected in Fig.6, since the higher energy recoil protons are dominated mainly near 0° in the two dimensional spectrum. Because of the interference of the recoil protons, the error of the measured reaction cross section is larger.

The recoil protons may come from the hydrogen absorbed by electrode surfaces. To solve this problem, more investigations should be done.

The authors are indebted to the crew of 4.5 MV accelerator, IHIP, Peking University for their kind cooperation.

References

[1] Tang Guoyou, et al., Chinese Journal of Nuclear Physics, 14.3(1993)239

[2] Tang Guoyou, et al., Chinese Journal of Nuclear Physics, 17.1(1995)45

[3] Yu. M. Gledenov, et al., Angular Distribution and Cross Section of the $^{58}Ni(n,\alpha)^{55}Fe$ and $^{54}Fe(n,\alpha)^{51}Cr$ Reactions at 6 and 7 MeV, ISINN-4, Apr., 1996

[4] Yu. M. Gledenov, Investigation of the Fast Neutron Induced (n,α) Reactions, E3-95-445

[5] C. Budtz-Jorgensen, H.-H. Kinnter et al., Nucl. Instr. and Meth. A 258(1987)209

CN9800582

Measurement of Activation Cross Sections for $^{159}Tb(n,\gamma)^{160}Tb$ and $^{169}Tm(n,\gamma)^{170}Tm$ Reactions

Chen Jinxiang Shi Zhaomin Tang Guoyou Zhang Guohui
(Institute of Heavy Ion Physics, Peking University)

Lu Hanlin Han Xiaogang Huang Xiaolong
(China Institute of Atomic Energy, Beijing)

Chang Yongfu Wang Jun Wang Wushang
(Northwest Institute of Nuclear Technology, Xian)

Introduction

Both ^{159}Tb and ^{169}Tm are rare-earth elements. Their activation cross sections are a good indicator for nuclear science and technology applications. Precise values of the neutron capture cross section of terbium and thulium also are of practical importance in relation to reactor design since they are the fission product poisons.

For the $^{159}Tb(n,\gamma)^{160}Tb$ reaction, capture cross sections were measured in neutron energy range 0.4−4.0 MeV in four laboratories[1-4]. In all these works were directly measured the prompt gamma-ray for capture events. No measurement of $^{159}Tb(n,\gamma)^{160}Tb$ cross section using activation technique has been reported. The cross sections for $^{169}Tm(n,\gamma)^{170}Tm$ were measured in the neutron energy range 0.16−3.0 MeV in four laboratories[5-8]. The cross section measured by Jian Sousheng[8] using activation method was lower than other one using the prompt gamma-ray method. The cross section at 0.5−1.6 MeV is necessary to be measured with higher resolution HPGe detector further so as to check the capture cross sections and obtain more accurate data.

In this experiment, the neutron capture cross sections for ^{159}Tb and ^{169}Tm relative to the $^{197}Au(n,\gamma)^{198}Au$ reaction were measured at neutron energies of 0.57, 1.10 and 1.60 MeV using the activation method.

1 Experimental Procedure

The experiments were carried out at the 4.5 MV Van de Graaff accelerator of the Institute of Heavy Ion Physics, Peking University. The monoenergetic neutrons with energies 0.57, 1.10 and 1.60 MeV were produced via the $T(p,n)^3He$ reaction on a solid T-Ti target of 1.42 mg/cm^2 in thickness.

The rare-earth samples were made from natural element oxides powder by pressing into disks of 10 mm in diameter and about 0.5—0.8 mm thick (about 353.1, 325.1, 339.8 mg/cm^2 for Tm, 500.5, 544.1, 615.2 mg/cm^2 for Tb, respectively) and being sealed in thin polyethylene foils. The purities were 86.88% for Tb and 87.56% for Tm. Each sample was sandwiched between two gold disks. The purity 99.9% gold disks each of 10 mm in diameter and 0.1 mm in thickness were used to measure the neutron fluence on the sample. The sample groups were wrapped with cadmium foils of 0.5 mm in thickness.

The irradiation was performed at 0° direction relative to the incident proton beam. The distance between the sample and target was 1.5 cm. In order to reduce wall-scattered and floor-scattered neutrons, the target for source neutrons was located in a non-scattering environment about 5.5 m away from the wall and at a distance of 1.8 m from the floor and under the target there was a underground hollow of 3.0 m in diameter and 1.8 m deep. The proton beam currents were generally 10—12 μA and the duration of irradiation was 23 to 24 hours at each energy. The fluctuation of neutron fluence rate was monitored with a BF_3 long counter at 0° at a distance of 315 cm from the neutron source. In order to record the neutron fluence rate as a function of time during the irradiation, the integral count rate of the long counter per 10 minutes was recorded continuously by microcomputer multiscaler and stored on magnetic disk for calculating the correction of non-uniform irradiation history.

After irradiation, the activities from residual nuclei were measured with a HPGe γ-detector (105 cm^3). The efficiency of the detector was calibrated by using a set of standard gamma ray sources in the energy range of 0.1 — 1.5 MeV and the efficiency curve was fitted with the least-square method. The γ-detection efficiency for ^{160}Tb was obtained from this efficiency curve. For the decay of ^{170}Tm, the dominant gamma ray is only 84.25 keV. In order to calibrate the efficiency of the detector for ^{170}Tm accurately, a standard gamma-ray source of ^{170}Tm was prepared specially by Institute of Atomic Energy and its activity was determined by the 4πβ–γ coincidence counting. The activities of these samples were also measured comparatively by gamma-ray spectroscope using a HPGe-N ORTEC model GX10185 and a HPGe-P Canberra well detector in the Northwest Institute of Nuclear Technology. Their measured results were in good agreement with our ones within the errors. The decay data used in present work are taken from Ref.[9] and listed in Table 1.

Table 1 Decay data of radioactive products

Resid. nucl.	$T_{1/2}$ / d	E_γ / keV	I_γ / %
^{160}Tb	72.3	1177.95	14.97
^{170}Tm	128.6	84.25	3.26
^{198}Au	2.696	411.8	95.57

Some corrections have been made and are described as follows:

(1) Neutron Energy

On account of the sample near the target, the incident neutron energy was calculated by

$$\bar{E}_n = \int_0^\alpha E(\theta)A(\theta)2\pi \sin\theta \, d\theta \Big/ \int_0^\alpha A(\theta)2\pi \sin\theta \, d\theta$$

where $E(\theta)$ = the energy angular distribution of incident neutron;

$A(\theta)$ = the angular distribution of incident neutron cross section;

α = the maximum angle subtended by the sample at the target.

(2) Gamma Ray Self-absorption in the Sample

The correction factor of gamma ray self-absorption in the sample is given by

$$f_s = [1 - \exp(-\mu x)] / \mu x$$

where μ is the total-mass absorption coefficient in cm^2/g;

x is the density thickness in g/cm^2.

At first, the total-mass absorption coefficient was measured experimentally as gamma-ray passed through a series of samples with different thickness. Because the 1173 keV gamma-ray of ^{60}Co almost equals 1177.95 keV gamma-ray of ^{160}Tb, the total-mass absorption coefficient of Tb sample was measured by using 1173 keV γ-ray of ^{60}Co instead of by using 1177.95 keV γ-ray of ^{160}Tb.

It is important for the correction factor of 84.25 keV gamma ray self-absorption in the Tm_2O_3 sample. Its total-mass absorption coefficient was measured experimentally by using 84.25 keV γ-ray of ^{170}Tm source.

The γ-ray peak area measured was analyzed using the program H developed for an IBM compatible computer. The counting rates under the concerned full-energy peaks based on the measured γ-spectrum were obtained. After the corrections for the detector efficiency, cascade effect, γ-intensity, fluctuation of neutron fluence rate and γ-ray self absorption in the samples, the activation cross sections of ^{159}Tb and ^{169}Tm were calculated by using well-known activation equation.

2 Result and Discussion

The cross sections measured in present work and the $^{197}Au(n,\gamma)^{198}Au$ cross sections recommended by ENDF/B-6 are listed in Table 2. The principal contributions of errors and their magnitudes are given in Table 3.

Table 2 Measured results of cross sections (in mb)

E_n/MeV	$^{159}Tb(n,\gamma)^{160}Tb$	$^{169}Tm(n,\gamma)^{170}Tm$	$^{197}Au(n,\gamma)^{198}Au$
0.57±0.03	298.8 ±15.5	160.3 ±10.1	118.6 ±4.1
1.10±0.03	179.0 ±10.7	99.7 ±6.9	77.2 ±3.4
1.60±0.04	120.6 ±7.2	95.5 ±6.7	66.5 ±2.9

Table 3 Principal sources of errors

Source of uncertainty	Relative errors/(%)	
	$^{159}Tb(n,\gamma)^{160}Tb$	$^{169}Tm(n,\gamma)^{170}Tm$
reference cross section	3.5−4.5	3.5−4.5
γ-counting statistics for sample	0.7−1.0	0.6−1.0
γ-counting statistics for ^{198}Au	0.6−0.8	0.5−0.7
γ-detection efficiency for sample	1.5	2.0
γ-detection efficiency for ^{198}Au	1.5	1.5
correction of self absorption for sample	2.0	4.0
correction of self absorption for ^{198}Au	1.5	1.5
sample weight	1.0	1.0
^{197}Au foil weight	0.1	0.1

Fig.1−2 show the capture cross sections of ^{159}Tb and ^{169}Tm as function of the incident neutron energy in comparison with the results of other published measurements, respectively.

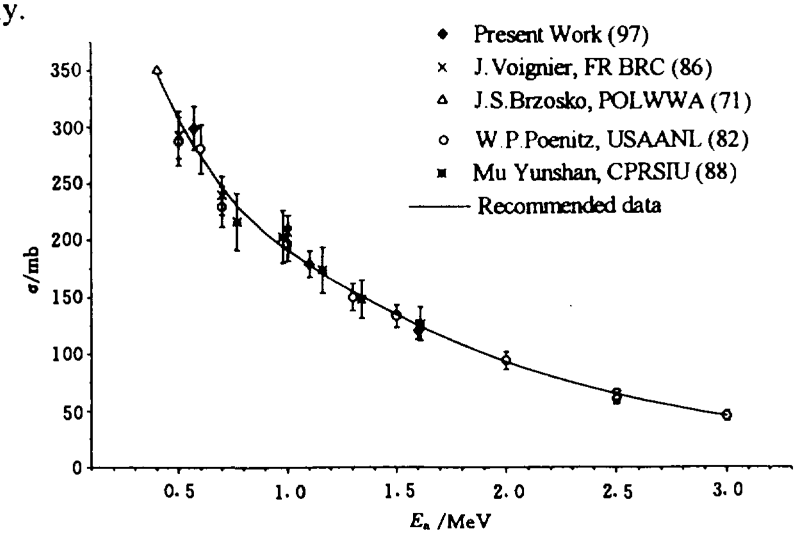

Fig.1 Cross sections for $^{159}Tb(n,\gamma)^{160}Tb$ reaction

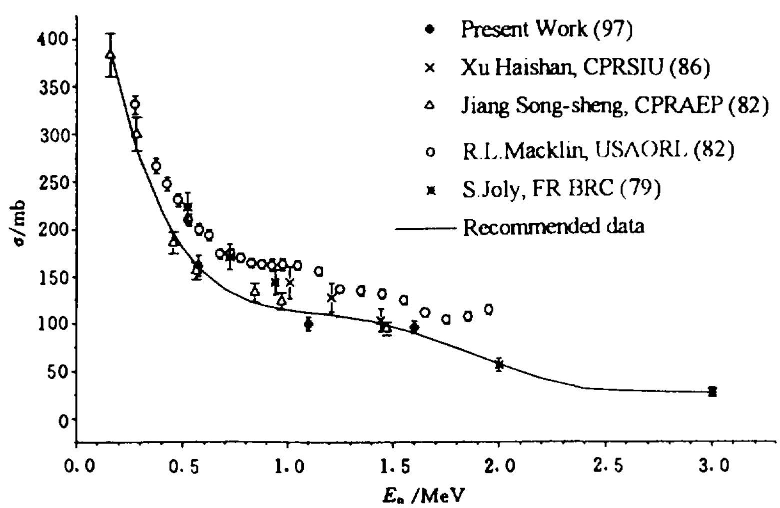

Fig.2 Cross sections for $^{169}Tm(n,\gamma)^{170}Tm$ reaction

Tb: The uncertainty of our measurement is 5%–6%, while W.P.Poenitz[1] 7.5%–10%, J.Voignier[2] 7%–8%, Mu Yunshan[3] 11%–12% and J.S.Brzosko[4] no error given. Our results obtained by the activation method are in good agreement with the experimental data of other authors[1-4], which are obtained by the prompt gamma-ray detection technique in the 0.4–3.0 MeV neutron energy range. From Fig.1, we can find out that they all have a same decreasing trend with increasing incident neutron energy. So we consider that the experimental data including our data are reasonable and reliable. These experimental data were fitted to get the recommended data. The recommended data in energy region 0.4–3.0 MeV are given in Table 4.

Tm: The uncertainty of the present experimental results is 6%–7%, while R.L. Macklin[5] about 5%, Xu Haishan[6] 10%–12%, S.Joly[7] 6.7%–18% and Jiang[8] 6%–7.5%. For this reaction, we and Jiang[8] measured this capture cross section by the same activation method. But, we measured the γ-activity of ^{170}Tm while Jiang measured the β-activity of ^{170}Tm. The other authors[5-7] all directly measured the prompt gamma-ray for capture events. From Fig.2, we can find out that our results are in good agreement with Jiang's experimental data but lower than the results of other authors. In the energy range higher than 1.5 MeV, there is a serious discrepancy between the experimental results of S.Joly and R.L.Macklin, obtained by the same prompt gamma-ray detection technique. So we consider that our and Jiang's experimental results are adequate. The recommended data in energy region 0.4–3.0 MeV for this reaction are given based on our and Jiang's results as well as

S.Joly's experimental data for energy higher than 1.5 MeV in Table 4.

Table 4 The recommended data for $^{159}Tb(n,\gamma)^{160}Tb$ and $^{169}Tm(n,\gamma)^{170}Tm$ reactions

neutron energy/MeV	cross section /mb	
	$^{159}Tb(n,\gamma)^{160}Tb$	$^{169}Tm(n,\gamma)^{170}Tm$
0.40	347.6 ± 20.8	218.5 ±10.9
0.50	306.9 ±15.3	179.4 ±8.9
0.60	273.6 ±13.6	152.7 ±7.6
0.70	246.2 ±12.3	135.3 ±6.8
0.80	224.1 ±11.2	124.5 ±6.2
0.90	206.1 ±10.3	118.1 ±5.9
1.00	191.2 ±9.5	114.1 ±5.7
1.20	166.1 ±8.3	108.9 ±5.4
1.40	144.3 ±8.6	101.7 ±5.1
1.60	124.8 ±7.5	89.9 ±4.5
1.80	107.9 ±6.5	74.1 ±3.7
2.00	93.1 ±6.5	56.8 ±5.6
2.20	80.2 ±5.6	41.5 ±4.5
2.40	69.1 ±4.8	31.1 ±3.4
2.60	59.8 ±4.2	28.9 ±3.2
2.80	51.9 ±3.6	27.4 ±3.1
3.00	45.4 ±3.2	27.0 ±3.0

Thanks to the Chinese Nuclear Data Center for its financial support. In addition, acknowledgement is also made to the crew of the 4.5 MV Van de Graaff accelerator at Peking University for numerous irradiations.

References

[1] Poenitz W P, Guenther P T and Smith A B. ANL-83-4, 1983, 4:239
[2] Voignier J, Joly S and Grenier G. Nucl. Sci. and Eng., 1986, 93:43
[3] Mu Yunshan, Li Yexiang, Wang Shiming, et al., Chin J Nucl Phys., 1988, 10(3):233
[4] Brzosko J S, Gierlik E, Soltan A, et al., J.Acta Physica Polonica Section /B, 1971, 2:489
[5] Macklin R L, Drake D M, Malanify J J, et al., Nucl. Sci. and Eng., 1982, 82:143
[6] Xu Haishan, Xian Zhengyu, Mu Yunshan, et al., Chin J Nucl Tech, 1986, 9:5
[7] Joly S, Voignier J, Grenier G, et al. Nucl. Sci. and Eng., 1979,70:53
[8] Jiang Songshemg, Luo Dexing, Zhou Zuying, et al., Chin J Nucl Phys, 1982, 4(2):136
[9] Firestone R B. Table of isotopes, 8th edition 1996, Vol.2

CN9800583

II THEORETICAL CALCULATION

Nuclear Level Density and Spin Cut-off Parameters of Light Nuclei

Z. Kargar A.N. Behkami
(Physics Department, Shiraz University, Shiraz, Iran)

Abstract

Nuclear level densities, thermodynamic functions and spin cut-off factors have been deduced for nuclei in the mass region $24 < A < 63$ from a microscopic theory which includes nuclear pairing interaction. Single particle levels for both Seeger and Nilsson potentials were used in the calculations. Level densities extracted from the theory are compared with their corresponding experimental values. It is found that the nuclear level densities are very sensitive to the energy gap parameter Δ. The reduction of energy gap results in an increase in the nuclear level density. The effects of pairing interaction on the thermodynamic functions are illustrated and discussed. The calculational procedure to account for an odd particle system blocking, as well as the effect of such blocking are also discussed.

Introduction

In all statistical theories the nuclear level denstity is the most characteristic quantity and plays an essential role in the study of nuclear structure. The Fermi gas model or non-interacting model[1] has often been used in the study of statistical treatment of nuclear properties, it is familiar and of convenient form.

However, computation of level density parameter 'a' from neutron resonance data using noninteracting model shows marked shell effects[2]. The use of single particle levels obtained from the shell model calculation in the evaluations of nuclear state densities has been discussed by various authors[3,4]

Furthermore, the superconductivity theory[5] predicts the existance of the transition energy, below which the Fermi gas model is invalidated. In this superconducting phase the energy temperature relation is much different from the one expected in the later model and the level density is much smaller than the one expected by the extrapolation from normal phase. In this way the prediction of the low energy behaviour of level densities has been much improved[6].

Since detailed and high resolution (n,γ) and transfer reaction data became available, the authors have considered it worth while applying the statistical approach to examine the effects of BCS pairing interaction in order to see to which extent the pairing interaction is needed to give agreement between measured and calculated level densities. In addition we would like to find out the influence of the discrete structure of single particle spectrum on the behavior of the thermodynamic functions, and to see whether one set of single particle energies is better than another for calculating level densities. In Section 1 the general theory will be discussed, in Section 2 the actual calculational procedure will be presented, in Section 3 the results obtained will be compared with their corresponding experimental values and discussed.

1 Nuclear State and Level Density

We consider a system of nucleons interacting each other with the pairing force. For a spherically symmetric nuclei, in addition to being characterized by energy ε_k, the single fermion states are also characterized by the projection of the angular momentum on the z-axis, m_k. In the superconducting theory, the nucleons having angular momentum $(m_{k'}\ -m_k)$ couple so as to form a quasi bound particle.

The state density of such an A nucleon system of energy E is related to the grand partition function[7],

$$\ln Z(\varepsilon,\beta) = -\beta\sum_k(\varepsilon_k - \lambda - E_k) + 2\sum_k \ln[1+\exp(-\beta E_k)] - \beta\frac{\Delta^2}{G} \tag{1}$$

Where α and β are two Lagrangian multipliers associated with the nucleon number and energy. $E_k = [(\varepsilon_k - \lambda)^2 + \Delta^2]^{1/2}$ is the single fermion energy and Δ is the gap parameter. $\lambda=\alpha/\beta$ is the chemical potential and G is the strength of pairing interaction.

Eq. (1) is valid only if the quantities Δ, λ and β satisfy the following gap equation:

$$\frac{2}{G} = \sum_k \frac{1}{E_k}\tanh\frac{\beta E_k}{2} \tag{2}$$

The state density is the inverse Laplace transform of the grand partition function,

$$\omega(A,E) = \left(\frac{1}{2\pi \mathrm{i}}\right)^2 \oint \mathrm{d}\alpha \oint \mathrm{d}\beta Z(\alpha,\beta)\exp(-\alpha A + \beta E) \tag{3}$$

The above contour integrals can be evaluated by the method outlined previously

[8-10], the result is:

$$\varpi(A,E)=\frac{\exp(S)}{2\pi D^{1/2}} \tag{4}$$

here the entropy S can be written as:

$$S=2\sum_k \ln[1+\exp(-\beta E_k)]+2\beta\sum_k \frac{E_k}{1+\exp(\beta E_k)} \tag{5}$$

and 'D' is a 2×2 determinant with its elements given in terms of the second derivations of the grand partition function.

In addition, we obtain the nucleon number N and the energy E given by

$$A=\frac{1}{\beta}\frac{\partial \ln Z}{\partial \lambda}=\sum_k n_k \tag{6}$$

$$E=\frac{-\partial \ln Z}{\partial \beta}=\sum_k \varepsilon_k n_k-\frac{\Delta^2}{G} \tag{7}$$

Where the occupation probability, n_k is given by

$$n_k=1-\frac{\varepsilon_k-\lambda}{E_k}\tan\mathrm{h}\frac{\beta E_k}{2} \tag{8}$$

The statistical properties of a nucleus is defined in terms of its neutron and proton N and Z and the total energy E. Since the neutron-proton superfluids are independent, their correlation can be neglected. We then extend the above derivation to include a nuclear system. For a nucleus of N neutrons of energies $\varepsilon_k^{(n)}$ with magnetic quantum numbers $m_k^{(n)}$ and Z protons of energies $\varepsilon_k^{(p)}$ with magnetic qunatum numbers $m_k^{(p)}$, the constants of motion are then neutron and proton numbers given by Eq.(6) and the total energy $E=E_p+E_n$ given by Eq.(7).

The total state density for a system of N neutrons and Z protons at an exitation energy $U=U_n+U_p$ is

$$\varpi(N,Z,U)=\frac{\exp(S)}{(2\pi)^{3/2}D^{1/2}} \tag{9}$$

here $S=S_n+S_p$ is the total entropy and 'D' is now a 3×3 determinant.

Finally, the total level density for a nuclear system at an excitation energy $U=E-E_{ground}$ is given by

$$\rho(N,Z,U)=\varpi(N,Z,U)/(2\pi\sigma^2)^{1/2} \tag{10}$$

where σ^2 is the total spin cut-off parameter defined as:

$$\sigma^2=\sigma_n^2+\sigma_p^2$$

with

$$\sigma_n^2=\frac{1}{2}\sum_k m_k^{n^2}\sin\mathrm{h}^2(\frac{1}{2}\beta E_k) \tag{11}$$

and a similar relation for σ_p^2, where ε_k and m_k are the single particle energies and magnetic quantum numbers respectively.

2 Calculational Procedure

2.1 Energy Gap and Critical Temperature

In view of the importance of the pairing energy in nuclear level density, we have calculated its dependence on nuclear temperature. For a nuclear system characterized by its single particle energies ε_k and magnetic quantum numbers m_k, calculations are done in the following way. (i) At zero temperature Eqs.(2) and (6) are solved for $\lambda(0)$ and the pairing strength G for known particle number A and gap parameter Δ. The initial values of gap parameters were obtained from the latest mass table of Audi et al[11]. (ii) The critical temperature T_c and the corresponding chemical potential λ_c are evaluated by setting $\Delta=0$ and solving the same equations for specified nucleon number A and pairing strength G. (iii) The quantities $\lambda(T)$ and $\Delta(T)$ are then evaluated for a given value of T by solving Eqs.(2) and (6) with the values of A and G from (i). These values of $\lambda(T)$ and $\Delta(T)$ are used to compute other thermodynamic quantities which will be discussed in the next sections.

It is worth noting that the pairing interacting strength G depends on the number of single particle levels which are included in the calculation. However, for a given value of Δ the final results are not sensitive to the number of single particle levels as long as sufficient levels are included so that the levels of largest 'k' have very small occupational probabilities. Temperature dependence of the energy gap parameters for both the neutron and proton system for ^{60}Ni nucleus are shown in Fig.1. It is seen from this figure that the energy gap parameter decreases rapidly with increasing temperature and it vanishes altogether at the critical temperature.

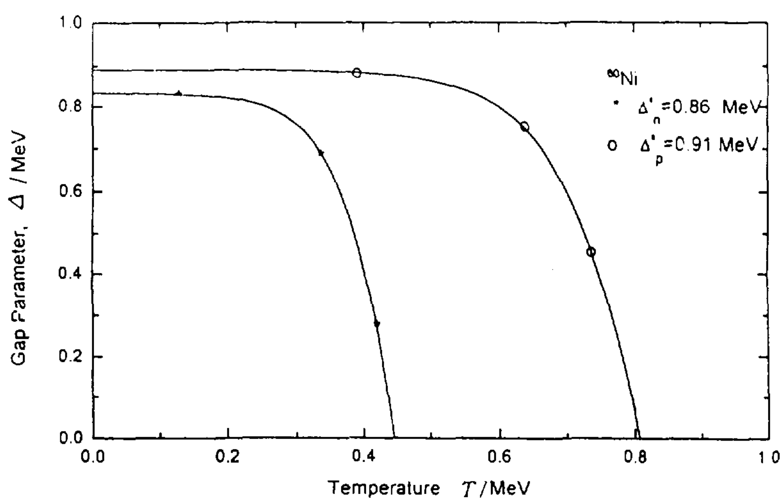

Fig. 1 Temperature dependence of the neutrons and protons gap parameters for ^{60}Ni

2.2 Excitation Energy and Entropy

The excitation energy of the nuclear system with temperature T can be evaluated as follows: (i) the intrinsic energy of the ground state $E_n(0)$ is obtained from Eq.(7) for known values of $\lambda(0)$ and G obtained in section 2.1. In the same way, the intrinsic energy $E_n(T)$ is obtained from known values of $\lambda(T)$ and $\Delta(T)$ obtained again in section 2.1. Thus, the excitation energy of the neutron system at temperature T is given by $U_n = E_n(T) - E_n(0)$. The excitation energy of the proton system is obtained in the same way, $U_P = E_P(T) - E_P(0)$, thus the total excitation energy at temperature T is $U = U_n + U_P$.

The excitation energy for neutron and proton system for ^{60}Ni nucleus are plotted as a function of tempeature in Fig. 2. The arrows indicate the energies of the phase transition from the superconducitng state to the normal state. We see from the examination of this figure that the functional relationship of the excitation energy and temperature is quite different above and below the critical temperature.

The entropy of the neutron and proton system is evaluated from Eq.(5) at temperature T from the values of $\lambda(T)$ and $\Delta(T)$ obtained in section 2.1. From the additivity property of entropy, the total entropy is obtained as $S=S_n+S_p$. The entropies are plotted as a function of temperature in Fig. 3 for ^{60}Ni nucleus. Again the arrows indicate the phase transition from superconducting state to the normal state.

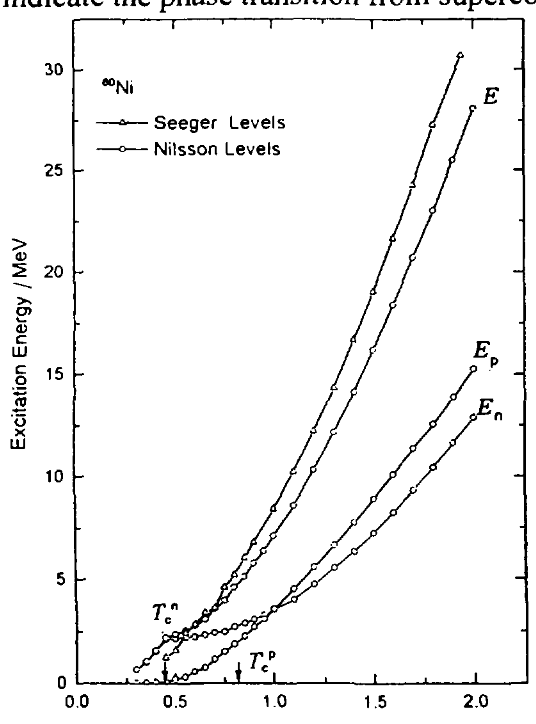

Fig. 2 Intrinsic excitation energy for ^{60}Ni

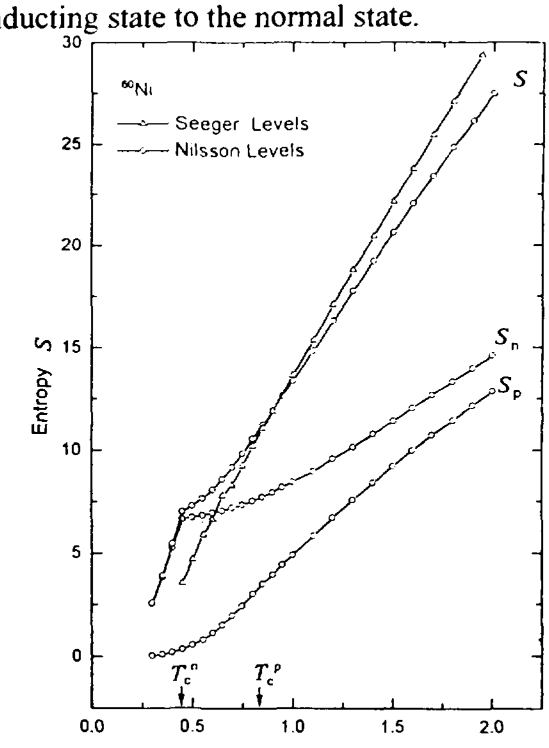

Fig. 3 Relation between the entropy and nuclear temperature, for ^{60}Ni

The calculational procedure just outlined is for even particle systems where the index 'k' sums over doubly degenerate levels.

2.3 Odd Particle System

For an odd particle system, blocking is important and must be included. When a level near the Fermi surface is occupied by an odd particle, the effect of the pairing correlation is reduced. The reduction necessarily depends on which level is occupied. The change in Δ between the even and odd case due to the blocking of one level by the odd particle is estimated as [10],

$$\Delta^{odd}(0) \cong \Delta^{even}(0) - \frac{1}{(\Delta^{even}(0))^2}\left(\sum_{k \neq k'} \frac{1}{E_k^3}\right)^{-1} \tag{12}$$

where k' indicates a state occupied by the odd particle. The actual calculation, in which the blocking effect has been included exactly indicates a difference in Δ between even and odd system in the order of 20%. These results are roughly in agreement with Eq.(12).

We have investigated the blocking effect by two different methods. (i) Reducing the strength of pairing parameter Δ. The change in Δ leads to a change in the particle occupational probabilities. After a proper reduction in Δ, the odd particle system is treated in a way analogous to the even particle system. (ii) Adjusting the ground state for nuclear pairing. The statistical functions were calculated from the adjacent doubly even nucleus and then the energy scale was shifted by an energy equivalent to that required to produce one quasi-particle. It turns out that the results of both procedures give generally identical level densities especially at higher excitation energies. This will be shown in the next section.

2.4 Nuclear State and Level Density

In performing calculations of state and level density the energies and spins of the single particle levels were first calculated with a program and parameters of Nilsson et al[12]. The quantities χ and μ which enter the Nilsson potential were taken from reference[12]. The relative energies and spins obtained from Nilsson program for two of the nuclei ^{56}Fe and ^{60}Ni for twenty eight doubly degenerate levels are given in Table 1 and for ^{60}Ni they are displayed in Fig. 4. Note that the Fermi energies are indicated for neutron and proton components. In actual calculation, however, many more single-particle levels were introduced.

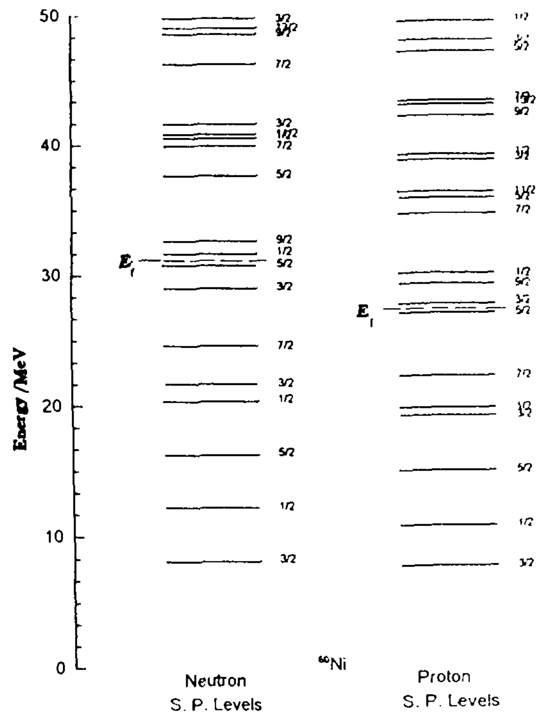

Fig.4 Energies of Nilsson single particle levels

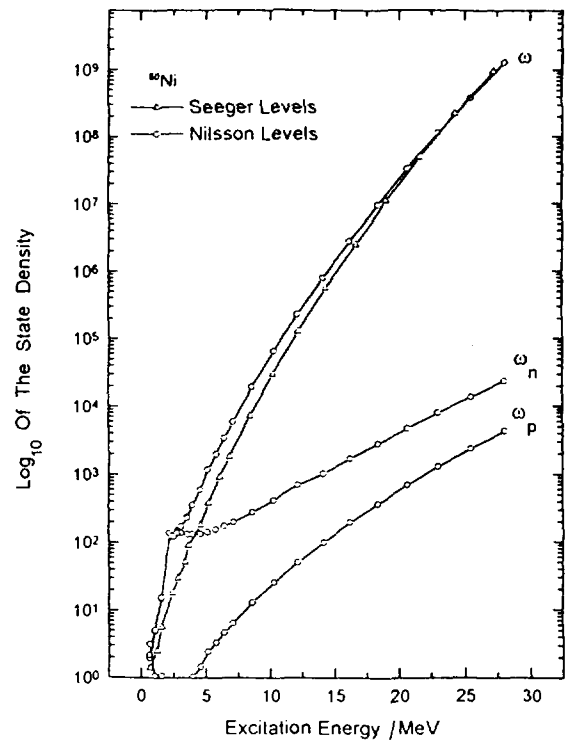

Fig.5 The logarithm of the state density for ^{60}Ni

Next the values of E_n, S_n and $\omega(N, U_n)$ were calculated from (7), (5) and (4) using the values of $\lambda(T)$ and $\Delta(T)$ obtained in Section 2.1. The spin cut-off factor σ_n^2 is calculated using Eqs.(11) from the known values of eigenvalues $\varepsilon_k^{(n)}$ and their corresponding magnetic quantum numbers $m_k^{(n)}$. Then the calculations are repeated for proton component. Finally, the qunatities σ^2, $\omega(N,Z,U)$ are calculated with Eqs.(11), (9) and (10). In Fig. 5 the logarithm of the state density is plotted as a function of excitation energy for ^{60}Ni nucleus. Again the effect of pairing energy and shell effect is quite apparent at lower energies.

2.5 Spin Cut-off Factor

The spin cut-off factor has been calculated with the microscopic theory from the known values of the single fermion energies ε_k and their corresponding magnetic quantum number m_k. This is done by using[13]

$$\sigma^2 = \frac{1}{2}\{\sum_k m_k^{n^2} \sinh^2(\frac{1}{2}\beta E_k^n) + \sum_k m_k^{p^2} \sinh^2(\frac{1}{2}\beta E_k^p)\} \tag{13}$$

which is made up of the sum of the neutron and proton components.

We have compared the results with that obtained on the basis of the macroscopic theory given by[14]

$$\sigma^2 = 0.0888 at A^{2/3} \tag{14}$$

where the nuclear temperature t is related to excitation energy through Eq. (15),

$$U = at^2 - t \tag{15}$$

Table 1 Relative Energies of Single Particle Level of Nilsson for ^{56}Fe and ^{60}Ni

	^{56}Fe				^{60}Ni			
K	State	Neutron Energy	State	Proton Energy	State	Neutron energy	State	Proton Energy
1	$1s_{1/2}$	0.00	$1s_{1/2}$	0.00	$1s_{1/2}$	0.00	$1s_{1/2}$	0.00
2	$1p_{3/2}$	10.27	$1p_{3/2}$	10.18	$1p_{3/2}$	7.89	$1p_{3/2}$	7.35
3		10.27		10.18		7.89		7.35
4	$1p_{1/2}$	12.37	$1p_{1/2}$	12.55	$1p_{1/2}$	11.93	$1p_{1/2}$	10.50
5	$1d_{5/2}$	20.15	$1d_{5/2}$	19.94	$1d_{5/2}$	16.01	$1d_{5/2}$	14.64
6		20.15		19.94		16.01		14.64
7		20.15		19.94		16.01		14.64
8	$1d_{3/2}$	23.66	$1d_{3/2}$	23.89	$2s_{1/2}$	20.13	$1d_{3/2}$	18.80
9		23.66		23.89	$1d_{3/2}$	21.35		18.80
10	$2s_{1/2}$	23.89	$2s_{1/2}$	24.04		21.35	$2s_{1/2}$	19.39
11	$1f_{7/2}$	29.64	$1f_{7/2}$	29.28	$1f_{7/2}$	24.19	$1f_{7/2}$	21.81
12		29.64		29.28		24.19		21.81
13		29.64		29.28		24.19		21.81
14		29.64		29.28		24.19		21.81
15	$2f_{5/2}$	34.55	$1f_{5/2}$	34.81	$2p_{3/2}$	28.76	$1f_{5/2}$	26.72
16		34.55		34.81		28.76		26.72
17		34.55		34.81	$2f_{5/2}$	30.50		26.72
18	$2p_{3/2}$	34.94	$2p_{3/2}$	35.07		30.50	$2p_{3/2}$	27.56
19		34.94		35.07		30.50		27.56
20	$2p_{1/2}$	37.05	$2p_{1/2}$	37.44	$2p_{1/2}$	31.47	$1g_{9/2}$	28.89
21	$1g_{9/2}$	38.74	$1g_{9/2}$	38.20	$1g_{9/2}$	32.36		28.89
22		38.74		38.20		32.36		28.89
23		38.74		38.20		32.36		28.89
24		38.74		38.20		32.36		28.89
25		38.74		38.20		32.36	$2p_{1/2}$	29.68
26	$1g_{7/2}$	45.06	$1g_{7/2}$	45.32	$2d_{5/2}$	37.34	$1g_{7/2}$	34.41
27		45.06		45.32		37.34		34.41
28		45.06		45.32		37.34		34.41

Here, 'a' is the level density parameter. The value of $\sigma = A/8$ is used in the present calculation. In Fig. 6 we show the variation of σ_n^2, σ_p^2 and σ^2 with excitation energy determined from the microscopic theory for the case of ^{60}Ni

nucleus. The results from the macroscopic theory is also shown for comparison. We see the role of the nuclear structure effect is quite apparent and will be discussed in the following section.

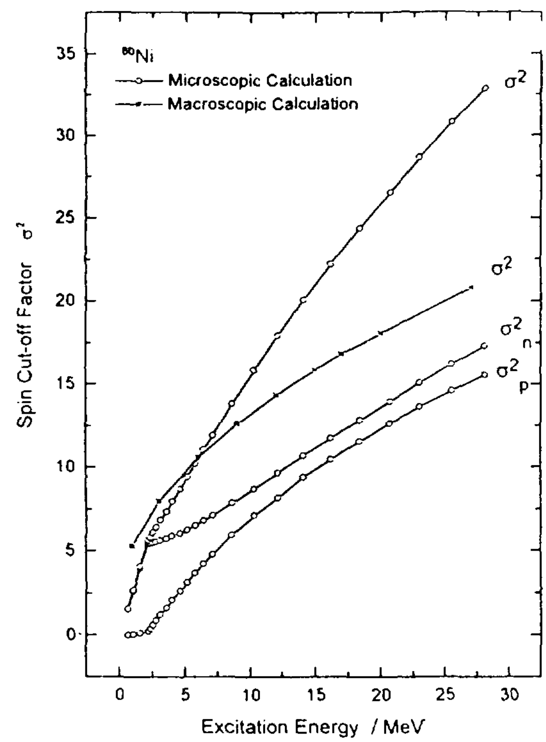

Fig. 6 The spin cut-off factor for ^{60}Ni

3 Result and Discussion

In this section, we present comparisons of the level densities and spin cut-off factors from the microscopic theory and experiments for $^{24}_{12}Mg$, $^{26}_{13}Al$, $^{28}_{13}Al$, $^{28}_{14}Si$, $^{29}_{14}Si$, $^{32}_{16}S$, $^{33}_{16}S$, $^{38}_{18}Ar$, $^{41}_{20}Ca$, $^{56}_{26}Fe$, $^{60}_{27}Co$, $^{60}_{28}Ni$ and $^{63}_{29}Cu$. The results of the comparison are shown in Figs. 7–9. Two different sets of single particle levels are used in the theoretical calculations, one set is due to Seeger and Parisho[15] and the other to Nilsson and coworkers[12].

The initial values of Δ_n and Δ_p for the even-even nuclei were taken from the literature[11] and then adjusted to improve the fit to the data. The final values of the pairing parameters for doubly even nuclei given in Table 2 were used for both the Seeger and Nilsson single particle levels.

Table2 Proton and Neutron Pairing Parameters Used in the Level Density Calculation

Nucleus	Δ_p / MeV	Δ_n / MeV
$^{24}_{12}Mg$	2.35	2.15
$^{28}_{14}Si$	2.28	2.18
$^{32}_{16}S$	2.50	2.39
$^{38}_{18}Ar$	2.06	2.20
$^{56}_{26}Fe$	1.45	1.08
$^{60}_{28}Ni$	0.91	0.86

The level density of the odd A nuclei as obtained using the procedure outlined in section 2.3. For example the level density of ^{33}S was obtained from the level density of ^{32}S by shifting the energy scale by Δ_n= 2.39 MeV. A similar level density was obtained by calculating $\Delta_n^{odd}(0)$ from Eq.(11) and doing the calculation for ^{33}S.

As can be seen from Figs. 7 — 19, the overall agreement between the experimental level densities and the microscopic theory with pairing is very good for both the Seeger and the Nilsson single fermion levels. The agreement for most nuclei is slightly better for the Nilsson single particle levels, whereas in a few cases the agreement is better with the Seeger single particle levels. The role of the nuclear structure effects is not directly apparent in the level density plots in Figs. 7—19, for example the contributions of the neutrons and protons to the total level density are comparable for ^{56}Fe, whereas the neutrons make much larger contribution for ^{60}Ni. The reason for this is associated with the strong participation of the highly degenerate $1g_{9/2}$ single particle levels in the case of ^{60}Ni.

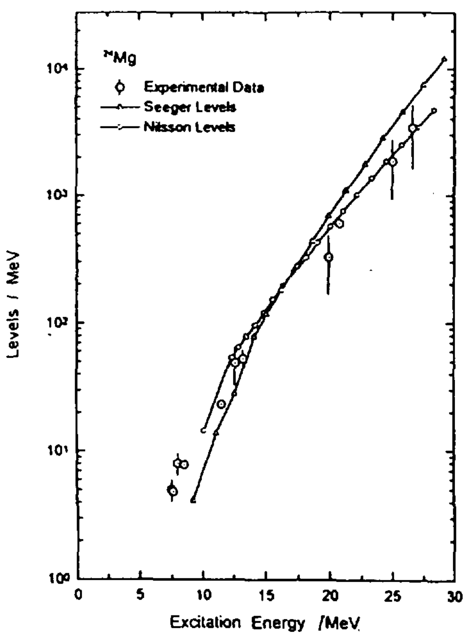

Fig.7 Comparison of the experimental level density with a microscopic theory for ^{24}Mg

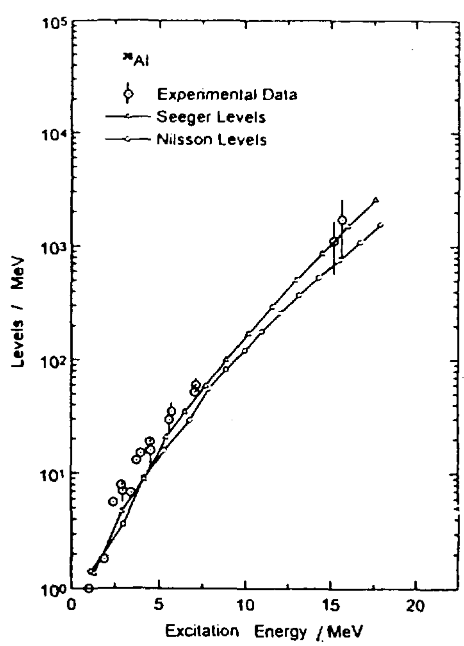

Fig.8 Comparison of the experimental level density with a microscopic theory for ^{26}Al

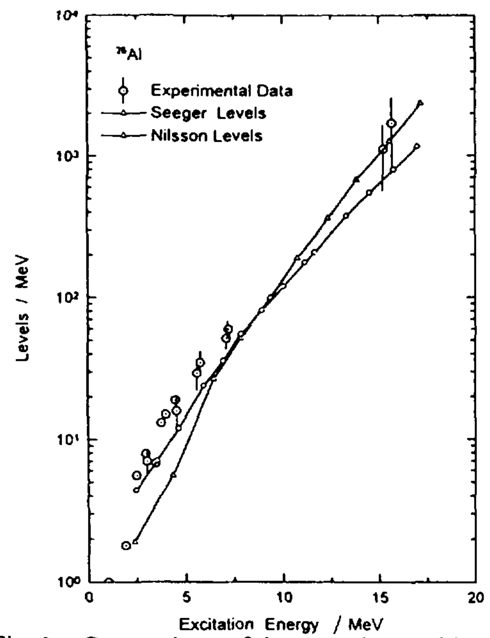

Fig.9 Comparison of the experimental level density with a microscopic theory for ^{28}Al

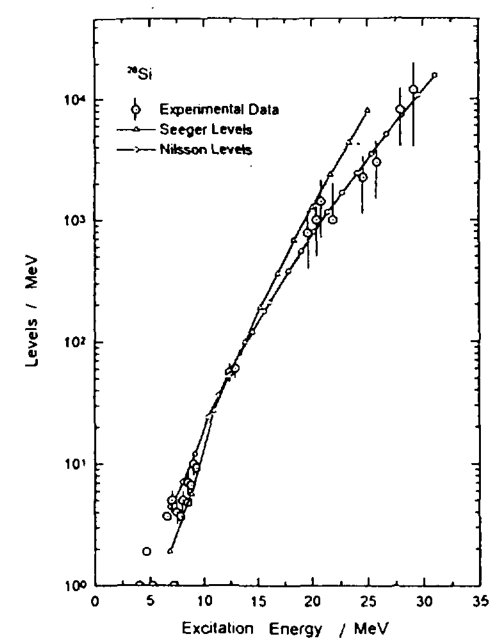

Fig.10 Comparison of the experimental level density with a microscopic theory for ^{28}Si

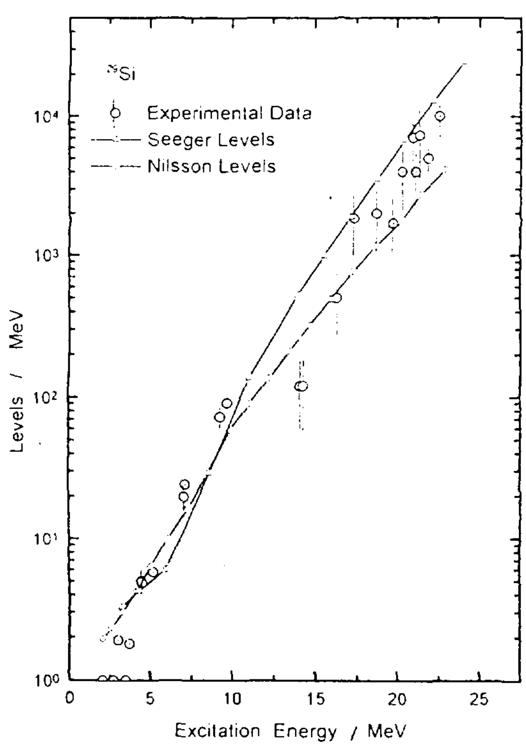

Fig.11 Comparison of the experimental level density with a microscopic theory for ^{29}Si

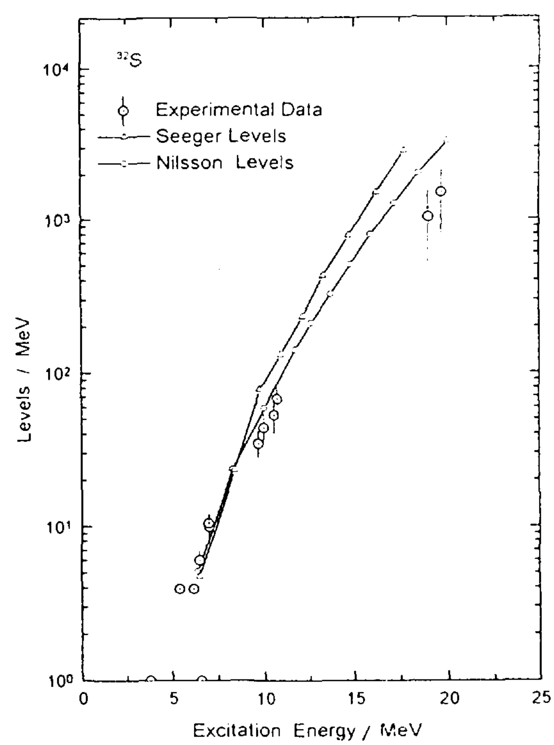

Fig.12 Comparison of the experimental level density with a microscopic theory for ^{32}S

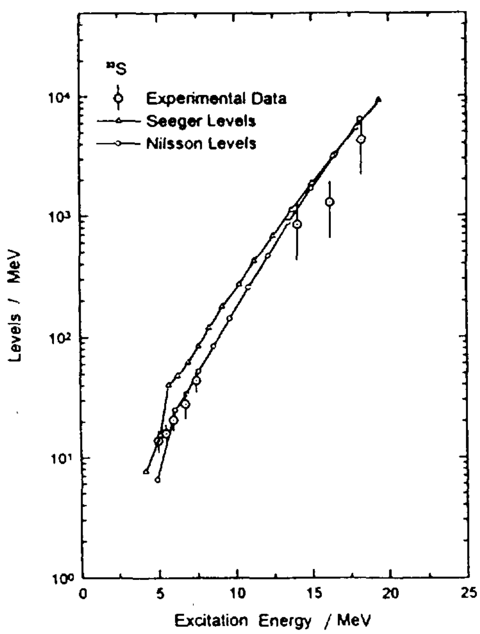

Fig.13 Comparison of the experimental level density with a microscopic theory for ^{33}S

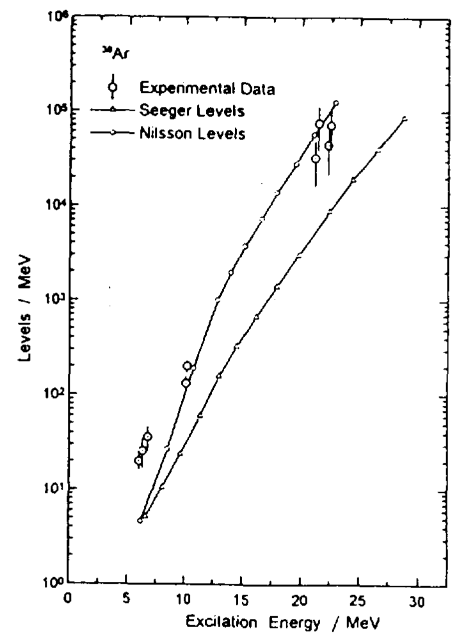

Fig.14 Comparison of the experimental level density with a microscopic theory for ^{38}Ar

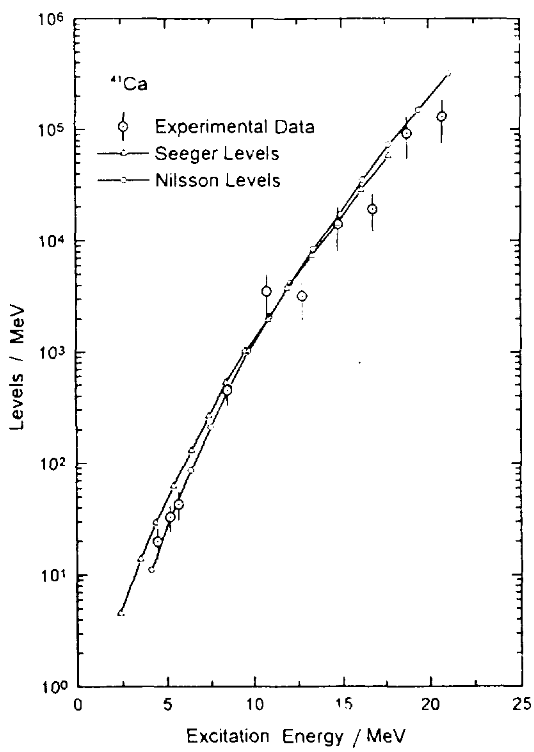

Fig.15 Comparison of the experimental level density with a microscopic theory for ^{41}Ca

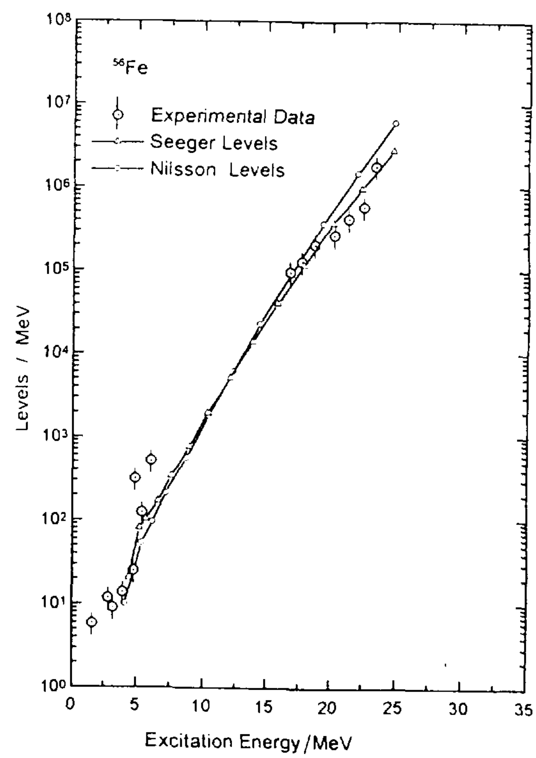

Fig.16 Comparison of the experimental level density with a microscopic theory for ^{56}Fe

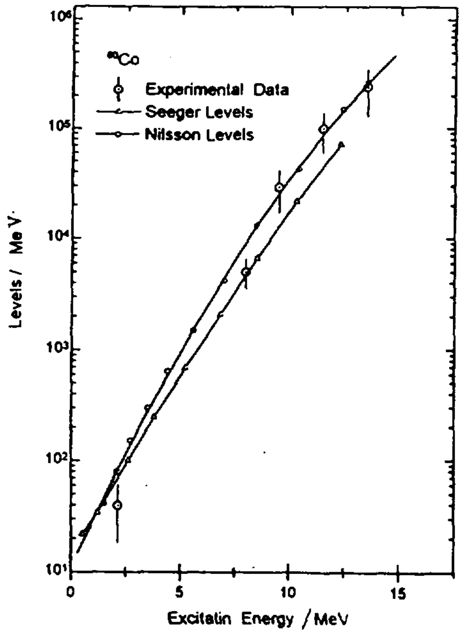

Fig.17 Comparison of the experimental level density with a microscopic theory for ^{60}Co

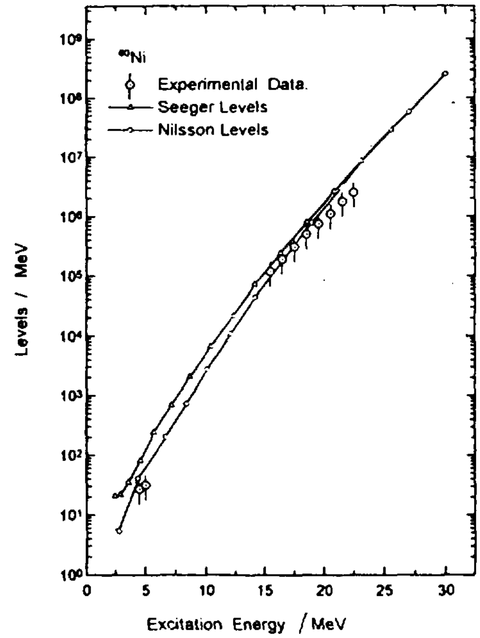

Fig.18 Comparison of the experimental level density with a microscopic theory for ^{60}Ni

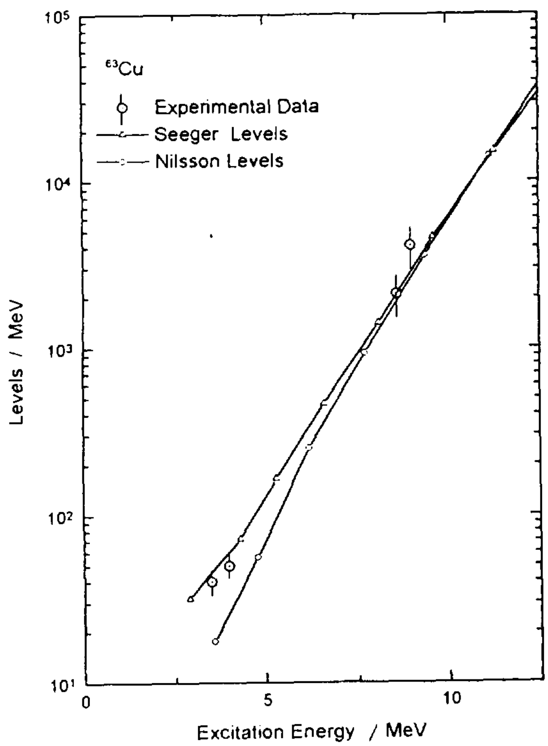

Fig. 19 Comparison of the experimental level density with a microscopic theory for ^{63}Cu

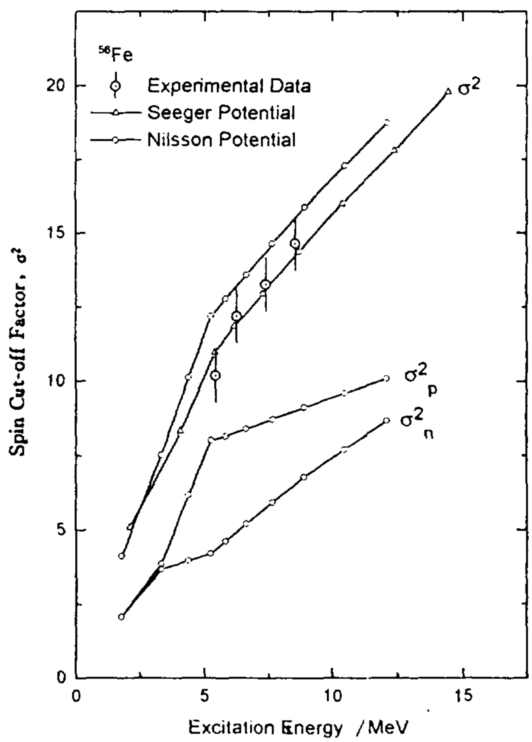

Fig.20 Comparison of the experimental spin cut-off factorwith a microscopic theory for ^{56}Fe

The calculated and measured values of the spin cut-off factor σ^2 are plotted in Fig. 20 for ^{56}Fe. The importance of the single particle shell structure is shown in this figure by the independent contributions of σ_n^2 and σ_p^2. It is interesting to note the proton contribution σ_p^2 dominates for ^{56}Fe, whereas the situation reverses for ^{60}Ni where the neutron contribution σ_n^2 dominates (see Fig. 6). The result that σ_p^2 is larger than σ_n^2 for ^{56}Fe is explained by the occupational probabilities for the various single particle levels. The enhancement in $\bar{\sigma}_p^2$ is mainly due to the large contribution from the $1f_{7/2}$ proton single particle levels. The addition of a few neutrons and protons in going from ^{56}Fe to ^{60}Ni completely reverses the importance of the roles of neutrons and protons. Now the $1f_{7/2}$ proton and neutron single particle levels are both nearly fully occupied and make only a minor contribution to σ^2. For ^{60}Ni, the $1g_{7/2}$ single particle levels have a sizable occupation for neutrons. Hence this level makes a major contribution to σ_n^2 resulting in a value of σ_n^2 for ^{60}Ni which is much higher than σ^2. The contribution of the higher angular momentum $1g_{9/2}$ single particle levels is evident also in the $\bar{\sigma}^2$ values for ^{60}Ni.

In summary, good agreement is obtained between expected and theoretical level densities and spin cut-off factors for several nuclei under investigation. The single particle levels of Seeger and Parisho and Nilsson et al were used in the microscopic theory which includes the nuclear pairing interaction.

Acknowledgment

We wish to acknowledge the staff and operating crew of the College of Science Computer Center for their assistance in providing the computer time.

References

[1] Weidenmuller HA. Phys.Lett.10,331(1964)
[2] Baba H Nucl. Phys. A159,162(1970)
[3] Glatz F et al., Z.Phys. A303,239(1981)
[4] Mustafa M.G., et al., Phys.Rev.C45,1078.(1992)
[5] Bardeen, J.Copper, L.N. and Schnieffer J.R. R. Phys. Rev.164 162(1957)
[6] Kargat et al., "*9th* Int. Sym. On Capture Gamma-Ray Spectroscopy" to be published(1996)
[7] Behkami et al. Bull. Am. Phys. Soc. Vol. 41 No.5 AD13(1996)
[8] Behkami A.N., Huizenga J. R. Nucl.Phys.A217 78(1973)
[9] Behkami A.N., Najafi S.I. J. Phys.G.Nucl.Part. 6 685(1980)
[10] Behkami A.N., Kargar Z. J. Phys.G.Nucl.Part. 18 1223(1992)

[11] Audi G. Wapstra A. H. Nucl.Phys. A566 1(1993)
[12] Nilsson et al., Nucl. Phys. A131 1(1961)
[13] Huizenga J.R., Rossner H.H., Schroder W.U. J. Phys. Soc. JPN. 54 257(1985)
[14] Gilbert A., Can. J. of Phys. 43 1446(1965)
[15] Seeger A., Perisho R.C. Nucl. Phys. A 238 491(1975)
[16] Iljinov A.S., Mebel M.V. Nucl. Phys. A543 517(1991)
[17] Beckerman M Nucl. Phys. A278 333(1975)
[18] Grimes et al., Phys. Rev. Vol. 27, No.6 2893(1983)
[19] Fischer R., Traxler G., Uhi.M., Vonach H. Phys. Rev. C30 No.1 72(1984)

n+^{239}Pu Coupled Channel Optical Model and DWBA Calculations

CN9800584

Wang Shunuan

(China Institute of Atomic Energy, P.O. Box 275-41, Beijing 102413)

Abstract

n+^{239}Pu coupled channel optical model and DWBA calculations are performed by using ECIS95 and PRECIS[1] codes. The calculated results of total cross section, reaction cross section, shape elastic and direct inelastic scattering cross sections and angular distributions getting from different methods are analyzed and compared. The different calculated methods used are reviewed.

It is now well known that the shape elastic and direct inelastic scattering cross sections and their angular distributions are one of the most important data in the evaluated data files for neutron induced reactions in the energy range between 1 MeV and 20 MeV in the fields of nuclear science and technology. For the theoretical calculations of neutron with incident energy in the range of 1–20 MeV on nuclei that are strongly deformed such as rare earths and actinides, the coupled channel optical model is usually used. As a whole, there are two methods to perform such coupled channel optical model calculations from the physics and mathematics point of view, one is the conventional matrix method called standard coupled channel (SCC) method, the other is ECIS (sequential iteration of coupled equations) method[2] which provides an alternative to the former. The distorted-wave Born approximation (DWBA) method calculations can be understood as a simple iterative expansion of the Lippmann-Schwinger equation in powers of the potential. It is thus a good approximation only when the coupling is weak.

In this work, taking n+^{239}Pu (E_n=1–20 MeV) as an example, mentioned above three methods (SCC, ECIS and DWBA) in two codes (ECIS95 and PRECIS) are used to calculate total cross section σ_t, reaction cross section σ_R, shape elastic scattering cross section σ_{se}, direct inelastic scattering cross section σ_{in}, shape elastic scattering angular distribution $\sigma_{se}(\theta)$, direct inelastic scattering angular distribution $\sigma_{in}(\theta)$ of each coupled isolated levels, respectively. The calculated results are analyzed and compared, and the methods used in each of the calculations are reviewed. In the whole calculations the compound nuclear contributions are not taken into account. The optical model parameters are chosen from the parametres of Madland[3] for actinides provided in code PRECIS.

The ^{239}Pu level (coupled each other) scheme[4] adopted is shown in Table 1.

Table 1 The ^{239}Pu levels (coupled each other) scheme

Energy / MeV	Spin Parity
0.00000	$1/2^+$
0.00786	$3/2^+$
0.05728	$5/2^+$
0.07571	$7/2^+$
0.16376	$9/2^+$
0.19400	$11/2^+$

The rotational model is used in the calculations. The deformed parameters β_λ with the static deformation of multipolarity λ=2 and 4 are considered and used as β_2=0.216, β_4=0.06.

From the comparison of the calculated results it can be concluded that for the whole neutron incident energies between 1 MeV and 20 MeV, the calculated σ_t, σ_R, σ_{se}, σ_{in} for the first a few levels coupled by using SCC and ECIS methods are in good agreement with each other. The calculated σ_t, σ_R, σ_{se}, and σ_{in} of levels $3/2^+$, $5/2^-$, $7/2^-$, $9/2^-$, $11/2^+$ for n+^{239}Pu at E_n=20 MeV and 5 MeV by using three different methods are shown in Table 2.

Table 2 The comparison between calculated σ_t, σ_R, σ_{se}, and σ_{in} for n+^{239}Pu (E_n=20 MeV and 5 MeV) by using DWBA, ECIS, SCC methods

Cross Section (mb)	DWBA		ECIS		SCC	
E_n / MeV	20	5	20	5	20	5
σ_t	6334.17	7981.16	6173.68	7234.64	6167.74	7236.04
σ_R	2444.52	2900.89	2776.77	3413.42	2771.25	3405.30
σ_{se}	3889.65	5080.27	3396.91	3812.22	3396.49	3830.74
σ_{in} (3/2+)	321.49	545.84	152.11	138.95	151.30	138.44
σ_{in} (5/2+)	482.26	817.04	228.15	212.15	227.14	212.16
σ_{in} (7/2+)	31.67	50.16	29.35	35.61	33.75	36.40
σ_{in} (9/2+)	39.55	65.56	44.78	77.68	47.00	79.05
σ_{in} (11/2+)	2.62	2.90	7.37	15.01	67.89	30.06

From Table 2 it can be discussed as the following: 1. In general, for σ_t, σ_R, σ_{se} calculated by SCC and ECIS methods, there are almost the same with high accuracy, but there are about 10% difference compared with those calculated by DWBA method, and the results calculated by DWBA method are always higher than the other two. So much differences between DWBA method and other two methods are actually due to the difference between the spherical optical model and the deformed optical model in σ_t, σ_R, σ_{se} calculations. In DWBA the distorted wave is calculated by using the spherical optical potential, and in inelastic scattering calculations the coupling between elastic and inelastic channels is taken into account by the first Born approximation, but in elastic scattering calculation, the coupling from inelastic channels is not taken into account. 2. For $\sigma_{in}(3/2^+, 5/2^+)$ calculated by SCC and ECIS methods are almost the same also with high accuracy, but for the results calculated by DWBA are almost twice for E_n=20 MeV and four times for E_n=5 MeV of the one calculated by SCC and ECIS methods. 3. For $\sigma_{in}(11/2^+)$ calculated by DWBA and ECIS methods at E_n=20 MeV are smaller than the one calculated by SCC method by a magnitude of order. From the above analysis it occurred to us that it was safe to use ECIS to calculate σ_t, σ_R, σ_{se} and σ_{in} for the first a few excited levels only for rare earths and actinides nuclei calculations in the incident neutron energies range of 1—20 MeV. Generally speaking, DWBA method presents much higher results for the first several levels, then it presents much lower results for the last one.

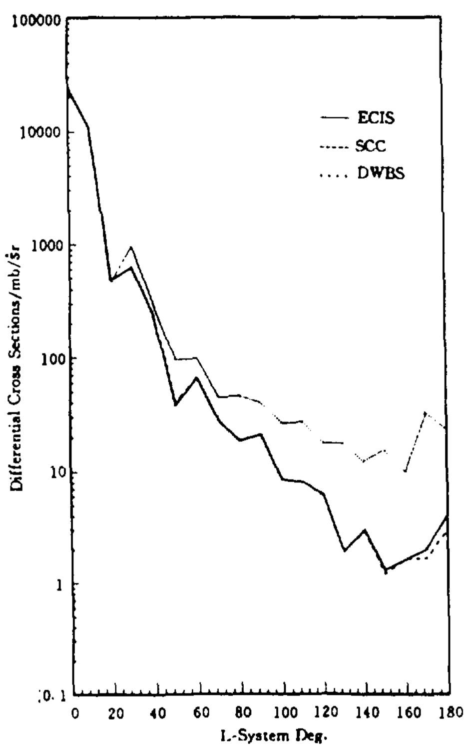

Fig.1 Elastic Scattering Angular Distribution n+^{239}Pu (E_n=20 MeV) ($1/2^+$)

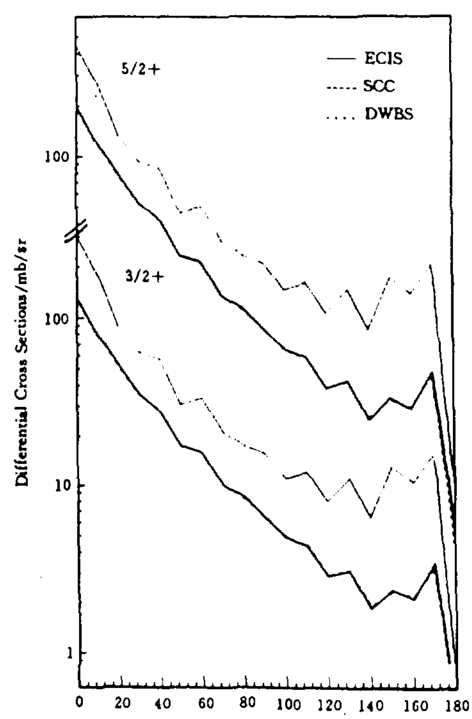

Fig.2 Scattering Angular Distribution n+^{239}Pu (E_n=20 MeV) ($3/2^+$ and $5/2^+$)

We take the calculated results at E_n=20 MeV as an example to analyze the angular distributions as follows. The $\sigma_{se}(\theta)$ calculated is shown in Fig.1. The $\sigma_{in}(\theta)$ calculated for $3/2^+$, $5/2^+$, $7/2^+$, $9/2^+$, $11/2^+$ are shown in Fig.2—4, respectively. In those Figs., the solid, dashed, and the dotted lines stand for the ECIS , SCC and DWBA methods calculations, respectively. The Fig.1 shows clearly that the $\sigma_{se}(\theta)$ calculated by ECIS and SCC methods are almost the same in the whole angular range, but the dotted line calculated by DWBA method is quite different from the other two at 20°—180°. It is much higher than the others. In Fig.2 is shown that $\sigma_{in}(\theta)$ at $3/2^+$ and $5/2^+$ states almost presents the same behavior and same magnitude contributions. The calculated results by using DWBA method are still much higher than the other two. The $\sigma_{in}(\theta)$ for $7/2^+$ and $9/2^+$ (seeing from Fig.3) presents same behavior and same magnitude contributions for three different methods. The $\sigma_{in}(\theta)$ for $11/2^+$ state shown in Fig.4 point out that even the absolute values of $\sigma_{in}(\theta)$ are much lower, but they are quite different from each other, the solid line and dotted line are much lower than the dashed line. The calculated $\sigma_{se}(\theta)$ and $\sigma_{in}(\theta)$ for $3/2^+$, $5/2^+$, $7/2^+$, $9/2^+$, $11/2^+$ at E_n=5 MeV have almost the same behavior analysis. The above analysis reminds us that if one needs to calculate the higher excitation states direct inelastic scattering angular distributions, it is better to use the SCC method to keep the correctness although the calculations need much more computer time and cost a lot.

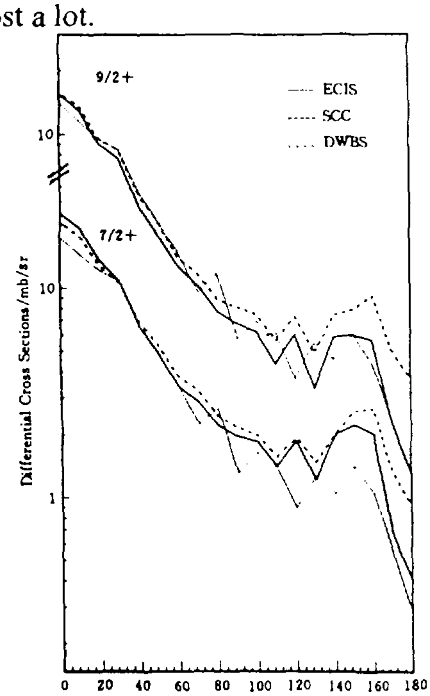

Fig.3 Scattering Angular Distribution $n+^{239}Pu$ (E_n=20 MeV) ($7/2^+$ and $9/2^+$)

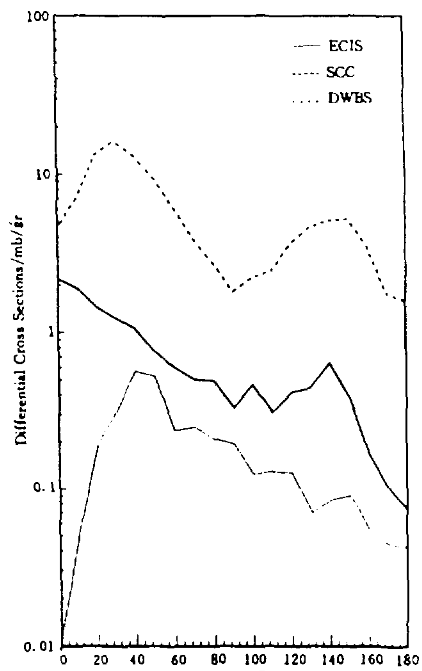

Fig.4 Scattering Angular Distribution $n+^{239}Pu$ (E_n=20 MeV) ($11/2^+$)

In the last comparison it could be point out in generally as the following. First of all, the DWBA method could not give reasonably various cross sections and angular distributions calculations in the incident neutron energies range of 1—20 MeV for rare earths and actinides nuclei which are strongly deformed and the coupling among the levels is not so weak. In addition, due to the direct inelastic scattering influence on the shape elastic scattering by using DWBA method is not taken into account, thus σ_t, σ_R, σ_{se} calculated by DWBA method have several hundreds mb differences from that of the other two methods (seeing from Table 1). Second, it stands to reason that using ECIS method to calculate various cross sections and angular distributions for the first a few excited levels for rare earths and actinides nuclei in the incident neutron energies range of 1—20 MeV, the reasonable results could be obtained, and the computer time is very much shorter than the one spent in the calculation by using SCC method. If the direct inelastic scattering contributions of the higher excited levels need to be calculated it is safe to use SCC method.

References

[1] Carlson. Workshop on Nuclear Reaction Data and Nuclear Reactors- Physics, Design and Safety, 15 Apr. —17 May 1996, Miramare Trieste, Italy, The Optical Model ECIS95, H4. SMR/921-3

[2] J.Raynal. Notes on ECIS94-Note, CEN-N-2772(1994)

[3] Madland and Young PG. International Conference on Neutron Physics and Nuclear Data for Reactors and Other Applied Purposes, 1978 Sep. 25-29, Harwell, OECD/NEA UKAEA, P.49(1978)

[4] Su Zongdi, Zhang Limin, Sun Zhengjun. CENPL-DLS,1994

CN9800585

Analyses of d+^{16}O and p+^{19}F Reaction

Han Yinlu Shen Qingbiao
(China Nuclear Data Center, CIAE)

Zhang Zhengjun Sun Xiuquan
(Department of Physics, Northwest University, Shaanxi)

Abstract

The nuclear data of d+^{16}O reaction at incident energies spanning 0.1 to 35.0 MeV were obtained by calculation with optical model, distorted wave Born approximation, preequilibrium nuclear reaction and Hauser-Feshbach theory. The cross sections of d+^{17}F and p+^{17}F reaction were predicted.

Introduction

The production and use of unstable radioactive nuclear ion beams are of considerable interest for astrophysical, nuclear physics studies and some nuclear engineering designs. Many laboratories have made efforts in producing the secondary radioactive beams for nuclear physical research[1-6]. The theoretical predictions of the nuclear data for secondary reactions have important reference value to experimental scientists.

According to the calculations and analyses of cross sections of d+^{16}O and p+^{19}F reactions, the cross sections of d+^{17}F and p+^{17}F reactions are predicted in this paper.

1 Calculation of the reaction d+^{16}O

The reaction d+^{16}O in the incident deuteron energy region of 0.1－35 MeV was calculated with optical model, Hauser-Feshbach theory, exiton model of preequilibrium nuclear reaction and distorted wave Born approximation. The charged particle induced reaction code CUNF[7], the searching optimal charged particle optical potential parameter code APCOM[8] and the distorted wave Born approximation code DWUCK[9] were used in our calculation.

Based on the experimental reaction cross sections of d+^{12}C and elastic scattering angular distributions of d+^{12}C, d+^{14}N and d+^{16}O reactions[10-13], a set of optimum deuteron optical potential parameters up to 35 MeV was obtained with code APCOM as follows:

$$V = 122.8750 - 0.01244E - 0.04392E^2 + 24.0(N-Z)/A + 0.006295Z/A^{1/3}$$

$$W_s = \max\{0, 5.2214 - 0.008095E\}$$

$$U_{so} = 7.0$$

$$r_r = 0.9046, \quad r_s = 1.5435, \quad r_{so} = 1.64, \quad r_c = 1.6338$$

$$a_r = 0.8549, \quad a_s = 0.7854, \quad a_{so} = 0.81$$

The calculated reaction cross sections of d+^{12}C reaction and elastic scattering angular distributions of d+^{12}C, d+^{14}N and d+^{16}O reactions with this set of optical potential parameters are shown in Figs.1 and 2, which fit the experimental data.

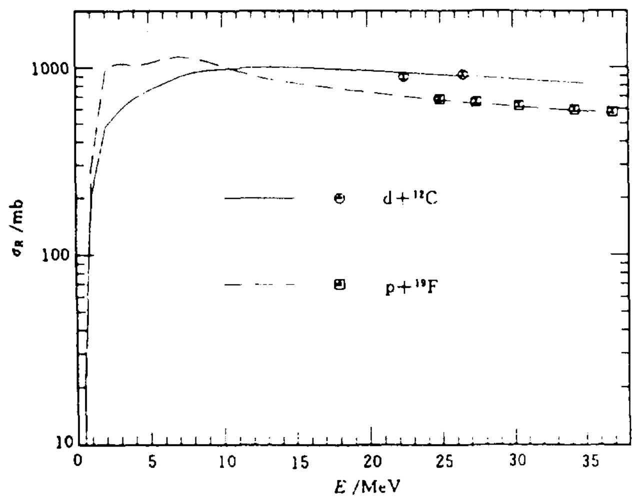

Fig.1 The reaction cross sections for d+^{12}C and p+^{19}F reactions

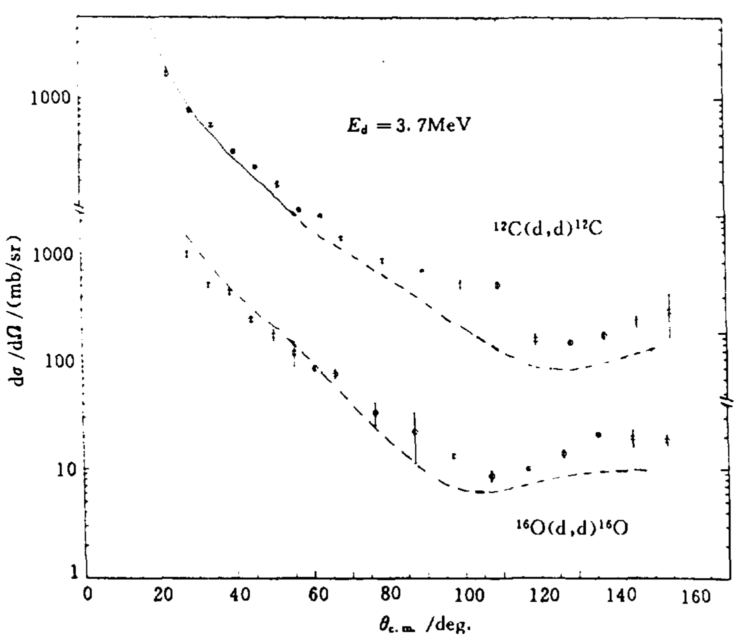

(a)

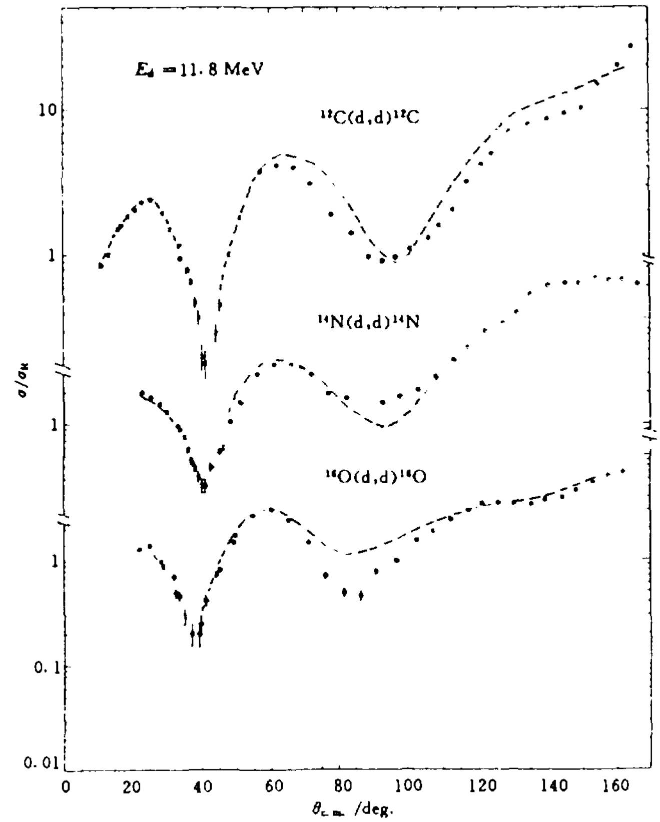

(b)

Fig.2 The elastic differential cross sections of deuteron reaction for ^{12}C, ^{14}N and ^{16}O

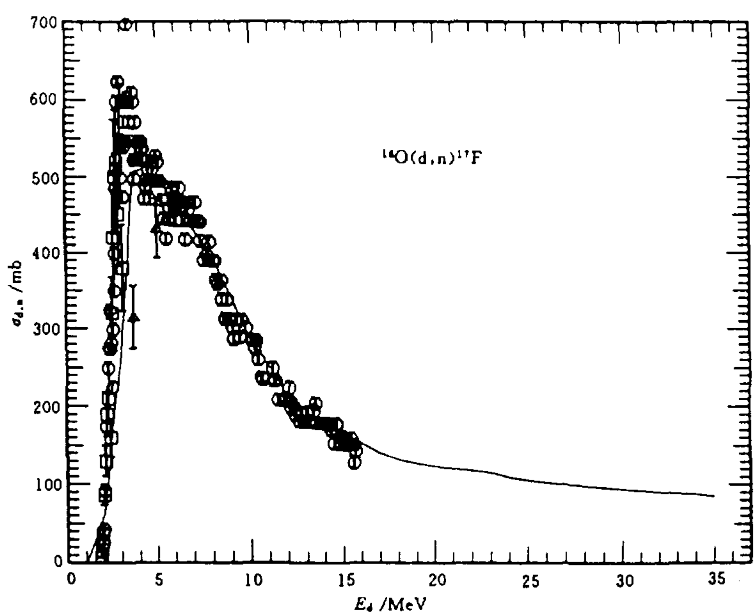

Fig.3 The cross sections of the $^{16}O(d,n)^{17}F$ reaction

The $^{16}O(d,n)^{17}F$ reaction is shown in Fig.3. The calculated results are agreement with experimental data for $E_d \geqslant 4.0$ MeV, while for $E_d < 4.0$ MeV, the calculated values are smaller than the experimental data. The theoretical calculated results are reasonable. The calculated discrete level (d,p_0), (d,p_1) and (d,p_2) angular distributions of d+^{16}O reactions at different energy are given in Fig.4. The calculated values are in agreement with experimental data, except at back angles. The experimental data of Figs.3 and 4 were taken from EXFOR.

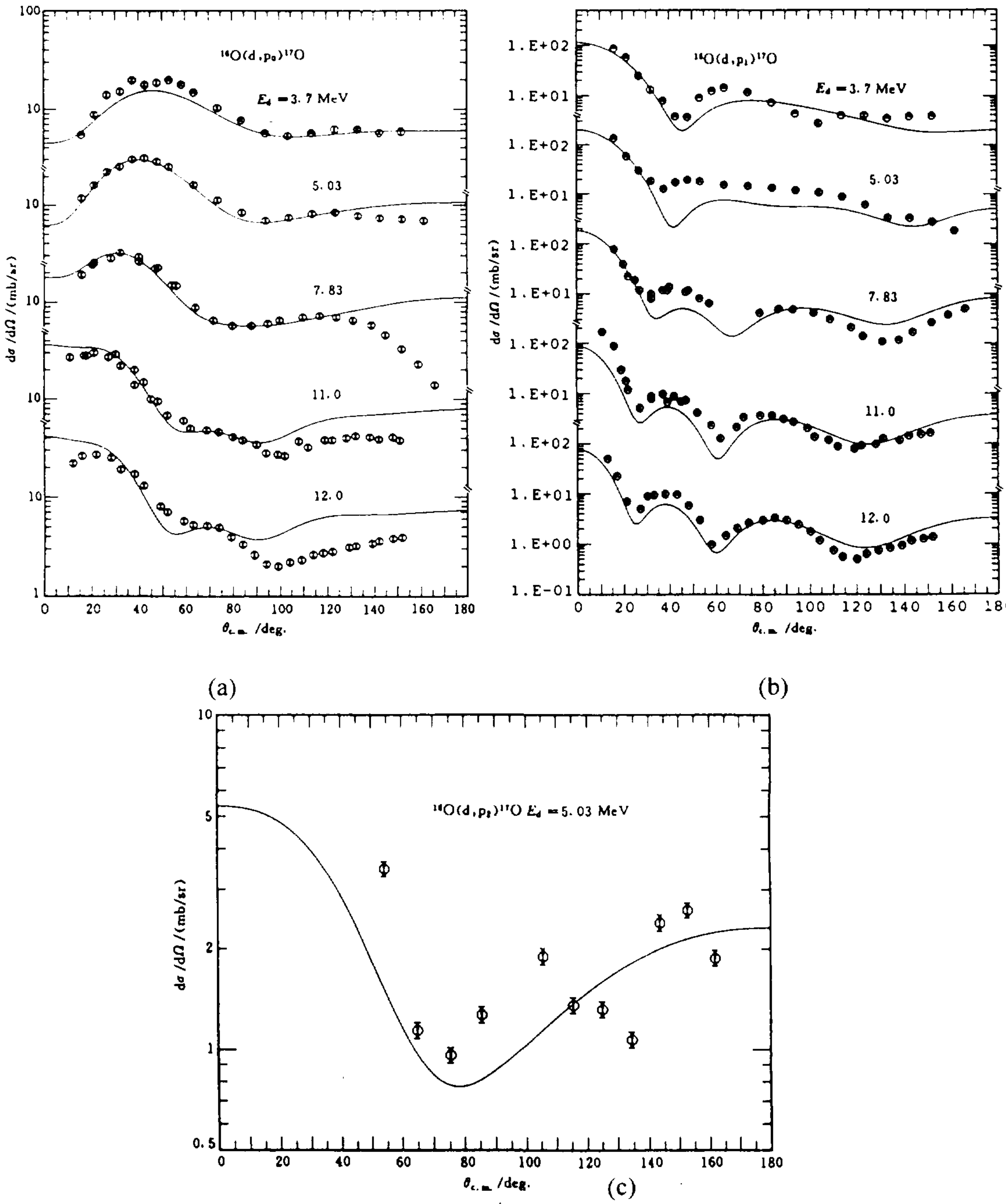

Fig.4 The discrete level angular distributions of $^{16}O(d,p)^{17}O$ reaction

Besides above results, the cross sections for which there is no experimental data are predicted for d+^{16}O reactions. The calculated values are shown in Fig.5. The ^{17}F radioactive beams were produced through ^{16}O(d,n)^{17}F reaction. Because the cross section of ^{16}O(d,n)^{17}F reaction is large and reaction channel is open at incident energy 1.5 MeV, this reaction is feasible to get the ^{17}F radioactive beam.

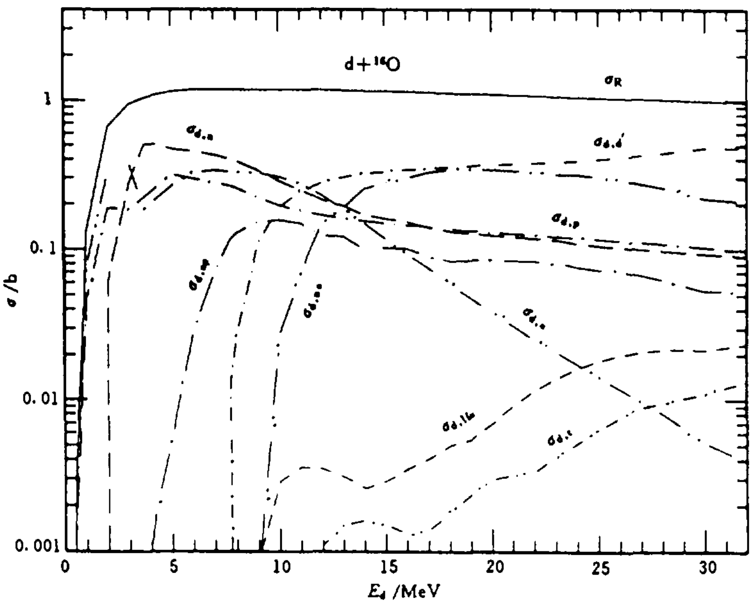

Fig.5 Cross sections of d+^{16}O reaction

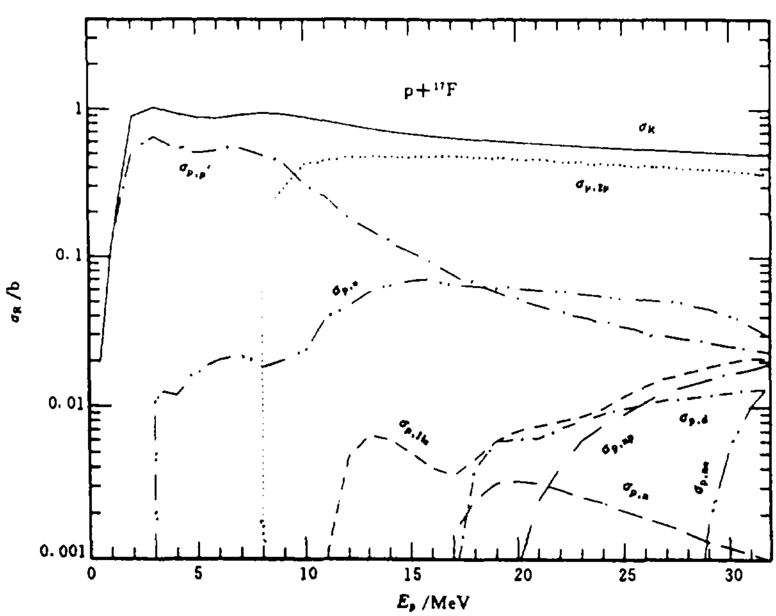

Fig.6 Cross sections of p+^{17}F reaction

The measurement of the secondary reaction induced by the radioactive ^{17}F is important. The cross sections of the reaction d+^{17}F in the incident deuteron energy region 0.5—30 MeV were calculated (Fig.6). When the incident deuteron energy is less than 1.5 MeV, the (d,p), (d,2p), (d,α) and (d,n) channels are open. The ions ^{15}O, ^{17}O, ^{18}F and ^{18}Ne may be detected.

2 Prediction of the Cross Sections of Reaction p+^{17}F

Based on the experimental reaction cross sections of p+^{19}F, a set of optimum proton optical potential parameters up to 38 MeV was obtained. The theoretical calculated results with this set of optical potential parameters are shown in Fig.1, which fit the experimental data[14]. With this set of parameters, the cross sections of reaction p+^{17}F were predicted. The calculated results were shown in Fig.7. When the incident proton energy is less than 10 MeV, the (p,p'), (p,α) and (p,2p) channels are open only. The cross sections of the other channels are less than 20 mb for energy E_p <30 MeV. The angular distributions of all reaction channels of p+^{17}F reactions are calculated in this work.

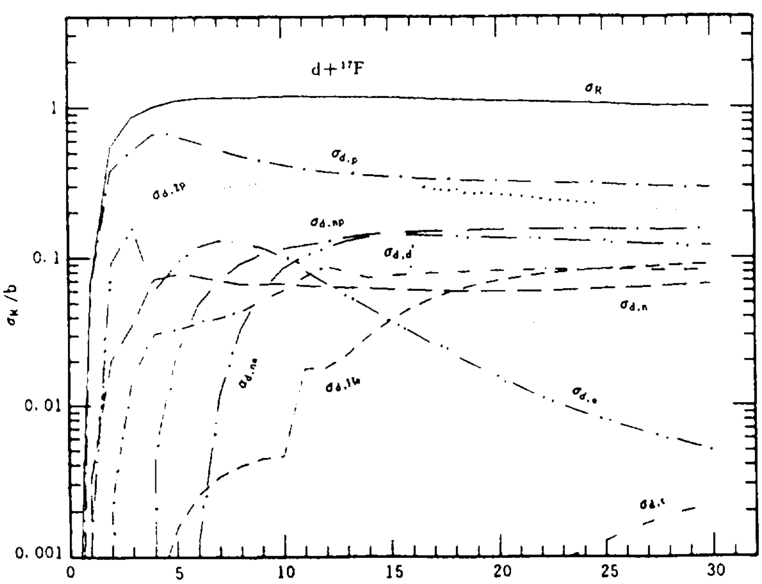

Fig.7 Cross sections of d+^{17}F reaction

3 Summary

The various nuclear data of the reactions d+^{16}O and p+^{19}F in the incident particle energy region 0.1—35 MeV were obtained with optical model, Hauser-Feshbach theory, exiton model of preequilibrium nuclear reaction and distorted wave Born approximation. The calculated results agree with the experimental data. The nuclear data for $d+^{17}F$ and $p+^{17}F$ reactions at some incident energies, for which there is no experimental data, were also reasonably predicted. The calculated results show that the experimental measurement for $d+^{17}F$ reaction is more feasible than for $p+^{17}F$ reaction. These results have important reference value to experimental scientists.

References

[1] W.D.Myers, et al., Proc. First Int. Conf. on Radioactive Nuclear Beams. Singapore:World Scientific, 1990.

[2] Bai Xixiang, et al., Atomic Energy Sci. Technol.27,385(1993).

[3] Liu Weiping, et al., Atomic Energy Sci. Technol.27,391(1993).

[4] Shen Qingbiao, et al. Chin. J. Nucl. Phys., 17,60(1995.)

[5] Liu Weiping, et al., Phys. Rev. Lett., 77,611(1996).

[6] Han Yinlu, et al., Chin. J. Nucl. Phys., 19,103 (1997).

[7] Zhang Jingshang. The Charged Particle Induced Reaction Code CUNF. China Institute of Atomic Energy (unpublished).

[8] Shen Qingbiao et al., Commu. Nucl. Data Prog., 7,41(1992).

[9] P.D.Kunz. Distorted Wave Code DWUCK4. University of Colorado, USA (unpublised)

[10] W.Fitz, et al., Nucl. Phys., A 101, 449(1967).

[11] Huang Bingyin, et al., Conf. on Nucl. Phys., Shanghai, 1974.

[12] B.Wilkins B. G. IGO. Phys. Lett., 3, 48(1962).

[13] S.Mayo S. et al., Nucl. Phys., 62,393(1965).

[14] W.Bauhoff. Atom. Data Nucl. Data Tables, 35,429(1986).

CN9800586

Calculation of the (n,p) Reaction Cross Sections for Zinc Isotopes

Huang Xiaolong Lu Hanlin Zhao Wenrong

(China Institute of Atomic Energy, Beijing)

Abstract

A model calculation of (n,p) reaction cross sections for Zinc isotopes in the neutron energy range below 20 MeV is carried out with UNF code. The theoretical models are briefly described and a new set of the neutron optical model potential parameters for natural Zinc is given. The results of the calculation are compared with the experimental data and a good agreement is obtained.

Introduction

Zinc is a useful nuclear material and has five isotopes with mass numbers of 64, 66, 67, 68 and 70 in its natural element. The (n,p) reaction cross sections for Zinc are very useful in fission and fusion reactors, especially the $^{64}Zn(n,p)^{64}Cu$ reaction. To do this calculation, a new set of optical parameters for neutron based on the total cross sections, nonelastic cross sections and elastic scattering angular distributions for natural Zn was studied firstly. Then this set of parameters was used to calculate the cross sections for the (n,p) reaction.

In the following sections we outlined the theoretical models and the global optical model calculation, and we also presented our results.

1 Codes and Parameters

The UNF code[1], which is based on the semi-classical theory of multi-step reaction processes, was employed in this work. It can be used to calculate the complete set of neutron nuclear data including reaction cross sections, neutron energy spectra and angular distributions, etc. and the output is in ENDF/B-6 format.

For the optical model potentials of neutron, a new set of parameters has been used. This new set of parameters have been obtained by using program APOM94[2], in which the optical potential parameters can be searched automatically.

The total cross sections, nonelastic cross sections and elastic scattering angular distributions for natural Zinc were adopted in the APOM94 calculation because these data for Zinc isotopes are very scarce. All of the measured data on the total cross sections and nonelastic cross sections in neutron energy range from 0.1 MeV to 20 MeV were collected and analysed. The elastic scattering angular distributions were adopted for some energy points too.

Based on the evaluated total cross sections, nonelastic cross sections and some elastic scattering angular distributions, a set of neutron optical potential parameters in neutron energy range from 0.1 MeV to 20 MeV was obtained and listed in Table1.

Table 1 Neutron optical model parameters for Zn isotopes

Optical Potential (MeV)	r / fm	a / fm
$V^{\text{real}} = 54.0230 + 0.3004E - 0.0165E^2 - 24\frac{(N-Z)}{A}$	1.1362	0.7392
$W_{\text{vol}}^{\text{imag}} = \max\{0,-2.6187 + 0.1162E - 0.0013E^2\}$	1.1870	0.4424
$V_{\text{s-o}} = 6.2$	1.1362	0.7392
$W_{\text{surf}}^{\text{imag}} = \max\{0.10.9778 - 0.0445E - 12\frac{(N-Z)}{A}\}$	1.3295	0.4178

With this set of parameters obtained above, the total cross sections and nonelastic cross sections of natural zinc were calculated, which are shown in Fig.1 and Fig.2, respectively. The calculated results are in good agreement with the experimental data. It means that this set of neutron optical potential parameters is reliable and can be used to calculate various reaction cross sections for zinc isotopes.

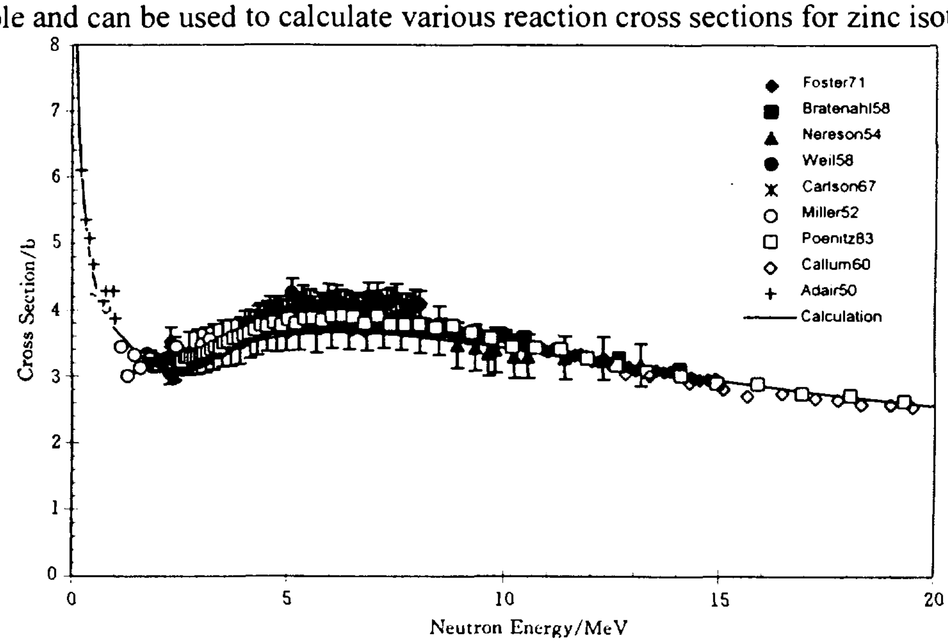

Fig.1 Total cross section for natural zinc

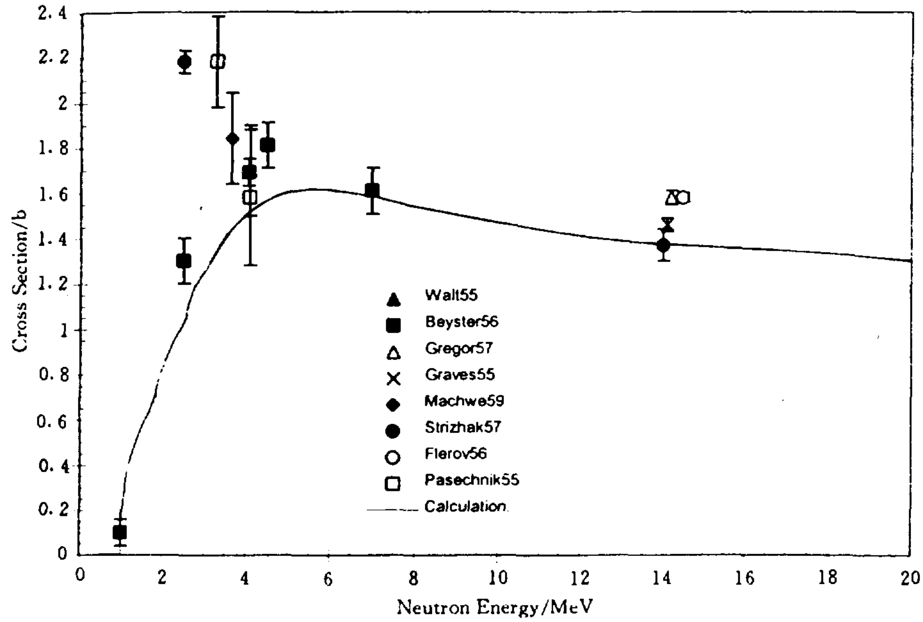

Fig.2 Nonelastic cross section for natural zinc

2 Results and Discussions

The theoretical calculation of (n,p) reaction cross sections for Zn isotopes has been done with the new set of neutron optical model potentials obtained above. The comparison between calculation and experiment were made for the reaction cross sections which have been measured, and shown in Figs. 3 to 5, respectively. The solid line in each figure represents the result of the present calculation.

(1) ^{64}Zn(n,p)^{64}Cu Reaction

It is well known that the effects of low energy neutrons in D(d,n) or T(d,n) neutron sources are very obvious and must be treated carefully in neutron activation measurement. If the reaction has a low threshold, the effects may be very serious, especially in 6 to 12 MeV range due to the influence of breakup neutrons, D-d neutrons and some other neutrons and above 15 MeV neutron energy region mainly owing to the influence of D-d neutrons.

^{64}Zn has the maximum proton production cross sections among Zn isotopes because it is the nucleus with the fewest neutrons. Fig.3 shows the calculated cross sections for the ^{64}Zn(n,p)^{64}Cu reaction, together with the relevant experimental data. The Lu Hanlin et al.'s[20] data from 4 to 11.4 MeV, Ikeda et al.'s[21] from 2 to 15 MeV, King et al.'s[22] from 2 to 5 MeV and Nemilov[23] from 7 to 9 MeV agree fairly well with the calculated cross sections. Meanwhile the Santry et al.'s[24] measurement shows about 5%—15% higher values. Their data were determined through detecting the β activities below 5 MeV and via counting 511 keV γ ray by NaI(Tl) spectroscopy above 5 MeV. It is possible that there exist some interfere reactions, such as $^{67}Zn(n,p)^{67}Cu$ and $^{68}Zn(n,\gamma)^{69m}Zn$ in their measurements, which made their data higher. Smith et al.'s[25] data in low energy are in good agreement with calculated ones, but in high energy are very low. Bormann et al.'s[26] high-energy data are very high, and Ghorai et al.'s[27] new measurement also shows higher values. The large discrepancy among the measurements may be due to the effects of the low energy neutrons in D(d,n) or T(d,n) neutron source. Because the $^{64}Zn(n,p)^{64}Cu$ reaction has a low threshold, this effect increases as the neutron energy increases.

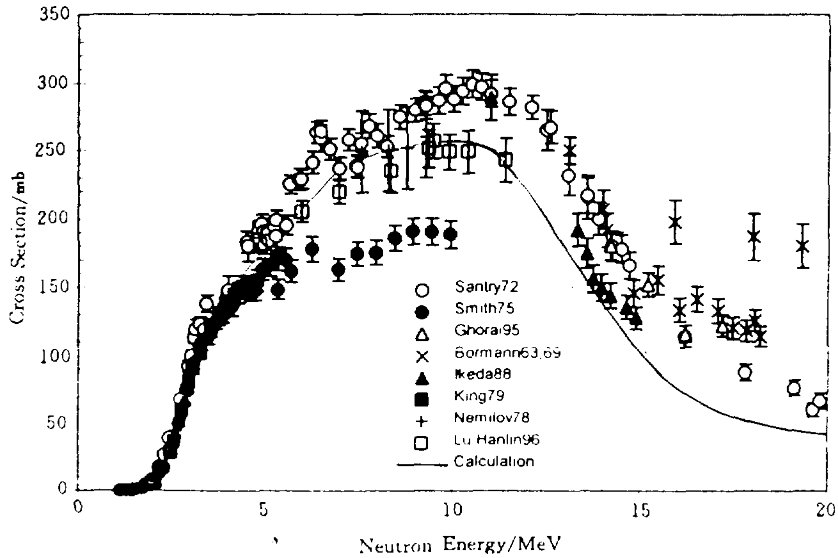

Fig.3 $^{64}Zn(n,p)^{64}Cu$ reaction cross section

(2) ^{66}Zn(n,p)^{66}Cu Reaction

The same situation can be seen in the $^{66}Zn(n,p)^{66}Cu$ reaction, which is shown in Fig.4. Smith et al.'s measurements agree with the calculation below 5 MeV. Above 5 MeV, however, their data are much lower than the calculation. Besides, in 14 MeV region, Viennot et al.'s[28] measurement is in agreement with the calculation too. In neutron energy range from 15 to 20 MeV, Bormann et al. and Ghorai et al.'s[29] measurements show higher values. Generally the measured cross sections of $^{66}Zn(n,p)^{66}Cu$ reaction are obtained by measuring the product of ^{66}Cu. Above 15 MeV, the contributions of $^{67}Zn(n,np)^{66}Cu$ and $^{67}Zn(n,d)^{66}Cu$ reactions are included and this might cause the measured data higher, although the abundance of ^{67}Zn is low (about 4.1%).

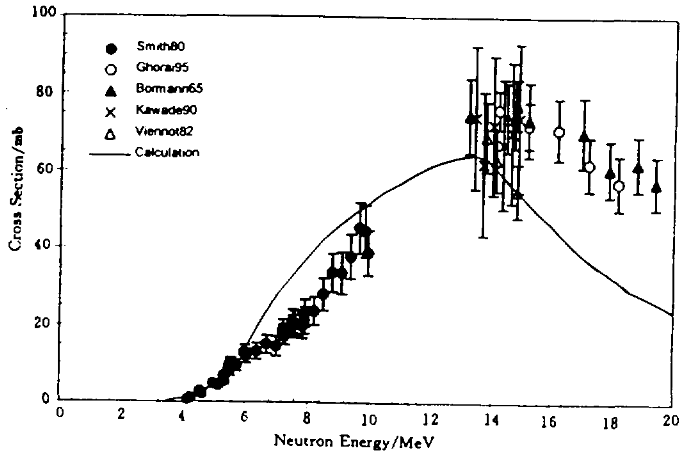

Fig.4 $^{66}Zn(n,p)^{66}Cu$ reaction cross section

(3) $^{67}Zn(n,p)^{67}Cu$ Reaction

The cross sections for $^{67}Zn(n,p)^{67}Cu$ reaction should be smaller than those of $^{64}Zn(n,p)^{64}Cu$ and $^{66}Zn(n,p)^{66}Cu$ reactions because of its nucleus with more neutrons. The calculation is shown in Fig.5. One can see that only Ikeda et al.'s data agree well with the calculation and Zhao Wenrong et al.'s[30] measurement shows higher values except 12.82 MeV, which agrees with the calculation. Above 15 MeV the calculation is lower, and some measurements, such as Ghorai et al.'s and Viennot et al.'s data show higher values. In experiment the $^{67}Zn(n,p)^{67}Cu$ reaction cross sections are determined by measuring activities of ^{67}Cu. Usually the contributions of $^{68}Zn(n,np)^{67}Cu$ and $^{68}Zn(n,d)^{67}Cu$ reactions are included and their effects are larger with the increase of neutron energy. That is why the measured results are considerable higher than the calculated.

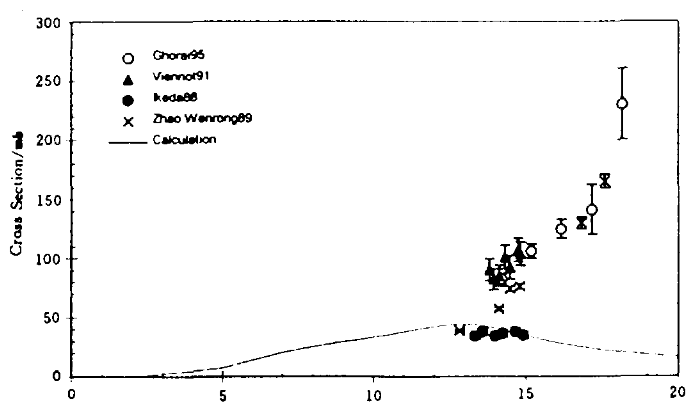

Fig.5 $^{67}Zn(n,p)^{67}Cu$ reaction cross section

3 Conclusions

Neutron activation cross sections for (n,p) reactions of Zinc isotopes have been calculated with UNF code in present work. The calculations were compared with the existing experimental data. Most of the calculated results are in good agreement with the relevant experimental data.

From Fig.3 to Fig.5, one can easily find that there are a few measurements for some (n,p) reactions and the existing data are still in large discrepancies. For example in neutron energy range from 5 to 12 MeV and 15 to 20 MeV, the existing data have a large amounts of discrepancies. Further experiments should be focused on these energy regions and more accurate measured data are necessary.

Since the pick-up mechanism in the preequilibrium reaction processes was introduced and the data for the low-lying discrete levels were considered in UNF code as well as a new set of neutron optical model potential parameters was used in this work, present calculation might be very successful. On the other hand, as it is very difficult to measure the activation cross sections for the (n,p) reactions above 15 MeV precisely because of their high sensitivities to neutrons with lower energy, the present calculation is very useful and may be used as the evaluated values.

References

[1] Zhang Jingshang. Fast Neutron Physics, Beijing, China, 201(1991); UNF program. Chinese Nuclear Data Center, Internal file(1995)

[2] Shen Qingbiao. APOM94 program. Chinese Nuclear Data Center, Internal file(1994)

[3] D.G.Foster, D.W.Glasgow, Phys. Rev. C3, 576(1971)

[4] W. P. Poenitz, J. F. Whalen, ANL-NDM-80, (1983)

[5] A. D. Carlson, H. H. Barschall, Phys. Rev. 158, 1142(1967)

[6] J. L. Weil. W. Jones, Phys. Rev. 110, 466(1958)

[7] G. J. Mc Callum et al., Nucl. Phys. 16, 313(1960)

[8] A. Bratenahl et al., Phys. Rev. 110, 927(1958)

[9] N. Nereson, S. Darden, Phys. Rev. 94, 1678(1954)

[10] D. W. Miller et al., Phys. Rev. 88, 83(1952)

[11] P. K. Adair, Phys. Rev. 77, 748(1950)

[12] M. Walt, J. R. Beyster, Phys. Rev. 98, 677(1955)

[13] J. R. Beyster et al., Phys. Rev. 104, 1319(1956)

[14] M.H.Mac Gregor et al., Phys. Rev. 108, 726(1957)

[15] V. I. Strizhak, AE 2, 68(1957)

[16] M. K. Machwe et al., Phys. Rev. 114, 1563(1959)
[17] E. R. Graves, R. W. Davis, Phys. Rev. 97, 1205(1955)
[18] N. N. Flerov, V. M. Talysin, AE 1, 155(1956)
[19] M. V. Pasechnik, 55GENEVA 2, 3(1955)
[20] Lu Hanlin et al., Private Communication
[21] Y. Ikeda et al., JAERI 1329, 1988; INDC(JPN)-142, 1990
[22] C. H. King et al., Nuclear Science 16, 71(1979)
[23] Y. A. Nemilov, Y. N. Trofimov, YK-27, 8(1977)
[24] D. C. Santry, J. P. Butler, Can. J. Phys. 50, 2536(1972)
[25] D. L. Smith, J. W. Meadows, Nucl. Sci. Eng. 58, 314(1975); Nucl. Sci. Eng. 76, 61(1980)
[26] M. Bormann et al., Z. Phys. 174, 1(1963); Nucl. Phys. 63, 438(1965); Nucl. Phys. A130, 195(1969)
[27] S. K. Ghorai et al., Ann. Nucl. Eng. 22, 11(1995)
[28] M. Viennot et al., MOH-5, 10(1982); Nucl. Sci. Eng. 108, 289(1991)
[29] K. Kawade et al., JAERI-M-90-171, 1990
[30] Zhao Wenrong et al., INDC(CPR)-16, 1989

CN9800587

Theoretical Calculation of Neutron Cross Sections for ^{176}Hf

Huang Xiaolong　　Lu Hanlin

(China Institute of Atomic Energy, Beijing)

Abstract

Neutron activation cross sections calculation for ^{176}Hf in the neutron energy below 20 MeV is carried out with UNF code. The calculated cross sections for (n,γ), (n,p), (n,α), (n,d), (n,t), (n,2n) and (n,3n) reaction are given. The results of the calculation are compared with the available experimental data and a good agreement is obtained. The calculation is also compared with the relevant evaluation data.

Introduction

Hafnium is an important material and its neutron activation cross sections are very useful in fission and fusion reactors. Cross section measurements for n+^{176}Hf have been made in several laboratories. But there are only a few measurements for (n,γ), (n,2n) reactions. Among these existing experimental data there are still large discrepancies, so the model calculation is needed.

To make this calculation, the UNF code which has been developed and documented in Ref.[1] was employed. The program can be easily used to calculate cross sections.

In the following discussions we outlined the theoretical models and also presented our results.

1 The Codes and Parameters

The UNF code based on the semi-classical theory of multi-step reaction processes was employed in present work. It can be used to calculate cross sections, double differential cross sections and output the data in ENDF/B-6 format.

The optical model potentials for n+^{176}Hf are taken from Ref.[2] and are given as follows:

$$V= 51.442860+0.154564E-0.020596E^2-24.0(N-Z)/A$$
$$W_s= \max\{0,9.100151-0.350662E-12.0(N-Z)/A\}$$
$$W_v= \max\{0,-1.215502+0.194002E+0.016019E^2\}$$
$$V_{so}=6.2$$
$$r_r=1.190571,\quad r_s=1.320246,\quad r_v=1.588077,\quad r_{so}=1.190571$$
$$a_r=0.578930,\quad a_s=0.668705,\quad a_v=0.361523,\quad a_{so}=0.578930$$

The cross sections for (n,γ), (n,p), (n,α), (n,d), (n,t), (n,2n) and (n,3n) reaction were calculated and the results are compared with the available experimental data and the evaluation data.

2 Results and Discussions

Comparisons between calculation and experiment were made for those reactions which have been measured. The reactions which have not been measured were also compared with the available evaluated data. Owing to the cross section for (n,^{3}He) reaction is very small (less than 0.1mb), it was not included in the present work. The comparison of calculation with experiment and/or evaluation for (n,γ), (n,p), (n,α), (n,d), (n,t), (n,2n) and (n,3n) reaction is shown in Figs.1—6, respectively. The line that is drawn in each of these figures represents the result of the present calculation. The results of these comparisons and discussions were given in the following.

(1) (n,γ) Reaction

For (n,γ) reaction, there is only one set of measurements which measured by H.Beer et al.[3] in neutron energy from 3.5 to 650 keV. The calculation is compared with this experiment and also the ENDF/B-6, JEF-2 and JENDL-3 evaluated data, which is shown in Fig.1. From Fig.1 one can notice that the present calculation is consistent with the measurements but higher than the data of ENDF/B-6 in low energy region.

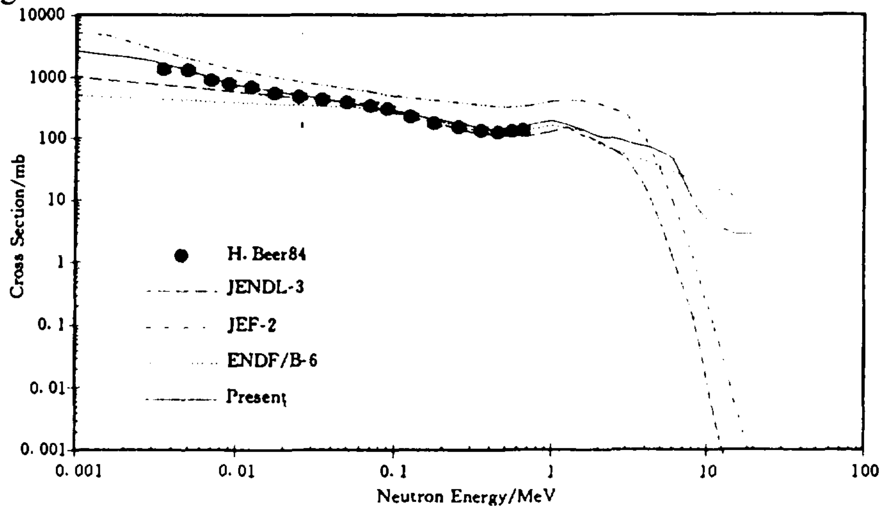

Fig.1 (n,γ) cross section for ^{176}Hf

(2) (n,p), (n,α), (n,d) and (n,t) Reaction

There are no experimental data for these reactions presently. And the evaluation data are available only for (n,p) and (n,α) reactions. So the comparison is carried out with the existing evaluation data for (n,p) and (n,α) reactions, which is shown in Figs.2 and 3, respectively. We also give the results of the present calculation for (n,d) and (n,t) reactions, which is shown in Fig. 4.

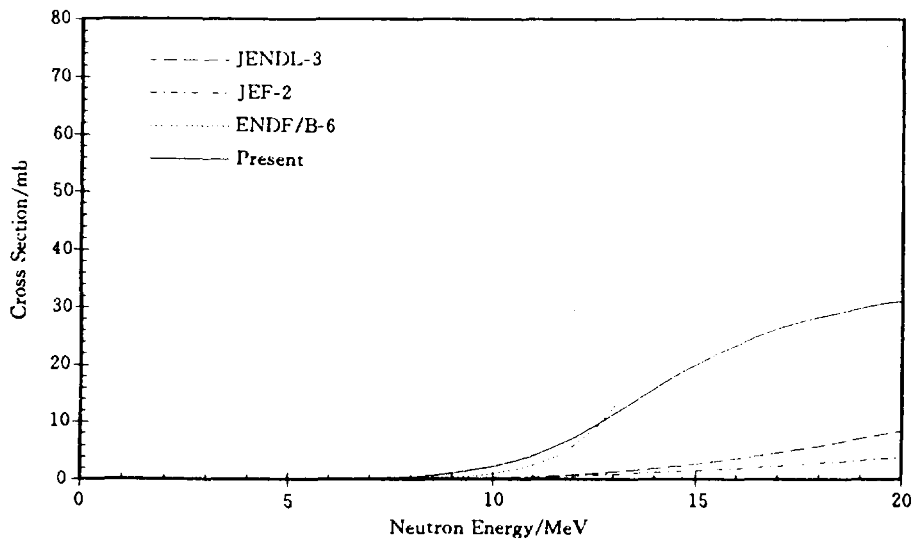

Fig.2 (n,p) cross section for ^{176}Hf

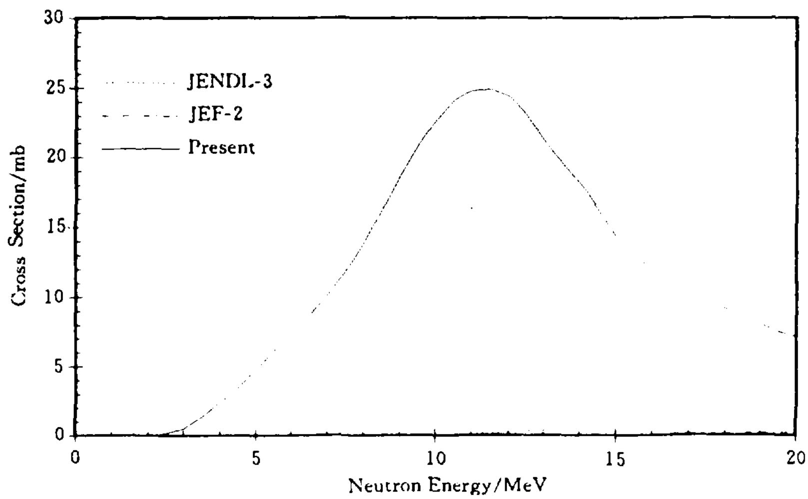

Fig.3 (n,α) cross section for ^{176}Hf

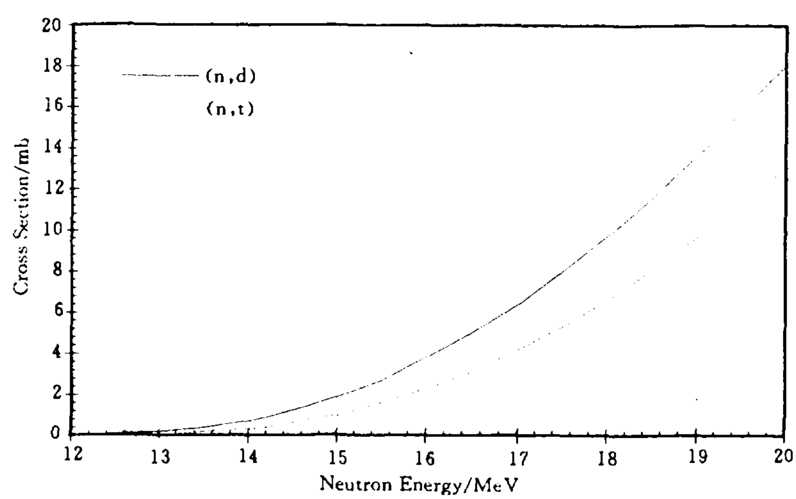

Fig.4 (n,d) and (n,t) cross section for ^{176}Hf

(3) (n,2n) Reaction

Fig.5 shows the calculated (n,2n) reaction cross section, together with the measurement and evaluation data. The calculation agrees very well with the measurements by S.M.Qaim et al.[5] and Lakchmann et al[11].

An experiment was performed recently[7] to determine the cross sections for ^{176}Hf(n,2n)^{175}Hf reaction in low and high energy region. These measurements provide a useful check to the present calculations. The results shows that the calculation is very consistent with these measurements. It means that the present calculation is reliable.

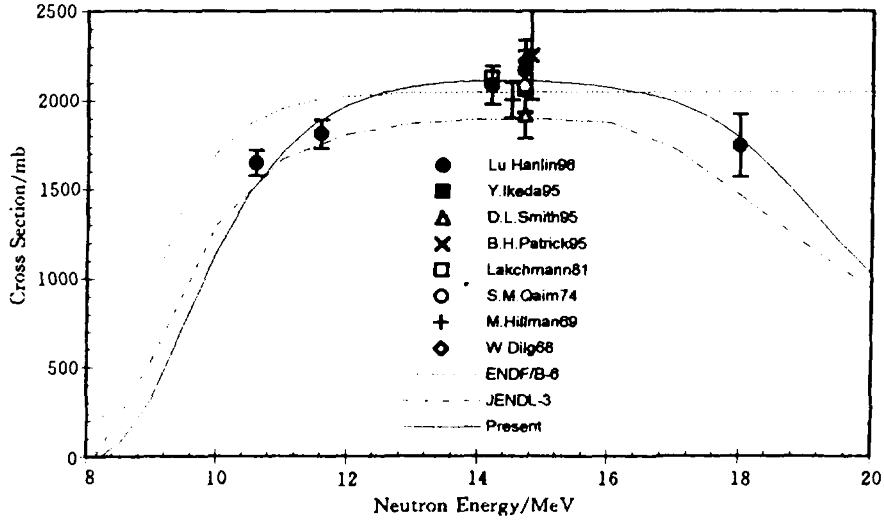

Fig.5 (n,2n) cross section for ^{176}Hf

(4) (n,3n) Reaction

For (n,3n) reaction, there is no available experimental data. So we only compared the calculation with the relevant evaluated data, which is shown in Fig. 6.

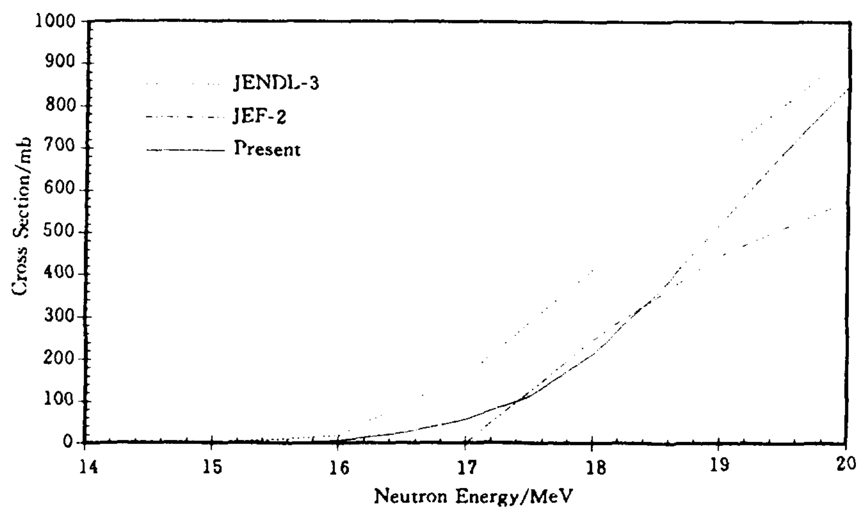

Fig.6 (n,3n) cross section for ^{176}Hf

3 Conclusions

Neutron activation cross sections for ^{176}Hf have been calculated with UNF code in the present work. The calculations were compared with the existing experimental data and/or evaluated data for each reaction. Most of the calculated results are in agreement with the relevant experimental data or evaluated data.

From Figs. 1−6, one can easily find that there are a few measurements and there are large discrepancies in the existing data. Further experiments should be focused on these reactions and more accurate measured data are necessary

Since the data for the low-lying discrete levels were considered and the pick-up mechanism in the preequilibrium reaction processes was introduced in UNF code, the consistent cross sections of calculation are easily obtained. It is easy to conclude that present calculation can be very successful and may be used as the evaluated values.

Acknowledgments

The authors thank Dr. Han Yinlu for his useful suggestions and kind help.

References

[1] Zhang Jingshang. Fast Neutron Physics. Beijing, China, 201(1991); UNF program. Chinese Nuclear Data Center. Internal file(1995)

[2] Han Yinlu, Private Communication

[3] H. Beer et al., Phys. Rev. C30, 464(1984)

[4] M. Hillman, E. Shikata, J. Inorg. Nucl. Chem. 31, 909(1969)

[5] S. M. Qaim, Nucl. Phys. A224, 319(1974)

[6] W. Dilg et al., Nucl. Phys. A118, 9(1968)

[7] Lu Hanlin, Private Communication

[8] Y.Ikeda et al., Private Communication

[9] D. L. Smith et al., Private Communication

[10] B. H. Patrick et al., Private Communication

[11] Lakchmann81et al., Private Communication

CN9800588

III DATA EVALUATION

Evaluation of ^{235}U Fission Product Yield Data and Study of the Dependence of Fission Yield Data on Neutron Energy

Liu Tingjin

(CNDC, CIAE, Beijing, China)

The ^{235}U(n,f) fission product yield data were evaluated for some important product nuclides ^{95}Zr, ^{99}Mo, ^{144}Ce and ^{147}Nd. The dependence of fission yield data on incident neutron energy was studied.

1 Data Collection

At first, the experimental data for these product nuclides were retrieved from master EXFOR data library by using EXFOR management system and some supplementary codes, as described in Fig.1. Then the data were taken from the EXFOR file, where the fission yield data measured in China were compiled and haven't been sent to the EXFOR master library. The data were also collected from some publications.

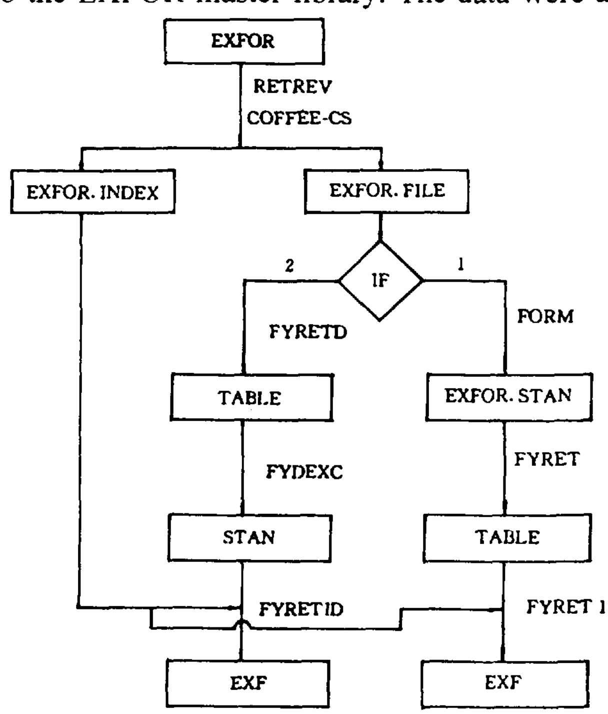

Fig.1 The flow chart of FY EXFOR data retrieval

1 Less than or equil to 6 column; 2 More than 6 column.

All together 83 EXFOR entries and papers were collected, they are listed in Table 1.

In general, the fission yield data can be retrieved according to the target, incident neutron energy, products by using EXFOR retrieval system. But when a product is given under the heading "ELEM/MASS", it could not be found. To solve this problem, the following programs were developed, and they can be used following the retrieving with EXFOR management system "RETREV", "COFFEE-CS" in the option "P" and default to the reaction field 4 (reaction product):

1) FORM Exchange the column position and make the data table standardization. Also change all the "DATA-ERR" into absolute error.

2) FYRET Extract the data table from EXFOR file.

3) FYRET1 Retrieve fission yield data according to the special Z and A, and read the reaction quantity, neutron energy, EXFOR entry number from the index file and write into the file.

If the quantities under the "HEADING" are over 6 (occupy two rows), instead of above, the corresponding programs FYRETD, FYEXC, FYRET1D can be used.

2 Evaluation of Experimental Data

The EXFOR BIB information and papers concerned were read carefully and were analysed in physics. The data were decided to be taken or abandoned according to the measurement date, method, facility, detector, monitor and discrepancy situation with others. In general, the following data were abandoned (marked by (×) in Table 1):

1) The quantity measured is not required;

2) Measured in 50's or earlier;

3) Large discrepancy with others and measured method is not reliable or no information in detail;

4) Incident neutron energy or other important quantities are not able or difficult to be known;

5) Something is wrong in the measurements or data processing.

The necessary corrections were made for the acceptable data:

1) Renormalization using new standards for decay data, standard fission yield, and fission cross section. The new standard data were taken from the Zhou's evaluation at CNDC[2] for decay data, the present evaluation for standard yield or Wang's evaluation (if there is no evaluation in this work) for thermal standard

yield[3], and ENDF/B for fission cross section.

2) Make the neutron energy standardization: 1.95 MeV for ^{235}U fission spectrum, 2.13 MeV for ^{252}Cf spontaneous fission spectrum. Some fast reactor spectra were also changed if they are considerably unreasonable.

3) Enlarge errors, if they were too small given by authors or the corresponding data are discrepant with those of others or even themelves and could not find the reason.

3 Data Processing

In general, the data were processed with the following codes:

1) AVERAG arithmetical average and weighted average and calculating the corresponding error for measured data more than two sets at same energy point, for example, thermal energy, 14.7 MeV, etc.

2) ZOTT developed by D.Muir[1], transplanted and modified. Used for simultaneously evaluating fission yield data at different energy points or for different products and their ratios. The covariance matrix can be calculated for the evaluated data. Concretely, the data were treated as follows:

a. Nuclides Zr, Mo, Ce, thermal yield: Only the absolute measured data were taken, averaging for each and their ratios. Simultaneous evaluation for fission yield and ratio.

b. Nuclide Zr: Averaging for data at fission spectrum, 14.8 MeV, 8.0 MeV. Simultaneous evaluation at thermal energy points, fission spectrum, 8.0 MeV.

c. Nuclide Mo: Averaging for fission yield at fission spectrum, 14.8 MeV, 0.5 MeV. Simultaneous evaluation at thermal energy, fission spectrum, ^{252}Cf fission spectrum.

d. Nuclide Ce: Averaging for fission yield at fission spectrum, 14.8 MeV, 0.5 MeV; Simultaneous evaluation at thermal energy, 14.8 MeV.

e. Nuclide Nd: Averaging for fission yield at thermal energy, fission spectrum, 14.8 MeV. Simultaneous evaluation at thermal energy, 8.0 MeV, 14.8 MeV.

4 Data Fitting and Dependence on Neutron Energy

After treating above, the data, including averaged and simultaneously evaluated ones instead of original measured data, were first fitted with linear fit program LIFIT, which is based on least square method, with a option for $Y=aE+b$ or $\ln(Y)=aE+b$, and the reduced chi-square is calculated. If the χ^2 is larger than about 1.5 (it means that the data could not be fitted with linear function), then the data were fitted with general spline fit program SPF[2], which is with knot optimization and spline order selection and for multi-sets of data of any shape curve, depending on the knots and order selection.

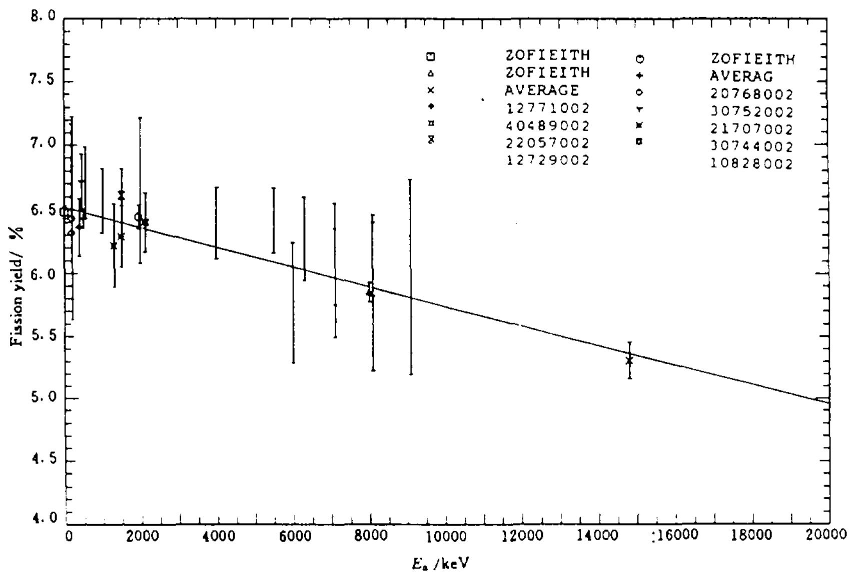

Fig.2 $^{235}U(N,F)^{95}Zr$ Cummu. Fission yield

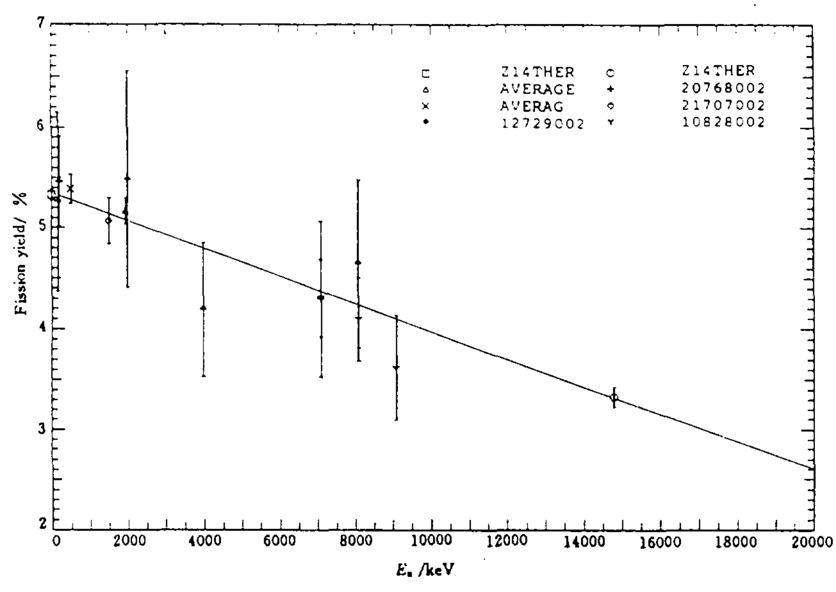

Fig.3 $^{235}U(N,F)^{144}Ce$ Cummu. Fission yield(processed)

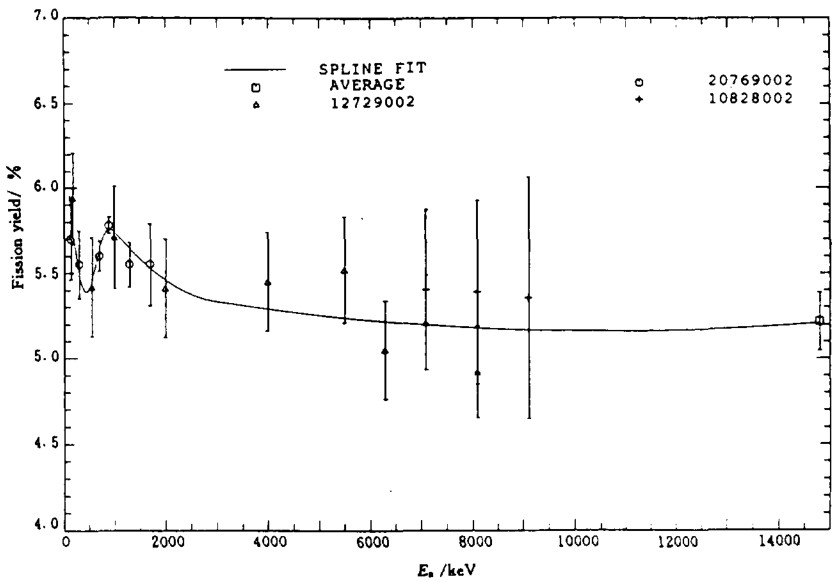

Fig.4 $^{235}U(N,F)^{99}Mo$ Cummu. FY (Mono energy)

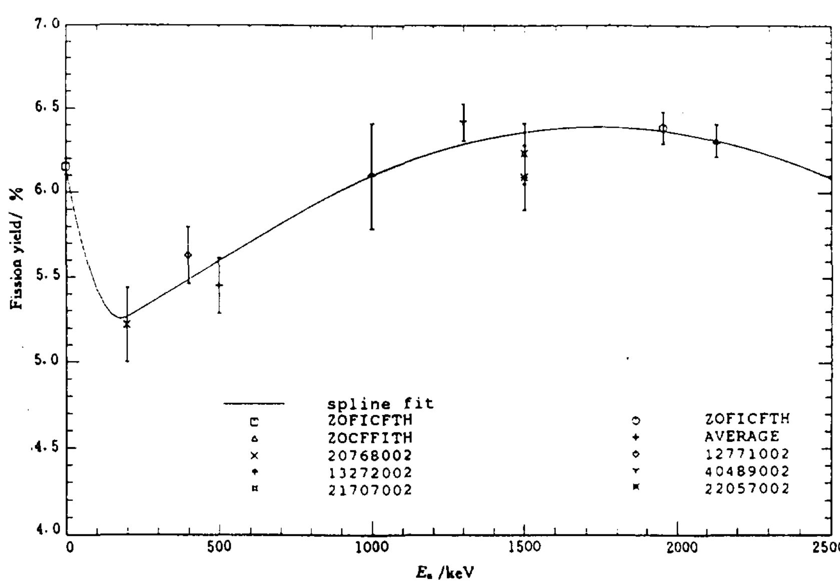

Fig.5 $^{235}U(N,F)^{99}Mo$ Cummu. FY (Spectrum average)

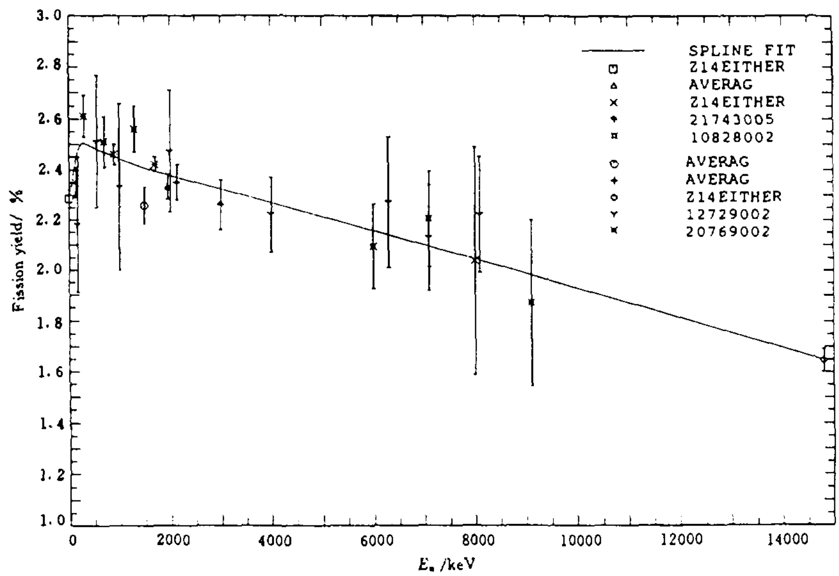

Fig.6 $^{235}U(N,F)^{147}Nd$ Cummu. FY

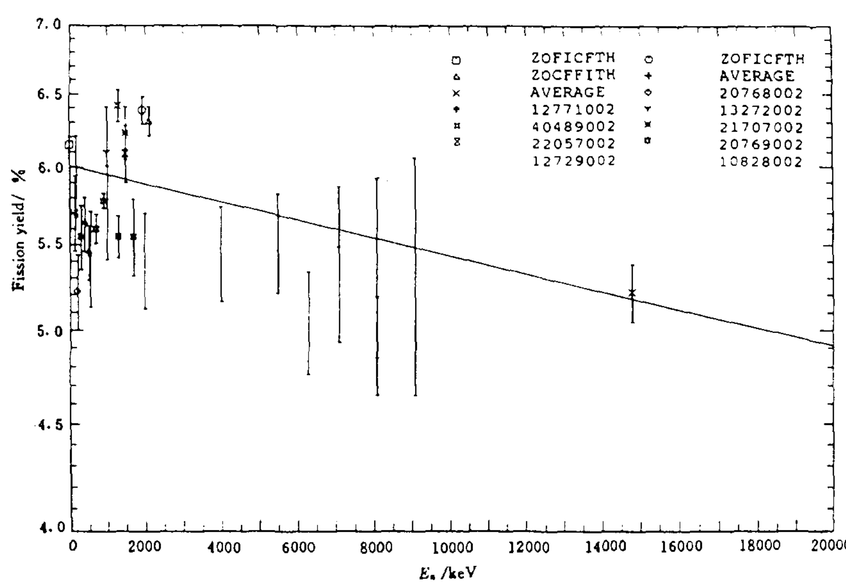

Fig.7 $^{235}U(N,F)^{99}Mo$ Cummulative Fission Yield

The results show that the dependencies of fission yield on incident neutron energy are simply linear for product nuclides Zr, Ce(Figs.2,3), but are quite complicated for Mo(Figs.4,5) and Nd(Fig.6), especially in the keV resonance region and for Mo. They could not be described by a straight line (in this case, χ^2=6.19 for Mo(Fig.7), and 2.07 for Nd). The deviation from linear line is over the experiment error and shown by several sets of data.

It should be pointed out that the fit values were obtained at the "optimum" condition, it's true in whole, but it's not true for some special energy points, for example, for thermal or 14.8 MeV points. Therefore, the recommended fission yield for some special data points, where there are more measured data are the data got through averaging or simultaneous evaluation instead of fit one.

5 Discussion

Dependence of fission yield on energy is a quite complicated problem, due to the complicated fission mechanism. So far it is not very clear but some trends can be seen from the available experimental data.

For studying the dependence of fission yield on incident energy, the measurement with monoenergetic neutron, like using Van de Graaff, Cockcroft-Walton, Tandem accelerator, is more valuable. The typical, important measurements at monoenergetic points were made by G.P.Ford et al. (Los Alamos Scientific Lab.)[3], L.E.Glendenin et al. (Argone National Lab.)[4], and T. C. Chapman et al. (Lawrence Livermore Lab.)[5].

Analyzing these data, the following trends have been found.

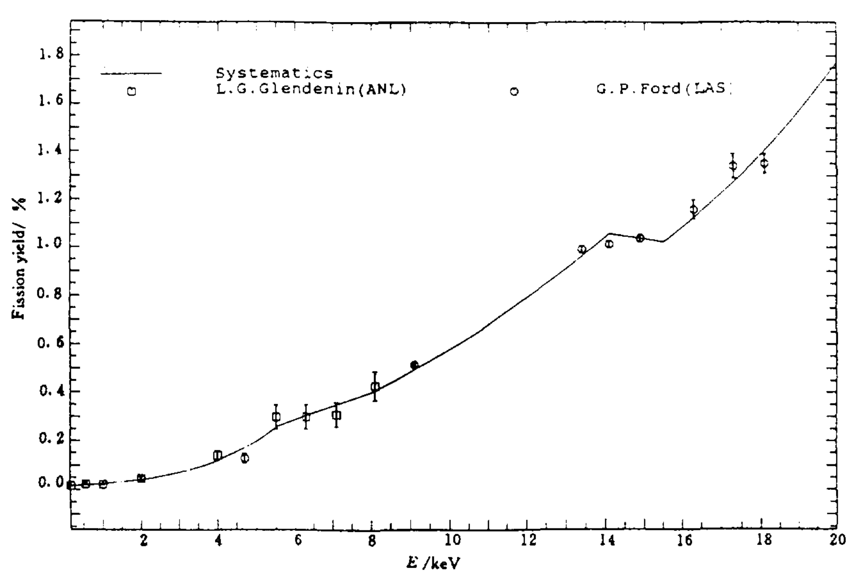

Fig.8 Fission yield measured at monoenergy for ^{111}Ag

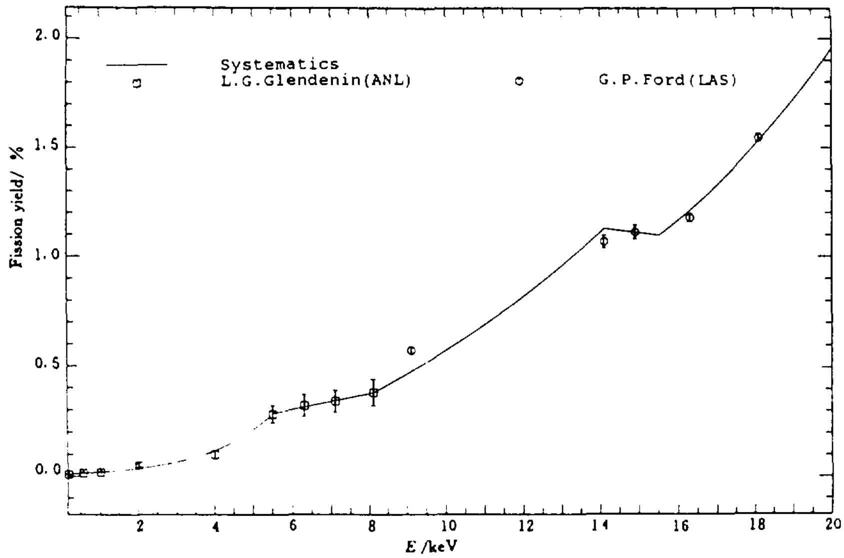

Fig. 9 Fission yield measured at monoenergy for ^{115}Cd

For symmetric fission, the yield increases with incident neutron energy in two steps. First, exponentially increase in the energy region up to about 5.5 MeV, then first step, a drop comparing the exponential increasing, from about 5.5 to 8.0 MeV, then again exponentially increase up to about 14.0 MeV, then second step from about 14.0 MeV to 15.5 MeV, at last, again exponentially increase up to 20.0 MeV. The two steps are approximately corresponding to the onsets of (n,n'f) and (n,2n'f) respectively, which make the excitation energy lower for the corresponding compound nucleus. These features are shown for fission products A=109—125, and some typical examples are given in Figs.8, 9.

For asymmetric fission, it is certain that the yield decreases slowly with increasing neutron energy, and roughly linearly (not exponentially). However if the dependence is studied carefully, it was found that the linear relation on energy is true for some products, for example for ^{95}Zr, ^{144}Ce, but not for others, for example for ^{99}Mo.

The dependence of fission yield on energy should be studied further in experimental measurement and theory investigation.

References

[1] D. Muir, Nucl. Sci. & Eng., 101,88(1989)
[2] Liu Tingjin, CNDP,2,58(1989)
[3] P. Ford et al., Phys. Rev., 137, 4B, 826(1965)
[4] E. Glendenin et al., Phys. Rev., C24(6) 2600(81)
[5] C. Chapman et al., Phys. Rev., C17(3), 1089(1978)

Table 1 Collected experimental FY data

EXFOR	$^{95}_{40}$Zr	$^{99}_{42}$Mo	$^{144}_{58}$Ce	$^{147}_{60}$Nd	EXFOR	$^{95}_{40}$Zr	$^{99}_{42}$Mo	$^{144}_{58}$Ce	$^{147}_{60}$Nd
10722002.3	√				20768002	√	√	√	
10994002				√(×)	21562002	√	√		
12729002	√	√	√	√	21590002	√	√	√	√
12771002	√	√			21605002	√	√		
12771005	√				21689002,4,6	√	√		
13059002-13				√(×)	21689012,19	√	√		
13064003			√		21707002	√	√	√	√
13064004				√	21708002			√	√
13065004	√				21743005		√		√
13086002					22054002	√			
13091002	√(×)		√(×)	√(×)	22057002	√	√		√
13116002					22066002	√	√	√	√
13174002					30495002		√		√
13211002.3	√				30496002				
13233006				√(×)	30504002		√		
13246002			√(×)		30744002	√	√		√
13251003				√	30752002	√			
13270017			√		30947002	√(×)		√(×)	√(×)
13272002		√			40206003			√(×)	√
13273003	√				40489002	√	√		
13283002	√			√	(Double Line heading)				
13283003			√		10828002	√	√	√	√
13286002	√		√	√	12919004	√(×)	√(×)	√(×)	√(×)
3306002.5	√		√		13054003	√(×)	√(×)	√(×)	
13335002	√				1307702				
13335008			√		13093002		√(×)		
13337002	√	√			13255002.4			√	√
13378002					13295002	√(×)	√(×)	√(×)	√(×)
13380002					13444003			√	
13339002	√				13445004			√	
13342002	√				20769002		√		√
13362002			√(×)		(Measured in China)				
13372003		√(×)			32628002			√(×)	√(×)
13374002.3		√(×)			32629002	√(×)	√(×)		√(×)
13382002		√(×)			32636002	√(×)	√(×)	√(×)	√(×)
13395002					32631002	√	√	√	√
13395003	√	√	√		32632002.3		√		
13403002	√(×)	√(×)			32633002,3	√	√	√	√
13425002					32634002-4	√(×)	√(×)		
13427003		√			32635002-5	√	√		
13428002	√(×)		√(×)		32636002	√(×)	√(×)		√
13448002	√(×)			√(×)	32638002,3	√	√	√	
13478002	√				32639002	√(×)	√(×)		
13478003			√		QiLinkun+(88)	√	√	√	√
13479002	√				Lize+(95)	√			√
13479003			√		H.R.Von Guntin(67)		√		

CN9800589

Decay Data Evaluation for Radionuclide ^{7}Be

Zhou Chunmei   Huang Xiaolong

(China Institute of Atomic Energy, CIAE)

^{7}Be is a radionuclide of ε decay. It can be useful as standard source of gamma-ray detector calibration. Therefore, its half-live and gamma-ray emission probability need to be known with good accuracy. The decay data were evaluated[1] in 1988. It is important for us to update them. The cutoff date of references retrieved from Nuclear Science References File (NSRF) is November, 1996.

1 Half-live

The measured half-lives are listed in Table 1. In this evaluation it is noted that variation of half-live with chemical environment ranges up to 0.2% and a proposal to the nuclear structure and decay data evaluator network—a limitation of relative statistical weights is adopted. Weighted mean value 53.26±0.05 days is recommended.

Table 1 Measured half-live for ^{7}Be

Value (in days)	Reference
53.12 ± 0.07	Jeager et al.(1996)[2]
53.29 ± 0.02&	Merritt et al.(1974)[3]
53.17 ± 0.07	Lagoutiue et al.(1975)[4]
53.52 ± 0.10	Johlige et al.(1970)[5]
53.61 ± 0.17	Kraushaar et al.(1953)[6]
53.50 ± 0.20	Wright et al.(1957)[7]
52.93 ± 0.20	Segre et al.(1951)[8]
53.00 ± 0.40	Bouchez et al.(1956)[9]
53.10 ± 0.30	England et al.(1965)[10]
53.00 ± 0.30	Cressy et al.(1974)[11]
53.22 ± 0.08	unweighted mean
53.26 ± 0.05	weighted mean

Notes to Table:

&: This value is the latest one for authors. The uncertainty was increased to 0.04 to ensure that this value did not contribute a weighting of greater than 50% in weighted mean calculation.

2 Emission Probability of Gamma-ray

^{7}Be is ε decay to ground state and the first excited state (477.62097 keV) of ^{7}Li. Only 477.6035 keV gamma-ray can be emitted. The measured gamma-ray emision probability is listed in the Table 2. P_r=10.45± 0.05 is recommended.

Table 2 Measured 477.6 keV gamma-ray emission probability

Value$^{\$}$, %	Reference
10.32 ± 0.16	Tayor et al.(1962) [12]
10.42 ± 0.18	Poentiz et al.(1973) [13]
10.35 ± 0.08	Goodier et al.(1974) [14]
10.10 ± 0.45	Balamuth et al.(1983) [15]
10.61 ± 0.23	Davids et al.(1983) [16]
10.60 ± 0.50	Donoghue et al.(1983) [17]
10.61 ± 0.17	Fisher et al.(1984) [18]
10.70 ± 0.20	Methews et al.(1983) [19]
9.80 ± 0.50	Norman et al.(1983) [20]
10.90 ± 0.50	Donald et al.(1983) [21]
10.40 ± 0.70	Evans et al.(1984) [22]
10.49 ± 0.07	Skelten et al.(1984) [23]
10.440 ± 0.083	unweighted mean
10.450 ± 0.044	weighted mean

Notes to Table:

$: Absolute emission probability for 477.6 keV gamma-ray per 100 parent decays.

3 Decay Scheme

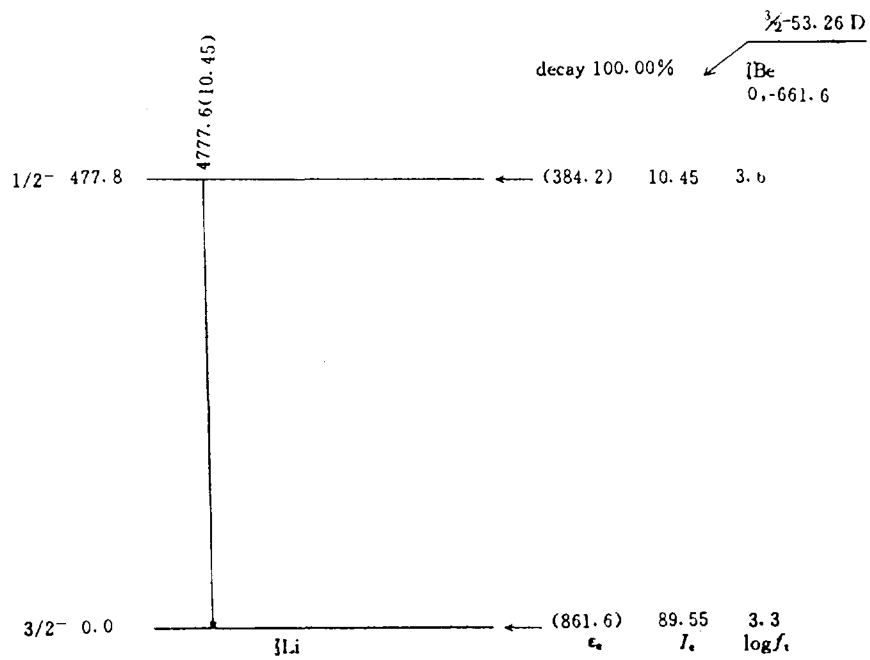

Fig.1 Decay scheme of ^{7}Be

The decay scheme for ^{7}Be radionuclide is shown in the Fig.1. The decay energy Q(EC)=861.82±0.02 keV[24]. The EC branching ratios P_{ε}(to ground state of

^{7}Li)=89.55±0.05 and P_ε(to 477.6 keV state of ^{7}Li)=10.45±0.05 are deduced from %EC=100 for ^{7}Be and P_γ(477.6 keV gamma-ray)=10.45±0.05. The *logft* values are calculated by LOGFT code. The level energy E_l=477.62095±0.00020 keV is calculated by using least-squares fitting to E_γ and nuclear recoil correction. Our recommended decay data for ^{7}Be are listed in Table 3.

Table 3 Recommended decay data for ^{7}Be

Decay type/ray	energy, keV	Intensity$^@$
EC 1		10.45±0.05
EC 2		89.55±0.05
γ 1	477.6035±0.0002	10.45±0.05

Notes to Table:

@: Absolute intensity per 100 parent decays.

4 Comparison with other Evaluations

The evaluated half-live comparison is listed in Table 4.

Table 4 Evaluated half-live comparison for ^{7}Be

$T_{1/2}$, days	Reference
53.26±0.05	this work
53.29±0.07	Ajzenberg-selove(1988)[1]
53.23±0.06	Horiguchi et al.(1992)[25]
53.29±0.07	Firestone et al.(1996)[26]
53.3±0.1	Lederer et al(1978)[27]

The comparison of evaluated emission probability of gamma-ray is listed in Table 5.

Table 5 Comparison of evaluated gamma-ray absolute intensity for ^{7}Be

$P_\gamma^\#$,%	Reference
10.45±0.05	this work
10.60±0.20	Huriguchi et al.(1992)[25]
10.52±0.06	Firestont et al.(1996)[26]
10.52±0.06	Ajzenberg-selove(1988)[1]

Notes to Table:

#: Absolute emission probability for 477.6 KeV gamma-ray per 100 parent decays

References

[1] F-Ajzenberg-selove, Nucl. Phys. A490, 1(1988)

[2] M. Jaeger et al., Phy. Rev. C54, 423(1996)

[3] J. S. Merritt, et al., AECL-3512, 30(1969); Private Communication (1974)
[4] F. L agoutiue, et al., Int. J. Appl. Radio. Isotopes, 26,131(1975)
[5] H. W. Johlige, et al., Phys. Rev. C2, 1616(1970)
[6] J. J. Kraushaar et al., Phys. Rev. 90, 610(1953)
[7] H. W. Wright et al., Nucl. Sci. Eng. 2, 427(1957)
[8] E. Segre et al., Phys. Rev. 75, 39(1949); 81, 284(1951)
[9] R. Bouchez et al., J. Phys. Radium, 17, 363(1956)
[10] J.B.A.England et al., Nucl. Phys. 72, 449(1965)
[11] P.J. Cressy et al., Nucl. Sci. Eng. 55, 450(1974)
[12] Tayor and Merritt, Can. J. Phys. 40, 926(1962)
[13] Poenitz and Devopl, Int. J. Appl. Radio. Isotopes, 24, 471(1973)
[14] Goodier, Mekepeace and Williams, Int. J. Appl. Radio. Isotopes, 25, 373(1974)
[15] Balamuth et al., Phys. Rev. C27, 1724(1983)
[16] Davids et al., Phys. Rev. C28, 885(1983)
[17] Donoghue et al., Phys. Rev. C28, 875(1983)
[18] Fisher and Hershbergen, Nucl. Phys. A423, 1219(1984)
[19] Mathews et al., Phys. Rev. C28, 879(1983)
[20] Norman et al., Phys. Rev. C27, 1728(1983)
[21] Knapp Mc Donald et al., Nucl. Phys. A411, 195(1983)
[22] Evans et al., Can. J. Phys. 62, 1139(1984)
[23] Skeiten and Kavanagh et al., Nucl. Phys. A414, 141(1984)
[24] G. Audi and A. H. Waptra, Nucl. Phys. A595, 409 (1995)
[25] T. Horiguchi et al., Chart of the Nuclides, 1992
[26] R. B. Firestone et al., Table of Isotopes, Vol. I (1996)
[27] C. M. Lederer et al., Table of Isotopes (1978)

CN9800590

Evaluation of Neutron Induced Helium Production and Activation Cross Sections for Some Nuclei

Yu Baosheng

(China Nuclear Data Center, CIAE)

The activation characters of chosen fusion materials are important in determining proper reactor technologies. In order to meet these requirements for fusion design studies, not only all activation cross sections for the fusion materials themselves have to be know, but also those for all possible impurities require to be considered if they lead to long-lived activities.

The helium production cross sections are extremely useful in the research of radiation damage caused by helium yield in materials, having experienced large fast-neutron doses, for they can induces nuclear transmutation and lattice deficiency. In some cases the activation cross sections of the production of long-lived associated with the (n,α) reactions are also extremely important for the radiation safety, maintenance and disposal of waste. Comparison of measured and evaluated data has indicated large discrepancies for several reactions. In order to meet the requirements from both viewpoint of the helium production and activation data, the cross sections of (n,α) reaction for ^{55}Mn, ^{54}Fe, ^{59}Co, ^{62}Ni and ^{63}Cu were further evaluated based on new measured data and theoretical calculation. The cross sections for (n,α) reaction with long lived radio nuclides directly or residual nuclei lead to long-lived one via neutron capture, (n,2n), (n,t) reactions, etc., were investigated and evaluated for some nuclei based on newly information available.

1 ^{55}Mn (n,α) ^{52}V Reaction

There are some difficulties measuring ^{55}Mn(n,α)^{52}V reaction cross section exist using activation method because the half-life of the residual nucleus ^{52}V is very short ($\approx$3.7 minutes). Previous measured cross sections for ^{55}Mn(n,α)^{52}V reaction have not only large fluctuation but also big errors. After 1980's the measured cross sections were improved, they can cover the energy region from threshold to 18 MeV.

In order to recommend properly the cross sections for ^{55}Mn(n,α)^{52}V reaction, the measured data around 14 MeV were evaluated. These data were adjusted to equivalent 14.7 MeV cross section, also adjusted properly for nuclear decay schemes, half-life and standard cross section. The weighted factor was used in the evaluation, which was based on the errors given by authors and quoted errors by us. Present evaluated value at 14.7 MeV is 25.4±2.7 mb.

The multiple sets of data were provided by F.Gabbard[1] in energy region 12 to 18 MeV, by M. Bormann[2] from 13 to 19 MeV, by E.Zupranska[3] from 13 to 18 MeV, respectively. Among these three group data, the data measured by F.Gabbard[1] were scattering, especially in energy region 13 to 14 MeV. But the shape of the data measured by M.Bormann[2] were in agreement very well with ones of E.Zuoranska[3]. Therefore, after the two group data were normalized to the evaluated value at 14.7 MeV, the complete cross sections measured in the energy region from 12 to 19 MeV can be obtained.

Recently the measurement was carried out by M.Bostan[4] in energy region from nearly threshold to 12 MeV at Julish laboratory in 1994. The measured data were corrected for other interfering decay and the back-ground neutrons (target invs-out) and breakup neutron.

These data can provide a complete shape of excitation function for ^{55}Mn (n,α)^{52}V reaction. Meanwhile, the evaluated data for ^{55}Mn were calculated with EGNASH Code by the author for JENDL-3 fusion file and CENDL-2 Rev.1. At present work, the evaluated data were performed based on the measured data by M.Bormann[2], E.Zuoransky[3], M.Bostan[4] and referring other measured data as well as theoretically calculated results. The recommended data were compared with other evaluated data from ENDF/B-VI, JENDL-3 and ADL-3I and shown in Fig. 1.

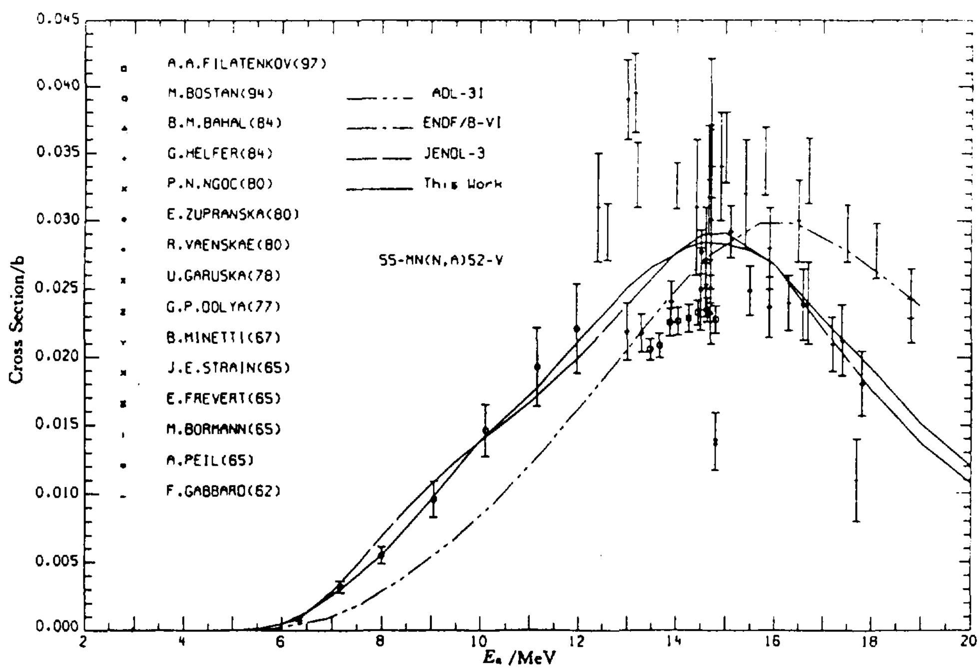

Comparison of evaluated & measured data

Fig.1

2 $^{54}Fe(n,\alpha)^{51}Cr$ Reaction

The many experimental data sets for $^{54}Fe(n,\alpha)^{51}Cr$ reaction were measured by different laboratories below 20 MeV and could describe sufficiently the trend for the reaction. Based on the experimental data mentioned above the evaluation was done in the previous work. The measured data of S.K.Saraf[5] are important to improve the evaluation near reaction threshold energy where the measured data did not exist until 1991.

Recently, the relation of the threshold value and shape of standard cross section to the effects of neutron back-ground has been carefully investigated by Lu Hanlin[6] in CIAE. The cross sections near threshold energy were accurately measured by him. Therefore, the new and accurate data measured supplemented the experimental data and updated the previous evaluated work. The present evaluated data based on new measured cross sections are lower ~2%—17 % than previous work in energy region 5 to 10 MeV. The present evaluation is compared with ones from ENDF/B-VI, JENDL-3 and BROND-2 and shown in Fig. 2.

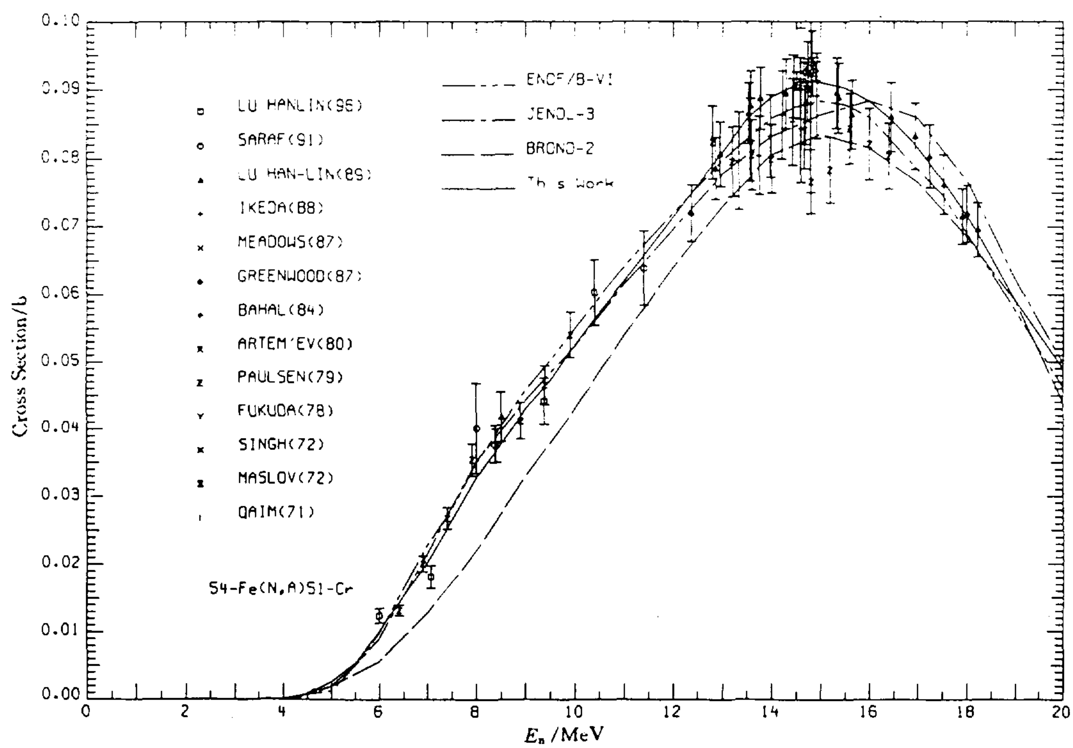

Comparison of evaluated & measured data

Fig.2

3 $^{59}Co(n,\alpha)^{56}Mn$ Reaction

Lot of the experimental data for $^{59}Co(n,\alpha)^{56}Mn$ reaction exist from threshold to 20 MeV. Our evaluated value at 14.7 MeV is 31.15±0.65 mb, which was used to normalize corresponding measured data above 13 MeV.

Recently, A.A.Filatenkov[7] has measured the cross sections from 13 to 15 MeV. In order to increase the reliability, two reference reactions of $^{27}Al(n,\alpha)^{24}Na$ and $^{93}Nb(n,2n)^{92m}Nb$ were used simultaneously, so as to determin the accurate neutron fluence. The back-ground from scattered neutron contribution was minimized using the thin-wall constructions and air cooling target. The measured value A.A.Filatenkov[7] is 31.80±0.78 at 14.7 MeV, which is consistent with our evaluated value within errors.

The data below 13 MeV were accurate measured by W.Mannhart[8]. In this measurement, the effects of back-ground were subtracted via measuring the "gas-out" target. The evaluated data were obtained based on the measured data and calculated results. The evaluated data are compared with other evaluated data from JENDL-3, ENDF/B-VI and ADL-3I and shown in Fig. 3.

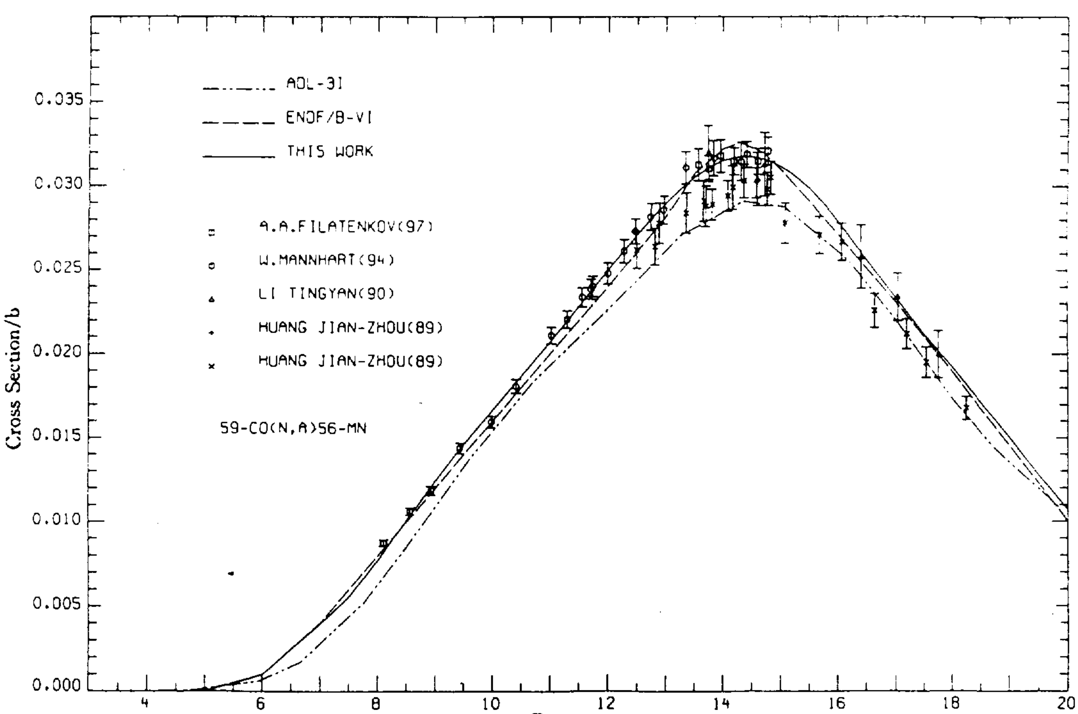

Comparison evaluated & measured data for $^{59}Co(n,\alpha)^{56}Mn$ reaction

Fig.3

4 $^{62}Ni(n,\alpha)^{59}Fe$ Reaction

The measured data were mainly performed around 14 MeV in some laboratories, especially the recent measured values by K.Fukuda[9], Wang Yongchang[10] and Li Tingyan[11] were consistent with each other. In order to recommend properly the cross section for $^{62}Ni(n,\alpha)^{59}Fe$ reaction, the measured data around 14 MeV were evaluated. The weighted factor was used in the evaluation, which was based on the given errors by authors and quoted errors by us. Present evaluated value of 14.7 MeV is 23.4±1.7 mb.

Recently, the accurate data were measured by Lu Hanlin[6] below 12 MeV energy region where the measured data are very scarce. In this measurement in order to subtracted the effects of neutron back-ground from "gas-out" and backup neutron from D(d,n) neutron source, the threshold value and shape of standard cross section were carefully investigated and selected. Therefore, these experimental data cover the energy region from threshold to 15 MeV. The evaluated data were obtained based on the evaluated measured data and theoretically calculated tend. The recommended data were compared with the other evaluations from ENDF/B-VI, JENDL-3 and BROND-2 and shown in Fig. 4.

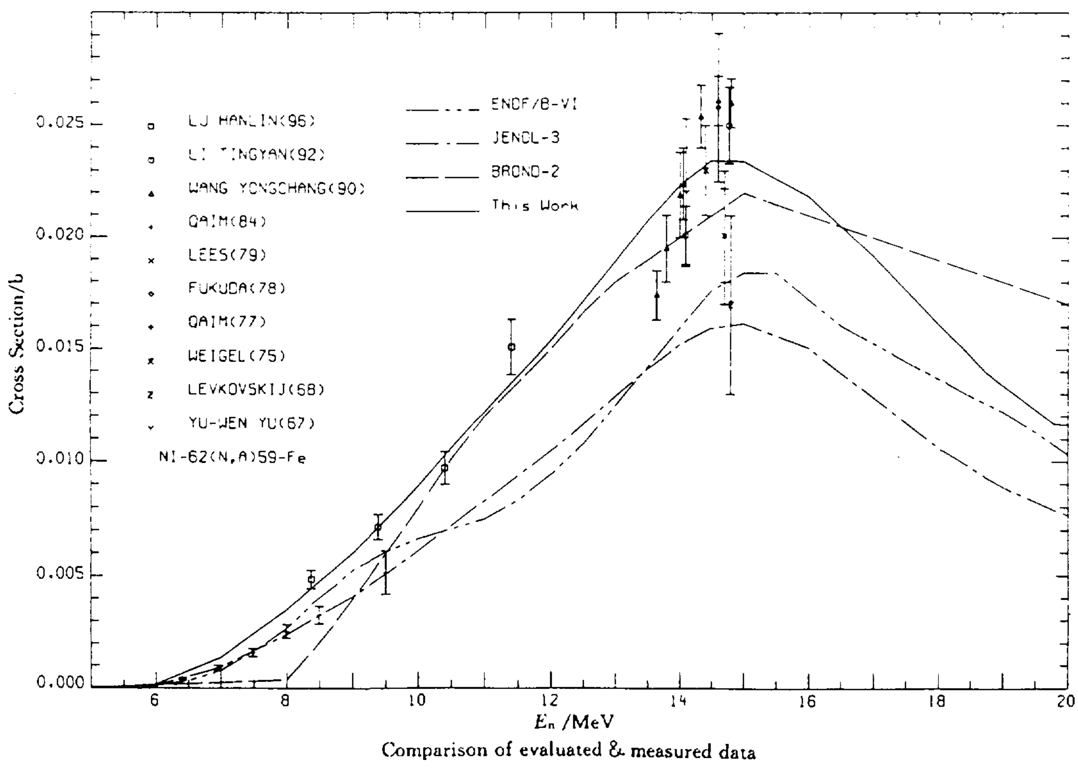

Fig.4

5 $^{63}Cu(n,\alpha)^{60}Co$ Reaction

The available measured cross sections for $^{63}Cu(n,\alpha)^{60}Co$ reaction were collected and analyzed, most of the experimental data up to year 1996 have been included, especially the new accurate measured data by Lu Hanlin[6] in energy region 6 to 12 MeV. Because the carefully selected standard cross section was used so that the effects of back-ground and breakup neutron were reduced and subtracted. The new measured data by Lu Hanlin[6] in 6 to 12 MeV have superseded and supplemented the scarce data in the energy region, and modified the previous evaluation.

All collected cross sections around 14 MeV were adjusted to energy 14.6 MeV cross section and re-normalized for the standard cross section used. The characters of gamma ray of ^{60}Co have not any significant change. The half-life of 5.271 a and the branching ratio 99.89% for 1173 keV characteristic gamma of ^{60}Co in this evaluation were unnecessary to revise. The evaluated data was obtained at 14.6 MeV and used to normalize the measured data above 13 MeV.

The cross sections for $^{63}Cu(n,\alpha)^{60}Co$ reaction were evaluated based on the experimental data and theoretically calculated values. It was shown that our evaluated data could reproduce experimental data very well. The present results for $^{63}Cu(n,\alpha)$ ^{60}Co reaction were compared with other evaluated data from ENDF/B-VI and JENDL-3 and shown in Fig. 5.

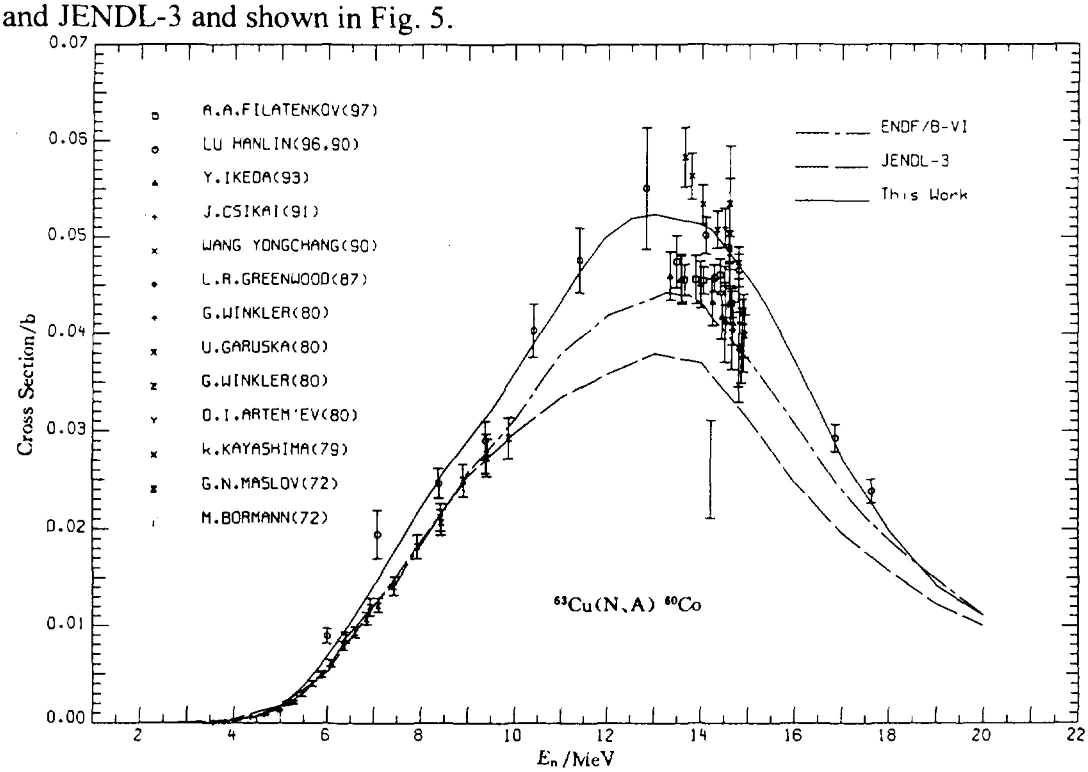

Comparison of evaluated & measured data

Fig.5

Acknowledgments

The authors are indebted to IAEA (International Atomic Energy Agency), CNNC (China National Nuclear Corporation) and CIAE for their supports, and thank Drs.A.B.Pashchenko, T.Benson, O.Schwerer, Lu Hanlin, Zhao Wenrong for kind help and suggestions.

References

[1] F. Gabbaro et al., Phys. Rew., 128,1276(1962)
[2] M. Bormann et al., Nucl. Phys., 63,438(1965)
[3] E. Zupranska et al., J. APP/B,11,853(1980)
[4] M. Bostan et al., Phys. Rew./C,49,266(1994)
[5] S. K. Saraf et al., Nucl. Sci. Eng.,107,365(1991)
[6] Lu Hanlin Private communication (1996)
[7] A. A. Filatenkov et al., INDC(CCP)-402 (1997)
[8] W. Mannhart et al., Conf. on Nucl. Data for Scie. and Tech., P258(1994) Gathinburg, USA.
[9] K Fukuda et al., ENANDC(J)-56/U,44(1978)
[10] Wang Yongchang et al., High Energy Physics and Nucler Physics, 14,1117(1990)
[11] Li Tingyan et al., ibid,16,151(1992)

CN9800591

Evaluation and Calculation of Activation Cross Sections for ^{158,159}Tb(n,2n), (n,3n), (n,γ) and (n,x) Reactions Below 20 MeV

Yu Baosheng Han Yinlu Gao Lan
(China Nuclear Data Center, CIAE)

Shi Zhaomin Tang Guoyou
(Institute of Heavy Ion Physics, Peking University)

Introduction

^{159}Tb is a rare-earth element. Its activation cross section is a good indicator for nuclear science and technology applications. However, the evaluated data are very scarce in several nuclear data libraries. The cross section for ^{159}Tb(n,2n)^{158}Tb reaction was one of the Coordinate Research Program of IAEA on activation cross sections for the generation of long-lived radionuclides of importance in fusion reactor technology. However, the results of all the theoretical calculations are larger than the experimental data for $^{159}Tb(n,2n)^{158}Tb$ reaction below neutron energy 11 MeV measured by Julich-Debrecen collaboration. The measurements for $^{159}Tb(n,2n)$ ^{158}Tb reaction by CIAE and Lanzhou University (LNZ) and for $^{159}Tb(n, \gamma)^{160}Tb$ reaction by CIAE and Peking University (BJG) were used in this work. The evaluation and calculation of the activation cross sections for $^{159}Tb(n,2n)$, (n,3n), (n,γ) and some charged particle emission reactions (n,x) below 20 MeV were performed based on experimental and theoretical data so as to meet the nuclear science and technology applications. The present results are compared with the values of averaged theoretical calculation and the experimental data.

1 Evaluation and Analysis of Experimental Data

1.1 ^{159}Tb(n,2n) Reaction

The investigation of the cross section for $^{159}Tb(n,2n)^{158}Tb$ reaction is very useful for activation indicator application and waste disposal assessment of fusion reactor materials due to the half-lived of reaction product ^{158}Tb having 1.8 a. At present evaluation, the much emphasis are to recommend accurate activation cross sections based on the newest measured and theoretically calculated data below 20 MeV. The new measured data were performed in CIAE and LNZ in 1996 and all of the collected data [1-7] are listed in Table 1.

Table 1 Collected Data and Relevant Information for $^{159}Tb(n, 2n)^{158}Tb$ Reaction

Year	Author	E_n / MeV	n flux	$T_{1/2}(^{158}Tb)Y$	E_γ / keV	P_γ / %
1974	S.M.Qaim	14.7	$^{27}Al(n,\alpha)^{24}Na$ $^{75}As(n,2n)^{74}As$	180	944	43.9
1984	R.J.Prestwood	14.8	$^{169}Tm(n,2n)^{168}Tm$	180	80 - 1187	43.9
1995	J.W.Meadows	14.7	$^{58}Ni(n, p)^{58}Co$	180	944	43.9
1995	Y.Ikeda	14.1 - 14.9	$^{93}Nb(n,2n)^{92m}Nb$	150	944.2	43.0
1996	S.M.Qaim	9.18, 9.6, 10.1,10.83	$^{27}Al(n, \alpha)^{24}Na$	180	944	43.9
1996	Lu Hanlin	13.7- 14.8	$^{197}Au(n,2n)^{196}Au$	180	944	43
1996	Yu weixiang	9.5, 9.9	$^{197}Au(n,2n)^{196}Au$	180	944	43

The existing measured cross section of (n,2n) reaction for ^{159}Tb is around 14 MeV and below 11 MeV. Most measurements for (n,2n) reaction have been performed around 14 MeV because of the availability of intense source of mono-energietic neutron of this energy from Cockcroft-Walton accelerator. Below 11 MeV, there are only 6 energy points for this reaction. In order to recommend the accurate cross sections around 14 MeV and below 11 MeV, the experimental measurements were performed by using the neutron source from $T(d,n)^4He$, $D(d,n)^3He$ reactions in neutron energy regions —14 MeV, 9—10 MeV. With Cockcroft-Walton and Tandem accelerator (CIAE).

The measured data for (n,2n) reaction around 14 MeV were collected and selected and renormalized to a common set of decay data and reference cross sections. The cross section evaluated from the renormalized selected data at 14.5 MeV is 1924±53 mb and consists with the evaluated value by H.Vonach[8].

In CIAE measurement for product activity below 11 MeV, the effects of low energy neutrons were considered. When the neutron of 9.5 and 9.9 MeV were produced by the $D(d,n)^3He$ reaction using a gas target, several kind of low energy neutrons in the main spectrum were also produced from the breakup neutron of deuteron, the multi-scattering of the main neutron, target structure materials. The difference of 130% at 9.5 MeV and 80% at 9.9 MeV were found for the neutron fluence measured using the monitor with different threshold of $^{58}Ni(n,p)^{58}Co$ and $^{197}Au(n,2n)^{196}Au$ reactions[7], respectively. For activation cross section measurement of long-lived radionuclides, the monitor reaction selected must be nearly the same in threshold and be of very similar shape in excitation function with the investigated reaction. In this way, the effect of low energy neutron can be suppressed largely. Now the measured data for $^{159}Tb(n,2n)^{158}Tb$ reaction was derived from the neutron fluence of the $^{197}Au(n,2n)^{197}Au$ monitor reaction because they have a similar threshold and similar shape of excitation function. The recommended decay parameters for the half-lived, gamma-ray energy and its probability consist each other.

Recently, the data were investigated by S.M.Qaim[5] at Julich/Debrecen laboratories again. Since the primary deuteron energies at the compact cyclotron CV 28 were recently redetermined, the old data were recalculated and revised.

Therefore, the evaluation for experimental data of (n,2n) reaction could be used to guide theoretical calculation at 14.5 MeV and below 11 MeV.

1.2 $^{159}Tb(n,\gamma)^{160}Tb$ Reaction

For the $^{159}Tb(n,\gamma)^{160}Tb$ reaction, there are experimental data at thermal energy and in the energy region of 0.00013 eV —4.0 MeV as well as around 14 MeV, these experimental data[9-14] are shown in Table 2.

Table 2 Collected Data and Relevant Information for $^{159}Tb(n,\gamma)$ Reaction

Year	Author	E_n	Detector	n flux	Comment
1961	J.H.Gibbons	11 - 170 keV	STANK	$In(n,\gamma)$	
1961	R.C.Block	0.2 - 9.4 keV	STANK		
1967	G.Peto	3.0 MeV	GEMUC	BF_3	Activation Method
1970	K.Knorr	0.00013 to 0.0032 eV			Transmission Measurement
1970	S.S.Malik	0.0253 eV 0.033 - 0.29 eV	Moxon-Rae	$^{197}Au(n,\gamma)$	
1971	F.Rigaud	14 MeV	NaI(Tl)	Absolute	Associated Particle
1971	J.S.Brzosko	0.4 MeV	STANK		
1974	T.B.Ryves	0.0253 eV	FISCH	$^{197}Au(n,\gamma)$ $^{54}Mn(n,\gamma)$	Activation
1974	K. Siddappa	23 keV	NaI(Tl)	$^{127}I(n,\gamma)^{128}I$	
1982	W.P.Poenitz	0.5 - 4.0 MeV	STANK	$^{197}Au(n,\gamma)$	
1986	J.Voignier	0.5 - 2.5 MeV	NaI	BF_3	
1988	Mu Yunshan	0.7 - 1.6 MeV	STANK	$^{197}Au(n,\gamma)$	
1996	M.V.Bokhovko	5 - 400 keV	NaI(Tl)	Absolute	^{6}Li-Glass
1997	Shi Zhaomin	0.5 - 1.6 MeV	HPGe(Li)	$^{197}Au(n,\gamma)$	Activation Method

STANK (Liquid scientillator Tank)
FISCH (Fission chamber and a Boron-Coated ionization chamber)
GEMUC (Mica End-Window Geiger muller counter)

Previous experimental data were measured by R.C.Block[10] in energy region of 0.2−9.4 keV, J.H.Gibbons[9] in energy region of 11 - 170 keV and S.S.Malk in energy region of 0.033−0.29 eV, the liquid scintillation tanks were used to measure the prompt γ ray for capture events.

During 1960−1970 s the measurements at 0.023, 0.4, 3.0, 14 MeV were performed by K.Siddappa[17], J.S.Brzosko[15],G.Peto[11] and F.Rigang[14]. In order to check the measured data in 0.5−4.0 MeV, after the 1980s some measurements were made by W.Poenitz[18], J.Voignier[19], Mu Yunshan[20].

The newly measurements in energy region of 5−400 keV were carried out by M.V.Bokhovko[21] with NaI(Tl) spectrometer at FEI laboratory in 1996. The measured data indicate that the old data measured by R.C.Blocl[10] and J.H.Gibbons[9] systematically higher than the new one.

To check these capture cross sections measured in energy region 0.1−4.0 MeV, which were measured by some laboratories with liquid scintillation tank to measure the prompt γ ray for capture events, Shi Zhaomin et al.[22] measured cross sections at 0.57, 1.10 and 1.6 MeV using 4.5 MV Van de Graaff accelerator with the $T(p,n)^3He$ reaction on a solid T-Ti target. The sample was made of powder terbium oxide, which was pressed into tablets and packed by nylon film. Each sample was sandwiched between two gold disks. The sample groups were wrapped with cadmium foils to prevent thermal neutron effects. The activity of the nuclide ^{160}Tb was measured in two Laboratories (CIAE, PU) and same standard γ-source was used to calibrate the efficiencies of HPGe(Li) spectrometers. At present work, the standards cross sections for $^{197}Au(n,\gamma)^{198}Au$ reaction were taken from ENDF/B-VI. The early measured data using liquid scintillation tank are consistent with new measured data within their errors. Therefore, these cross sections[26] based on the measured data mentioned above are reliable.

The thermal cross sections were measured by S.S.Malik[13] and T.B.Ryves[16]. They are in agreement within errors. But the thermal cross section from S.S.Malik[13] was deduced indirectly. The measured value by T.B.Ryves[16] was adopted due to its small errors.

The capture cross sections for $^{159}Tb(n,\gamma)^{160}Tb$ reaction, measured by T.B.Ryves[16], W.Poenitz[18], Mu Yunshan[20], J.Voignier[19], M.V.Bokhovko[21] and Shi Zhaomin[22] were adopted and previous measured data were also referred in theoretical calculation in the energy region where experimental data are scarce.

Some previous measured data were examined and corrected based on the accurate data measured from CIAE, PU and FFI. The evaluated data were obtained between 0.00013 eV—4.0 MeV.

1.3 ^{159}Tb(n,p) and (n,α) reactions

For $^{159}Tb(n,p)^{159}Eu$ reaction, experimental data are only available around 14.7 MeV measured by 5 laboratories. The measured data of E.T.Bramlitt[23] and P.R.Prasad[24] were lower and higher than other values, respectively. The value measured by Havlik[25] was corrected using new reference cross section, the revised value is consistent with the recently measured value of A.Barn[27]. The values with large errors measured by S.M.Qaim[26] are consistent with those of E.Havlik[25] and A.barn[27]. At present work, the measured values of E.Havlik[25] and A.Bari[27] were taken as references for theoretical calculation.

For $^{159}Tb(n,\alpha)^{156}Ho$ reaction, there are only 3 sets of experimental data at 14.8 MeV measured by E.Havlik[25], P.Kulisic[28] and S.M.Qaim[29]. The cross sections measured by S.M.Qaim[29] and P.Kulisic[25] are consistent with each other within their errors. The old measured data of E.Havlik[25] are very high since it was a maximum value estimated. The measurement was performed by P.Kulisic[28] using a multi-channel analyzer with particle discrimination character. The values measured by P.Kulisic[28] are consistent with the one by S.M.Qaim[29] using activation method. Then, the measured values of P.Kulisic[28] and S.M.Qaim[29] were recommended.

Except existing measured data for $^{159}Tb(n,\alpha)^{156}Ho$ and $^{159}Tb(n,p)^{159}Eu$ reactions, there are no other experimental data. Therefore, the cross sections of emission charged particle for $^{159}Tb(n,x)$ reactions must be calculated theoretically.

2 Theoretical Calculation and Recommendation

2.1 For ^{159}Tb

In order to recommend the cross sections for $^{159}Tb(n,2n)$, (n,3n), (n,γ) and (n,x) reactions, the theoretical calculation was performed with UNF code. A set of neutron optical potential parameters for ^{159}Tb was obtained, which are based on the available total, nonelastic cross sections and elastic scattering angular distributions. Adjusting this set of neutron optical potential parameters and the relevant level density and giant dipole resonance parameters, the cross sections of (n,2n), (n,3n),(n,γ) and (n,x) reactions were calculated using the UNF Code[30] and the neutron radiation capture cross sections of ^{159}Tb were also calculated using other Code[31]. The comparison of experimental data with the theoretically calculated results was made. The calculated data can reproduce the measured data very well.

The recommended cross sections for (n,γ) were given based on measured and calculated theoretically data, the cross sections in resonance energy region were from JFE-2 and in 0.1－4 MeV from fitting values of evaluated experimental data. The recommended activation cross sections for ^{159}Tb (n,2n), (n,γ) reactions are based on evaluated and calculated results and shown Figs. 1－3.

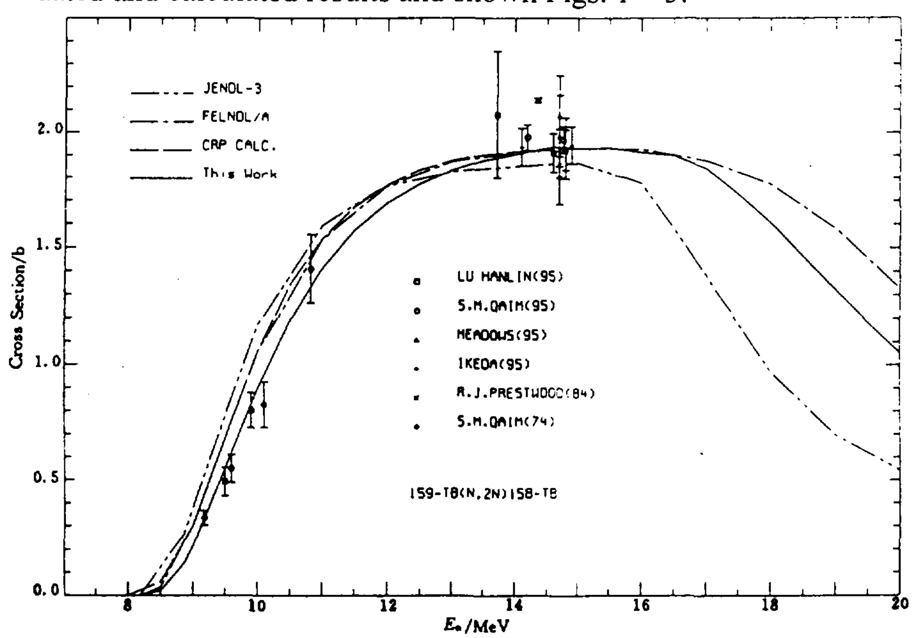

Comparison of evaluated & measured data

Fig.1

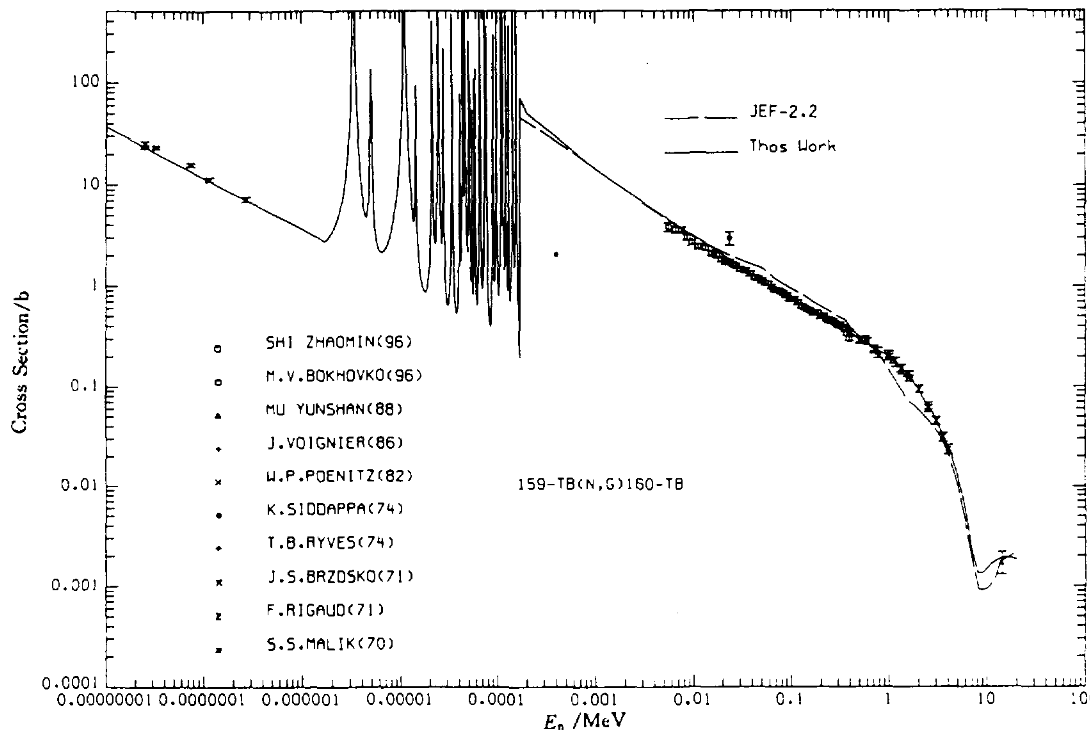

Evaluated Data for ^{159}Tb(n,γ) Reaction

Fig.2

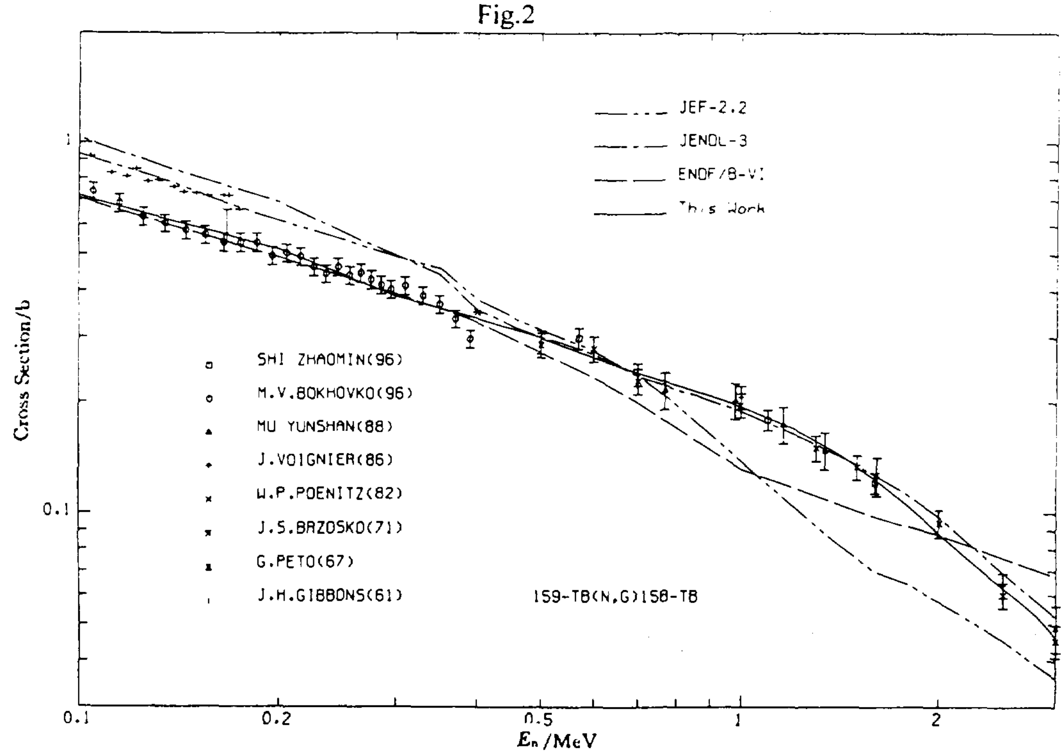

Comparison of evaluated & measured data

Fig.3

The threshold energies of (n,x) reactions are above 8 MeV. The calculation gives cross sections with the order of a few ten mb or less, generally much less. The calculated results were in agreements with existing experimental data. For the (n,α) and (n,p) reactions, the calculated curve could pass the evaluated data measured around 14 MeV. The calculated results for (n,x) reactions are recommended and shown Figs. 4—5.

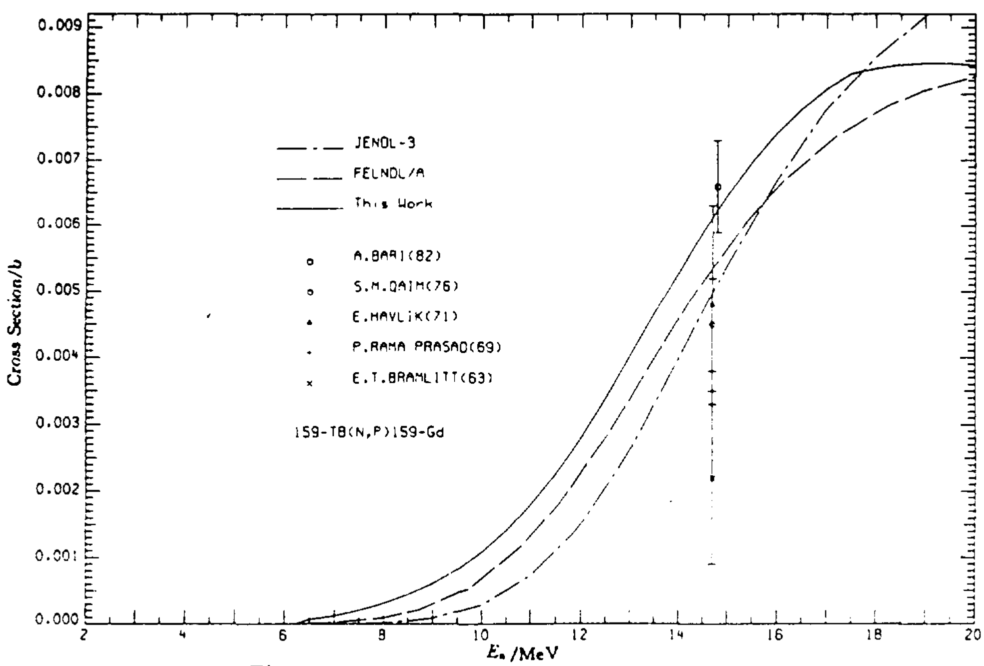

Fig.4 Comparison of evaluated & measured data

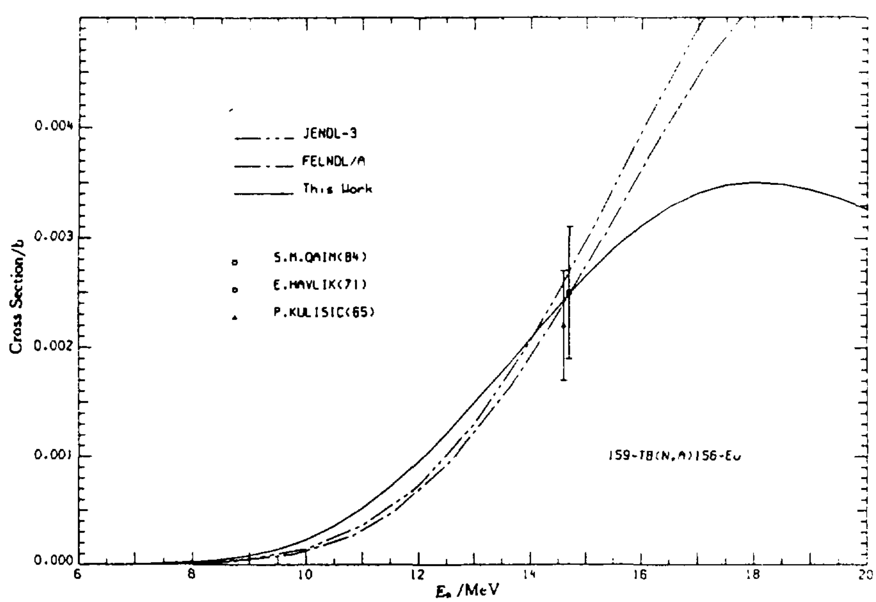

Fig.5 Comparison of evaluated & measured data

Then the cross sections of all reactions by neutron induced on ^{159}Tb are recommended and shown in Fig. 6.

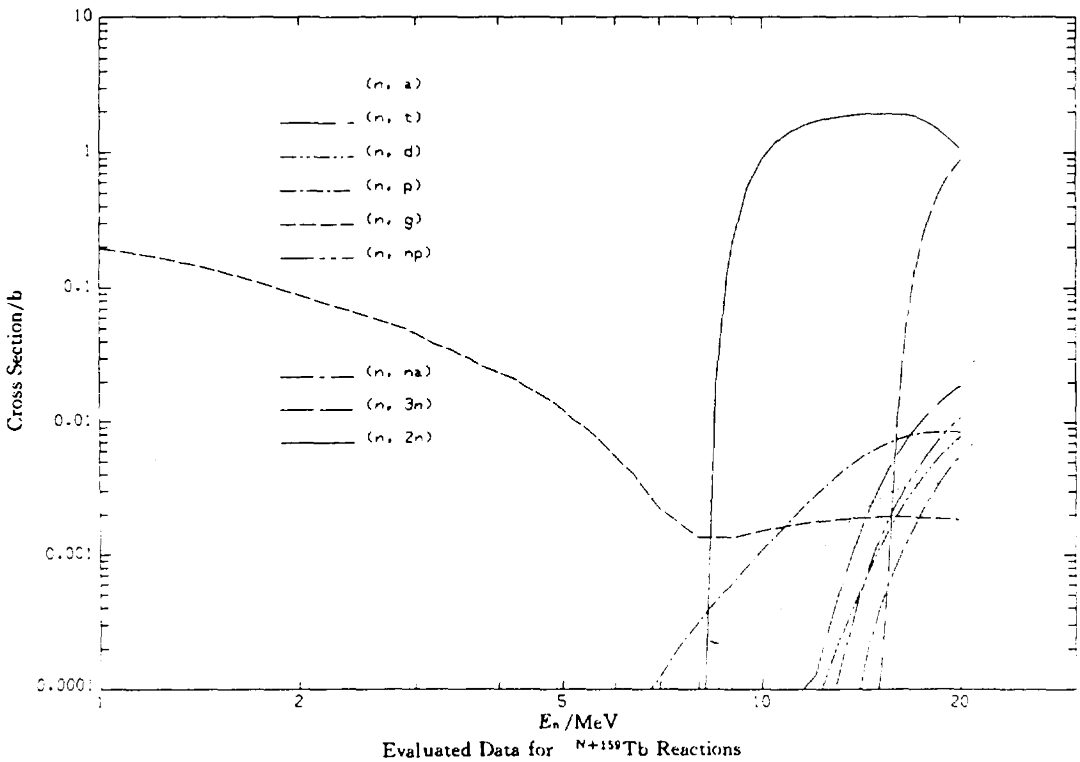

Fig.6

2.2 For ^{158}Tb

Because the ^{158}Tb is a radionuclide, there are no measured data available. In order to recommend the cross sections for $^{158}Tb(n,2n)$, $(n,3n)$, (n,γ) and (n,x) reactions, the theoretical calculation was performed with UNF code[30]. A set of neutron optical potential parameters of ^{159}Tb and the relevant level density and giant dipole resonance parameters of ^{158}Tb were used. The activation cross sections of $^{158}Tb(n,2n)$, (n,γ) and (n,x) reactions are recommended on the basis of calculated results and shown in Fig. 7

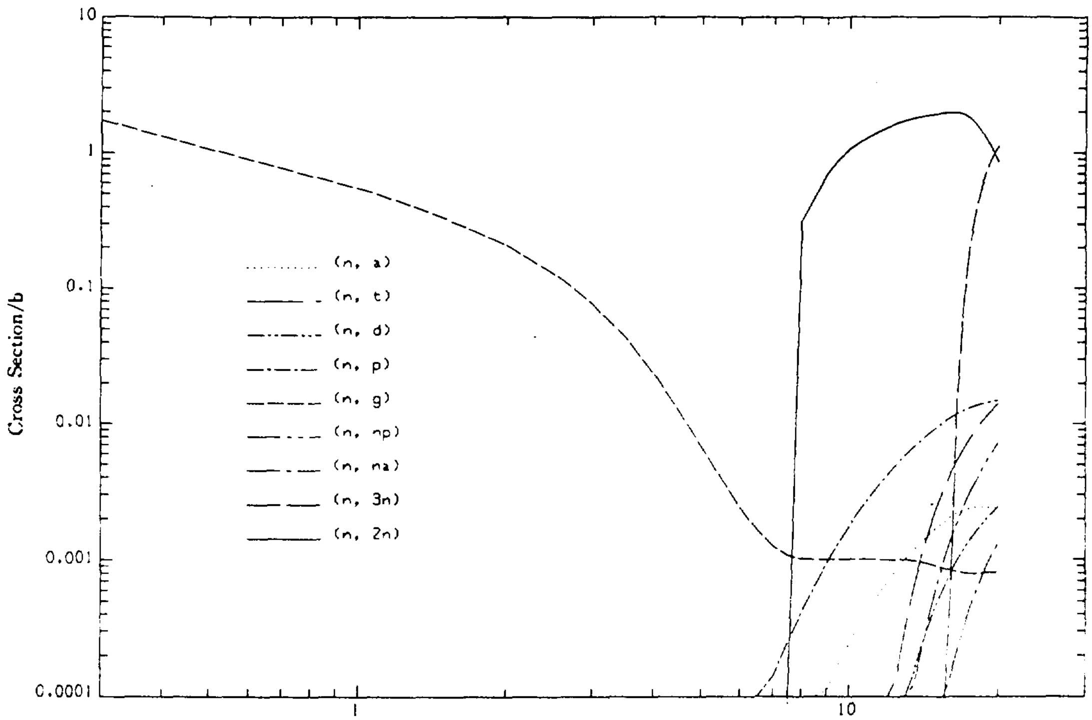

E_n /MeV

Evaluated Data for N+158Tb Reactions

Fig.7

3 Summary

The evaluated cross sections for ^{159}Tb (n,2n)^{158}Tb reaction are compared with other evaluated ones and consistent with experimental data, which were better than the evaluated data from other nuclear libraries.

The cross sections for ^{159}Tb(n,γ)^{160}Tb reaction were measured from thermal to 4.0 MeV and 14 MeV in several laboratories. At present work, the recommended data were given based on the accurate measured and calculated data. The cross section measured by Shi Zhaomin[22] in 0.5—1.6 MeV are used to check the cross sections in the energy region. The recommended cross sections are reliable.

Acknowledgments

The authors are indebted to IAEA (International Atomic Energy Agency), CNNC (China National Nuclear Corporation) and CIAE for their supports, and thank Drs.A.B.Pashchenko, T.Benson, O.Schwerer, Lu Hanlin, Zhao Wenrong for their kind helps and suggestions.

References

[1] S. M. Qaim et al., Nucl. Phys./A, 224, 319(1974)

[2] R. J. Prestwood et al., Phys. Rev. /C, 30, 823(1984)

[3] J. W. Meadows et al., J. ANE, 23, 877(1996)

[4] Y. Ikeda et al., JAERI - M - 91(1991)

[5] S. M. Qaim et al., INDC(NDS) - 342, 47(1996)

[6] Lu Hanlin et al., ibid, p-37

[7] Yu Weixiang et al., ibid, p-41

[8] H. Vonach et al., ibid, p-49

[9] J. H. Gibbons et al., Phys. Rev.,122,182(1961)

[10] R. C. Block et al., Inter. Conf. on Nuclear Data for Science and Technology p203 Saclay(1961)

[11] G. Peto et al., JNE, 21, 797(1967)

[12] K. Knorr et al., AKE, 16, 49(1970)

[13] S. S. Malik et al., NIM, 86, 83(1970)

[14] F. Rigaud et al., Nucl. Phys. A, 176,545(1971)

[15] J. S. Brzosko et al., APP/B,2, 489(1971)

[16] T. B. Ryves et al., JP/A, 7, 2318(1974)

[17] K. Siddappa et al., AP, 83, 355(1974)

[18] W. P. Poenitz et al., ANL - 83 - 4, 239 (1982)

[19] J. Voignier et al., Nucl. Sci. Eng., 93, 43(1996)

[20] Mu Yunshan et al., Journal of China Nucl. Phys., 10, 233(1988)

[21] M. V. Bokhovko et al., EXFOR Data 41225007(1996)

[22] Shi Zhaomin Private Communication(1997)

[23] E. T. Bramlitt et al., Phys. Rev., 131, 2649(1963)

[24] P. R. Prasad et al., Nucl. Phys./A, 125, 57(1969)

[25] E. Havlik et al., APA, 34, 209(1971)

[26] S. M.Qaim et al., RRP, 25, 335(1976)

[27] A. Bari et al., JRC, 75, 189(1982)

[28] P. Kulisic et al., Nucl. Phys, 73, 548(1965)

[29] S. M. Qaim et al., EXFOR Data N0. 21997012(1984)

[30] Zhang Jingshang, INDC(CPR)-027/L, 14(1992)

[31] Tang Guoyou and Liu Jianfeng, Private Communication(1996)

CN9800592

IV SYSTEMATICS RESEARCH

The Systematics Research on (p,n) and (p,2n) Reaction Excitation Functions

Ma Yinqun Zhuang Youxiang

(China Nuclear Data Center, CIAE, Beijing 102413)

Abstract

On the basis of Planck formula of black body radiation and experimental excitation functions of (p,n) and (p,2n) reactions, an empirical systematics formula with two parameters is presented, which can describe experimental data of (p,n) and (p,2n) reactions well for incident proton energies from threshold to 150 MeV, target masses from 30 to 243.

Introduction

With the development of nuclear science and technology, charged particle nuclear data are used in a wide range, such as spallation neutron sources, radiation damage, radioisotope production for medical application and so on. The existing charged particle nuclear data can not meet the requirements mentioned-above.

It is necessary for these purposes to do systematics research. There are two ways: one is from simplified theory formula, and the other from empirical one. Up to now, there is a few systematics research on charged particle nuclear data, especially (p,n) reaction excitation functions; Letaw et al.(1983)[1], Pearlstein (1989)[2] and Shen (1991)[3] have searched the systematics of nonelastic cross sections in intermediate energy for proton.

The present work takes the second way. Due to the enlightenment of Planck black radiation formula, based on survey and analysis of many experimental data, we have found that the curves of (p,n) reaction excitation functions are very similar to the ones of black body radiation. The reaction channels of different outgoing neutrons for charged particle q incident on target nucleus A are corresponding to the black body radiation in different temperatures one by one.

The intensity with different photon energy $h\nu$ of black body radiation in certain temperature is described by Planck formula, thus the cross section of nuclear reaction at an incident energy can be obtained by means of a revised Planck formula.

1 Establishment of Empirical Formula

1.1 Preliminary Formula

The Planck radiation formula of black body is as follows:

$$M(\nu) = \frac{C_0 \nu^3}{e^{C_1 \nu / T} - 1} \tag{1}$$

Where $M(\nu)$ is the intensity of black radiation at temperature T in a unit of time and a unit of surface area, ν is the radiation photon frequency, T is the absolute temperature of black body, C_0 and C_1 are the two constants. Accoding to the mentioned-above analogy, we have:

$M(\nu) \Leftrightarrow \sigma(E)$	(reaction cross section)
$\nu \Leftrightarrow E$	(incident energy)
$C_1 / T \Leftrightarrow \beta_0$	(a parameter related to a reaction channel)
$C_0 \Leftrightarrow C_0$	(a parameter awaiting determination)

Thus a preliminary formula of reaction cross section is obtained:

$$\sigma(E) = \frac{C_0 E^3}{e^{\beta_0 E} - 1} \tag{2}$$

Because there exits a threshold E_{th} for a certain reaction, $\sigma(E)=0$, when $E \leqslant E_{\text{th}}$, we replace E with $(E-E_{\text{th}})$ in formula (2)

$$\sigma(E) = \frac{C_0 (E - E_{\text{th}})^3}{e^{\beta_0 (E - E_{\text{th}})} - 1} \tag{3}$$

It can describe the curves of (p,xn) reaction excitation functions roughly, at E<30 MeV.

1.2 Improved Formula Function

In order to raise the values of curves at E>30 MeV, we put some β functions into formula (3). For (p,n) reaction, we have:

$$\sigma_{\text{p,n}} = \frac{C_0 (E - E_{\text{th}})^3}{e^{\beta_0 (E - E_{\text{th}}) - 1}} \prod_{i=1}^{6} \beta_i \tag{4}$$

where,

$$\beta_0 = E^{-C_1}$$

$$\beta_1 = \frac{1}{1+(\dfrac{C_2}{E-E_{\text{th}}})^2}$$

$$\beta_2 = \frac{1}{1-\sin(E-E_{\text{th}})^{C_3}}$$

$$\beta_3 = 1 - C_4 e^{(-C_5|E-25|^5)}$$

$$\beta_4 = 1 - C_6 e^{(-C_7|E-38|)}$$

$$\beta_5 = e^{(E/25)^{C_8}}$$

$$\beta_6 = e^{(-E/120)^{C_9}}$$

For (p,n) reaction, we have:

$$C_1 = \begin{cases} 0.3669/A^{1/12} & A>51 \\ 0.2644 & A \le 51 \end{cases} \qquad C_3 = 0.08907$$

$$C_4 = 0.7683 \qquad C_5 = 0.00008299 \qquad C_6 = 0.6985$$

$$C_7 = 0.06811 \qquad C_8 = 1.6772 \qquad C_9 = 7.5$$

For (p,2n) reaction we have:

$$\sigma_{\text{p,2n}}(E) = \sigma_1(E) + \sigma_2(E)\delta_{\text{E,C}_5} \tag{5}$$

where,

$$\delta_{\text{E,C}_5} = \begin{cases} 0 & , \quad E = C_5 \\ 1 & , \quad E \ne C_5 \end{cases}$$

$$\sigma_1(E) = \frac{C_0(E-E_{\text{th}})^3}{e^{\beta_0(E-E_{\text{th}})}-1}\beta_1\beta_2\beta_3,$$

$$\sigma_2(E) = \sigma_1(C_5)(C_5/E)^{C_6}\beta_4,$$

$$\beta_0 = E^{-C_1/A^{1/12}}, \qquad \beta_1 = e^{-C_2\left|\frac{C_7-E}{E}\right|}, \qquad \beta_2 = e^{(E/C_8)^{C_3}},$$

$$\beta_3 = \frac{1}{1+C_4 e^{30(E-C_5)}}, \qquad \beta_4 = \frac{1}{1+C_4 e^{30(C_5-E)}},$$

$$C_1 = 0.3669, \qquad C_4 = 0.000001, \qquad C_5 = 35\text{MeV},$$

$$C_6 = 1.5, \qquad C_7 = C_8 = 25\text{MeV}$$

and C_2 is independent on E and A of the target.

where C_0, C_2 for (p,n) and C_0, C_3 for (p,2n) are adjustable parameters (also the socalled local parameters).

2 Systematics of Parameters C_0, C_2 and C_3

2.1 Collection of Experimental Data

The experimental data of 25 targets from ^{11}B to ^{238}U for (p,n) reaction and of 22 targets from ^{45}Sc to ^{241}Am for (p,2n) reaction were collected from EXFOR experimental data library, respectively. These data were evaluatied roughly.

2.2 Determination of Local Parameters C_0, C_2 and C_3

In order to get the optimum values of C_0, C_2 and C_3, we define

$$\chi^2 = \frac{1}{N}\sum_{i=1}^{N}\left(\frac{\sigma_c(i) - \sigma_E(i)}{\Delta\sigma_E(i)}\right)^2 \tag{6}$$

where σ_c is the calculated value of cross section, σ_E is the experimental value of cross section. $\Delta\sigma_E$ expresses the experimental error, and N denotes the sum of all chosen energies. The parameters C_0, C_2 and C_3 can be obtained in search of the minimum deviation between the calculated results and experimental data by computer automatically. After careful researching, the parameters C_0, C_2 and C_3, have been acquired, see Table 1 and 2.

Table1 Local Parameters C_0 and C_2 from (p,n) experimental data

Target	$(N-Z)/A$	E_{th} / MeV	C_0 / MeV	C_2 / MeV
^{11}B	0.09091	3.0175	0.002491	0.000
^{13}C	0.76920	302355	0.001377	0.000
^{15}N	0.06667	3.7702	0.001450	0.000
^{45}Sc	0.06667	2.9080	0.003546	0.000
^{51}V	0.09803	1.5654	0.006877	0.000
^{52}Cr	0.07692	5.5990	0.006877	0.000
^{56}Fe	0.07143	5.4443	0.002687	0.000
^{62}Ni	0.09677	4.8060	0.005753	0.000
^{63}Cu	0.07937	4.2156	0.003867	0.000
^{65}Cu	0.10770	2.1668	0.007077	0.000
^{66}Zn	0.09091	6.0460	0.004882	0.000
^{67}Zn	0.10450	1.8100	0.008908	2.500
^{75}As	0.12000	1.6680	0.008899	4.850
^{77}Se	0.11690	2.1740	0.008540	4.390
^{79}Br	0.11390	2.4370	0.009336	4.391
^{87}Sr	0.12640	2.6730	0.012990	6.190
^{89}Y	0.12360	3.6550	0.010980	6.450
^{96}Mo	0.12500	3.7950	0.011210	3.450
^{107}Ag	0.12150	2.2200	0.012420	8.450
^{111}Cd	0.13510	1.6630	0.012872	8.845
^{123}Te	0.15450	2.0310	0.014200	10.85
^{127}I	0.16540	1.4560	0.014630	22.84
^{181}Ta	0.19340	0.9760	0.016980	32.85
^{209}Bi	0.20570	2.6878	0.029980	36.85
^{238}U	0.22690	0.9316	0.026980	125.9

Table2 Local Parameters C_0 and C_3 from (p,2n) experimental data

Target	$(N\text{-}Z)/A$	E_{th}, MeV	C_0 / MeV	C_3
^{45}Sc	0.06667	12.65	0.001599	1.6197
^{52}Cr	0.07692	16.74	0.004954	1.1619
^{56}Fe	0.07143	15.72	0.002001	1.4576
^{57}Fe	0.08772	13.22	0.009589	0.9589
^{63}Cu	0.07936	13.50	0.004259	0.9698
^{68}Zn	0.11760	12.16	0.034530	0.8500
^{69}Ga	0.10140	11.66	0.023520	0.7859
^{76}Se	0.10530	15.15	0.016590	0.5786
^{78}Se	0.12820	12.81	0.031980	0.7123
^{88}Sr	0.13640	13.95	0.041390	0.5879
^{93}Nb	0.11830	9.354	0.045000	0.6850
^{96}Mo	0.12500	11.76	0.042000	0.6000
^{109}Ag	0.13760	8.358	0.048500	0.6850
^{111}Cd	0.13510	11.81	0.041050	0.5850
^{112}Cd	0.14290	11.11	0.043840	0.7735
^{124}Te	0.16130	11.51	0.050480	0.9695
^{181}Ta	0.19340	7.700	0.129800	0.9775
^{197}Au	0.19790	8.200	0.167300	1.5600
^{206}Pb	0.20390	11.62	0.082790	1.7610
^{207}Pb	0.20770	11.23	0.067680	0.3592
^{209}Bi	0.20570	9.690	0.049890	2.8668
^{241}Am	0.21160	10.12	0.001299	0.8855

2.3 Systematics of Local parameters C_0, C_2 and C_3

Are there systematics behaviour of parameters C_0, C_2 and C_3? The answer is certainly yes.

Using the minimum deviation, the systematic formulas of parameters C_0, C_2 and C_3 are as follows:

For (p.n) reaction we have:

$$C_0 = (-0.009556 + 0.1665\frac{N-Z}{A})(1-0.3e^{-1800(\frac{N-Z}{A}-0.185)^2}) \tag{7}$$

$$C_2 = \frac{0.000412A^{2.1484} - (A/100)^{2.9888} + (A/150)^{6.7} + (A/200)^{24}}{1+0.4e^{10(67-A)}} \tag{8}$$

For (p,2n) reaction, we have:

$$C_0 = \begin{cases} 0.002635e^{(20.485X + (\frac{0.06514}{X})^{20} - (\frac{0.08}{X})^5)} & X < 0.19796 \\ 2.476935 - 11.7X & X \geq 0.019796 \end{cases} \tag{9}$$

$$C_3 = \begin{cases} 0.6057e^{(3.5|X-0.1323| + 132|X-0.1323|^{1.899})} & X < 0.2055 \\ (260.7769 - 1253.8X) & \\ (1 - \frac{5.65X}{1+0.0000001e^{1000000(0.20775-X)}}) & X \geq 0.2055 \end{cases} \tag{10}$$

where $X = \dfrac{N-Z}{A}$.

The values of C_0, C_2 and C_3 extracted from the above systematics are called regional parameters .The comparison between local and regional parameters is given in Figs.1—4.

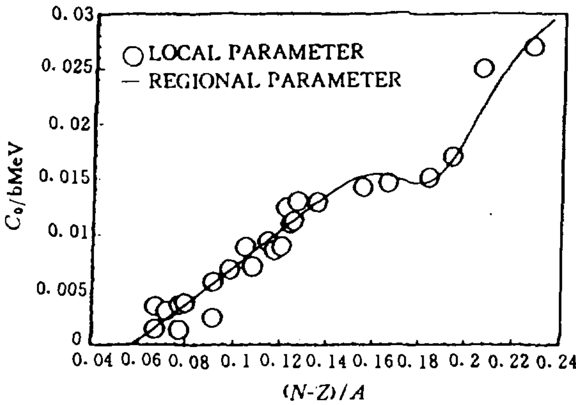

Fig.1 For(p,n) reaction

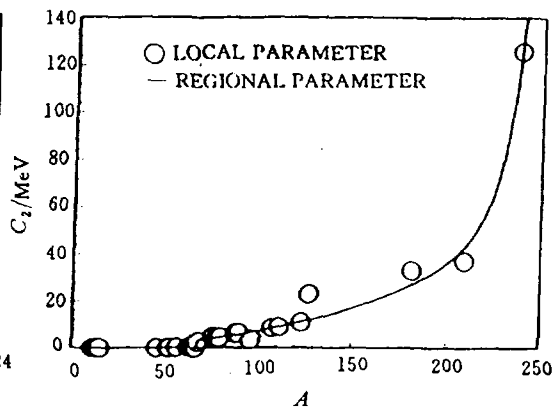

Fig.2 For(p,n) reaction

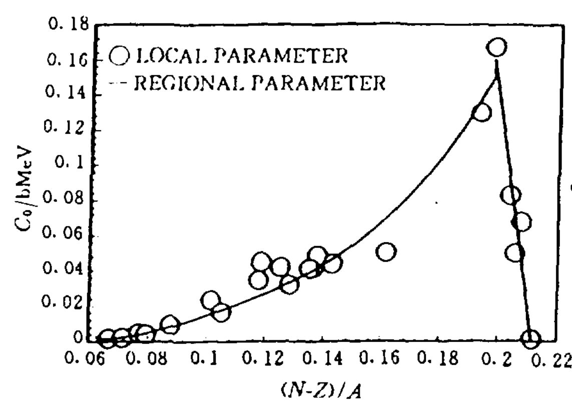

Fig.3 For(p,n) reaction

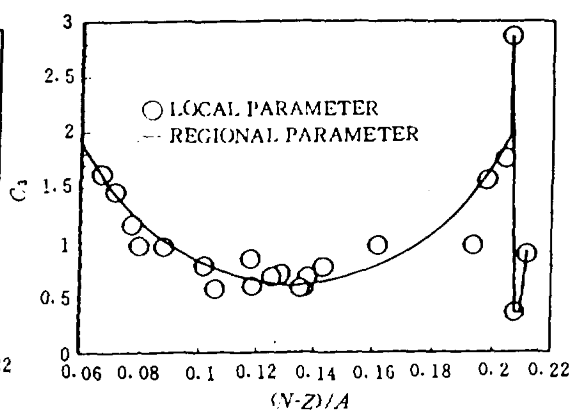

Fig.4 For(p,n) reaction

It can be seen that the fit curves for parameters C_0, C_2 and C_3 are in agreement with those from experimental data.

3 Conclusions and Discussion

Using the regional parameters C_0, C_2, the excitation function of the (p,n) reaction can be predicted. When $50<A<120$, the comparison with the existing measured excitation functions shows that the agreements between the predicted and measured curves are good (see Figs.5, 6); while for A<51 and A>120 nuclei, agreement between the excitation function predicted by the systematics and the existing measured excitation functions is not satisfactory. For (p,2n) reaction, agreement between the excitation function predicted by the systematics and the existing measured excitation functions is very satisfactory (see Figs.7, 8).

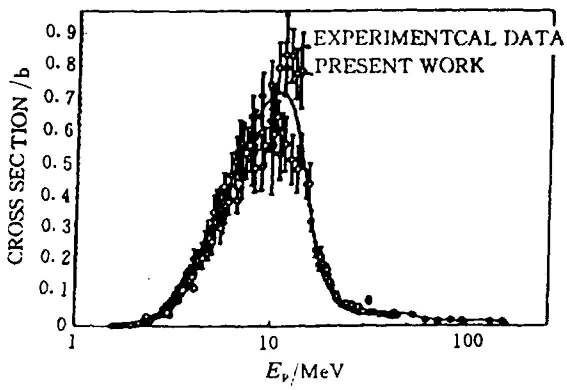

Fig.5 ^{51}V(p,n) reaction

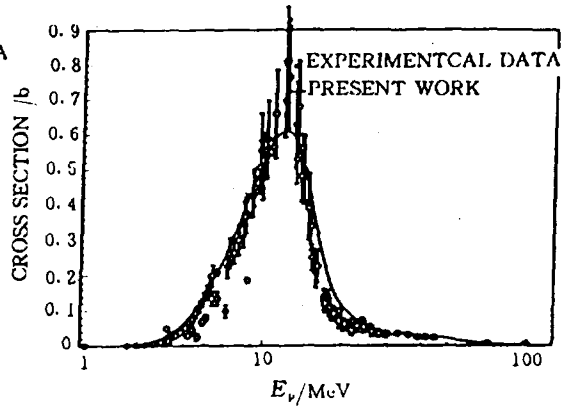

Fig.6 ^{111}Cd(p,n) reaction

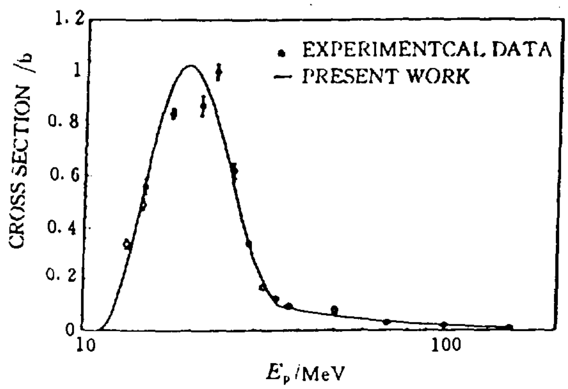

Fig.7 ^{111}V(p,2n) reaction

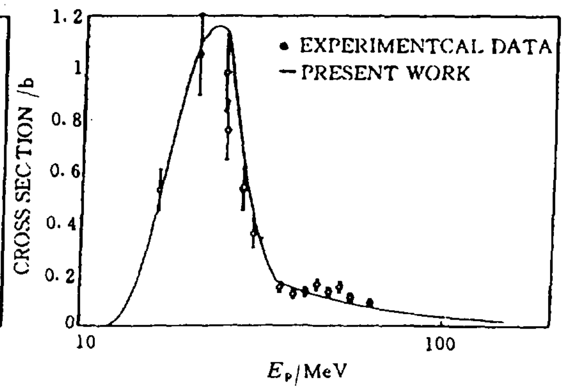

Fig.8 ^{206}Pb(p,2n) reaction

It would be of interest to note that the equation (5) could be applied to (q,xn) (where q=p, d, t, ^{3}He, α; x=1,2,3,4,5.) reactions as well.

Acknowledgements

The authors would like to express gratitude to Profs. Zhou Delin, Zhao Zhixiang and Lu Hanlin for their helpful discussion.

References

[1] Letaw, John R; Siberberg, R; Tsao, C.H. The Astrophysical Jourunl Supplement Series.51:271-275,1983

[2] Pearlstein, S. Astrophysical Jourunl.346: 1049-1060,1989

[3] Shen, Qingbiao.INDC (CPR)-020 Distr.: L:1-12, 1991(in Vienna)

CN9800593

V DATA AND PARAMETER LIBRARIES

The Sub-Library of Atomic Masses and Characteristic Constants of Nuclear Ground States (CENPL-MCC 2) (IV)*

Su Zongdi Sun Zhenjun
(China Institute of Atomic Energy, P.O.BOX 275, Beijing)

Zheng Chunkai
(Department of Technical Physics, Peking University, Beijing)

The MCC 2 (the Second Version) is an updated edition of the sub-library of atomic masses and characteristic constants of nuclear ground states (MCC) of the Chinese Evaluated Nuclear Parameter Library (CENPL). It contains data files: "MCC2-1.DAT" and "MCC2-2.DAT".

1 "MCC2-1.DAT" File

The "MCC2-1.DAT" file contains the most recent measured[1], systematics[1] and calculated[2] mass excesses, total binding energy[1], deformations[2] for nuclei between the proton and neutron drip lines and superheavy nuclei. There are altogether 9066 nuclei ranging from Z=0, A=1 to Z=136, A=339. The mass excesses of this file are from the experimental and systematics data compiled by G.Audi and A.H.Wapstra in 1995[1], and the calculated ones of P.Moller, J.R.Nix, W.D.Myers and W.J.Swiatecki in 1994[2] by using a nuclear mass formula with a finite-range droplet macroscopic model and the Folded-Yukawa single-particle microscopic model (FRDM). An appended "s" denotes that the value is of systematics, and "t" denotes calculated one.

2 "MCC2-2.DAT" File

The "MCC2-2.DAT" file contains the abundance[3], magnetic and quadrupole moments[4] of nuclear ground state for neutron and 286 stable nuclei ranging from Z=1, A=1 to Z=92, A=238.

The authors would like to thank NDS/IAEA, NNDC/BNL and Dr.G.Audi for providing the data tapes and so on.

References

[1] G. Audi and A. H. Wapstra, Nucl. Phys.A595(1995)409

[2] P. Moller, J. R. Nix, W. D. Myers and W. J. Swiatecki, Atomic Data and Nucl. Data Tables, 59(1995)85

[3] N. E. Holden, Table of the Isotopes, CRC Handbook of Chemistry and Physics(71st edition), in 1990

[4] R. B. Firestone, Table of Isotopes(8th Edition), in 1996

* The project supported in part by the International Atomic Energy Agency.

CINDA INDEX

Nuclide	Quantity	Energy/ eV		Lab	Type	Documentation				Author, Comments
		Min	Max			Ref	Vol	Page	Date	
^{16}O	(d,x)	1.0+5	3.5+7	AEP	Theo	Jour CNDP	18	34	Dec 97	Han Yinlu+, MDL CALC, DA, SIG
^{17}F	(d,x)	1.0+5	3.5+7	AEP	Theo	Jour CNDP	18	34	Dec 97	Han Yinlu+, MDL CALC, DA, SIG
^{51}V	(p,n)	Thrsh	1.5+8	AEP	Revw	Jour CNDP	18	83	Dec 97	Ma Yinqun+, (p,n) SYSTEMATICS
^{55}Mn	(n,α)	Thrsh	2.0+7	AEP	Eval	Jour CNDP	18	66	Dec 97	Yu Baosheng, CS
^{54}Fe	(n,α)	Thrsh	2.0+7	AEP	Eval	Jour CNDP	18	66	Dec 97	Yu Baosheng, CS
^{59}Co	(n,α)	Thrsh	2.0+7	AEP	Eval	Jour CNDP	18	66	Dec 97	Yu Baosheng, CS
^{58}Ni	(n,p)	4.1+6		BJG	Expt	Jour CNDP	18	1	Dec 97	Tang Guoyou+, GIC, DA, DE, GRPH
^{62}Ni	(n,α)	Thrsh	2.0+7	AEP	Eval	Jour CNDP	18	66	Dec 97	Yu Baosheng, CS
^{63}Cu	(n,α)	Thrsh	2.0+7	AEP	Eval	Jour CNDP	18	66	Dec 97	Yu Baosheng, CS
^{64}Zn	(n,p)	Thrsh	2.0+7	AEP	Theo	Jour CNDP	18	41	Dec 97	Huang Xiaolong+, MDL CALC, SIG
^{66}Zn	(n,p)	Thrsh	2.0+7	AEP	Theo	Jour CNDP	18	41	Dec 97	Huang Xiaolong+, MDL CALC, SIG
^{67}Zn	(n,p)	Thrsh	2.0+7	AEP	Theo	Jour CNDP	18	41	Dec 97	Huang Xiaolong+, MDL CALC, SIG
^{68}Zn	(n,p)	Thrsh	2.0+7	AEP	Theo	Jour CNDP	18	41	Dec 97	Huang Xiaolong+, MDL CALC, SIG
^{111}Cd	(p,n)	Thrsh	1.5+8	AEP	Revw	Jour CNDP	18	83	Dec 97	Ma Yinqun+, (p,n) SYSTEMATICS
	(p,2n)	Thrsh	1.5+8	AEP	Revw	Jour CNDP	18	83	Dec 97	Ma Yinqun+, (p,2n) SYSTEMATICS
^{158}Tb	(n,x)	Thrsh	2.0+7	AEP	Eval	Jour CNDP	18	72	Dec 97	Yu Baosheng, CS
^{159}Tb	(n,x)	6.0+6	2.0+7	AEP	Eval	Jour CNDP	18	72	Dec 97	Yu Baosheng, CS
	(n, γ)	4.5+5	4.0+6	BJG	Expt	Jour CNDP	18	9	Dec 97	Chen Jinxiang+, ACTIV, HPGE, CS, GRPH
^{160}Tb	(n, γ)	1.6+5	3.0+6	BJG	Expt	Jour CNDP	18	9	Dec 97	Chen Jinxiang+, ACTIV, HPGE, CS, GRPH
^{176}Hf	(n,x)	Thrsh	2.0+7	AEP	Theo	Jour CNDP	18	47	Dec 97	Huang Xiaolong+, MDL CALC, SIG
^{206}Pb	(p,2n)	Thrsh	1.5+8	AEP	Revw	Jour CNDP	18	83	Dec 97	Ma Yinqun+, (p,2n) SYSTEMATICS
^{235}U	Fission Yield	2.5-2	2.0+7	AEP	Eval	Jour CNDP	18	53	Dec 97	Liu Tingjin, YLDS VS EN, GRPH
^{239}Pu	Total	1.6+6	2.0+7	AEP	Theo	Jour CNDP	18	29	Dec 97	Wang Shunuan, COUPLED CHANNEL, DWBA, SCC
	Diff inelastic	1.0+6	2.0+7	AEP	Theo	Jour CNDP	18	29	Dec 97	Wang Shunuan, COUPLED CHANNEL, DWBA, SCC
	Diff Elastic	1.6+6	2.0+7	AEP	Theo	Jour CNDP	18	29	Dec 97	Wang Shunuan, COUPLED CHANNEL, DWBA, SCC

（京）新登字 077 号

图书在版编目（CIP）数据

中国核科技报告：CNIC-01230，CNDC-0021：核数据进展通讯：英文/刘廷进等著. -北京：原子能出版社，1997.12
ISBN 7-5022-1776-2

Ⅰ. 中… Ⅱ. 刘… Ⅲ. 核技术-研究报告-中国-1997-英文 Ⅳ. TL-2

中国版本图书馆 CIP 数据核字（97）第 24923 号

©原子能出版社，1997

原子能出版社出版发行

责任编辑：李曼莉

社址：北京市海淀区阜成路 43 号 邮政编码：100037

中国核科技报告编辑部排版

核科学技术情报研究所印刷

开本：787 × 1092 1/16 · 印张 6 · 字数 95 千字

1997 年 12 月北京第一版 · 1997 年 12 月北京第一次印刷

CHINA NUCLEAR SCIENCE & TECHNOLOGY REPORT

This report is subject to copyright. All rights are reserved. Submission of a report for publication implies the transfer of the exclusive publication right from the author(s) to the publisher. No part of this publication, except abstract, may be reproduced, stored in data banks or transmitted in any form or by any means, electronic, mechanical, photocopying, recording or otherwise, without the prior written permission of the publisher, China Nuclear Information Centre, and/or Atomic Energy Press. Violations fall under the prosecution act of the Copyright Law of China. The China Nuclear Information Centre and Atomic Energy Press do not accept any responsibility for loss or damage arising from the use of information contained in any of its reports or in any communication about its test or investigations.

ISBN 7-5022-1776-2

9 787502 217761 >